CHAPTER ONE

1.0 INTRODUCTION

1.1. BACKGROUND AND MOTIVATIONS

Stainless steels are widely used for corrosion resistant equipment in the chemical, petroleum, process, food, and power industries**.** Recently, because of their high degree of corrosion resistance, stainless steels also often have applications as architectural materials such as the roofs and walls of buildings (Tochihara *et al., 1986;* Avesta, 1999; Asami and Hashimoto, 2003). According to Tochihara *et al.* (1986); Wallinder *et al*. (2006), stainless steels have been increasingly used in outdoor constructions and architectural applications over the last two or three decades. It is reported that stainless steels have been applied to building construction as early as the 1920s and 1930s because of their low maintenance cost due to their high degree of corrosion resistance and stability in an unpolluted atmosphere (LaQue, 1969; Osozawa, 1980). Traditionally, austenitic stainless steels have been used for roofs and exterior facades, especially AISI grade 304 (typically 18% Cr, 8% Ni) in urban environments and AISI grade 316 (typically 18% Cr, 10% Ni, 2% Mo) in marine environments (Tochihara *et al.,* 1986; Wallinder *et al.,* 2006). The most common stainless steel used for roofing applications in both environments is grade 316 (Avesta, 1999). De Abreu *et al.* (2006) have recently reported that the general corrosion resistance of 444 is comparable to that of austenitic AISI 316. Its higher levels of chromium yield better oxidation resistance and the presence of nickel-molybdenum results in its excellent resistant to stress corrosion cracking and good properties in sulphur-containing environments at high temperatures (Grobner, 1973; Leffler, 2005). Although originally developed for industrial purposes, these materials have been tried for biomaterial uses due to their relatively high corrosion resistance and excellent mechanical properties. However, when used as biomaterials, these materials pose several problems due to the presence of nickel. These problems include toxicity of corrosion products and fretting debris to the human body, fracture due to corrosion fatigue and fretting corrosion fatigue, lack of biocompatibility, and inadequate affinity for cells and tissues. In particular, the toxicity problem brought about other problems such as allergy reaction, tumor formation, teratogenicity, and inflammation (Nakayama *et al.,* 1989; Teoh, 2000). According to Sumita *et al.* (2004) the release of nickel trace elements which cause

toxicity has prompted the development of nitrogen-containing nickel-free austenitic stainless steels.

The type 444 is a low-carbon, low nitrogen, ferritic stainless steel that provides pitting and crevice corrosion resistance superior to most ferritic stainless steels (AK Steel, 2007a). Every application requiring superior corrosion resistance and resistance to chloride stress corrosion cracking is ideal for this alloy. The type 444 finds many applications in petroleum refining plants, food processing, brewery and wine-making equipment; hot-water tanks and heat exchanger tubing and automotive components etc. (De Abreu *et al*, 2006: AK Steel, 2007a). Comparative investigations on the importance of initial surface film in the degradation of different types of stainless steels by atmospheric exposure reported by Asami and Hashimoto (2003) indicated that the corrosion resistance of 444 is higher than 316. The order of corrosion-resistance was type 444, type 316, type 304, and type 430. The improvement of passivity in the 444 stainless steel is mainly attributed to the substitution of chromium oxide by molybdenum oxide in the passive film (Doh *et al*, 2003). These properties makes it ideal to use this steel in petroleum refining plants, replacing austenitic grades 316 and 317 L (De Abreu *et al*, 2006).

1.2 PROBLEM STATEMENT

The corrosion behavior of both 444 and 316 stainless steels have been reported to be very similar in certain media (Leffler, 2005). Type 316 may possess some outstanding characteristics in some media, while 444 may have some distinctive advantages in most media where 316 might be ineffective. The characteristic behaviors of these alloys can be linked, attributed to and observed to be dependent on the probably type of passivating film. According to Asami and Hashimoto (2003), corrosion resistance does not only depend on the type of passivating film, but on the film formation process and film structure. Since the type of passivating film formed on the surfaces of stainless steels is a function of the alloying elements, the differences in the composition and the alloying elements of 316 and 444 will therefore influence the film formation process and thus affect their behavior in different media. Owing to the differences in the alloying elements of these alloys, the variations in the amounts of nickel and chromium in 316 and 444 respectively would thus determine the

mechanisms of formation and degradation, as well as the stability of the passivating film.

The stability of passive films on different alloys may be affected by several factors. Hydrogen may enter into the passivating oxide film as a proton due to the ionic bonding character of the passive film and changes the electrochemical properties of passive film; that is the average valence state of the cations in the passive film (Pyun and Oriani, 1989). Hydrogen may also change the electric structure, increase the dielectric constant and capacitance of passive film (Li *et al*., 2003). Hydrogen has been observed to have a detrimental effect on 316. According to Li *et al*. (2003), some hydrogen atoms produced during the cathodic corrosion reactions may enter the 316 surface and hence give rise to a decrease in passivity and corrosion resistance.

Despite the fact that the corrosion resistance of type 444 stainless steel is attributed to the amount of its chromium contents, it has been observed that simple enrichment of chromium in the surface film is not sufficient to explain the origin of corrosion resistance (Asami and Hashimoto, 1979; Hashimoto *et al*., 1979). The passive film could be enriched in chromium close to the alloy, whereas some amounts of hydroxides and water may be concentrated in the outermost layers of the film (Lorang *et al.,* 1987; Lorang *et al.*, 1988). As a means of improving passivity, molybdenum could be effectively used to augment the corrosion resistance effects of chromium.

The addition of molybdenum to stainless steels improves their pitting corrosion resistance in aggressive chloride solutions (Habazaki *et al*., 1991; AK Steels, 2007b). Molybdenum additions aid in the development and stability of an amorphous passive film which further provides resistance against $C1^-$ ion attack and subsequent pitting (Clayton and Lu, 1986). The oxidation of the chromium oxide from Cr_2O_3 to CrO_4^{2-} could also decreases the passivity of the film formed on the surface of this material. According to Doh *et al*. (2003), the Cr_2O_3/Fe_2O_3 ratio in the passive film could gradually decrease with passivation time, while the oxidation of Cr_2O_3 to CrO_4^{2-} could lead to the weakening of passivity. Molybdenum may effectively substitute chromium to a certain level by forming molybdenum oxide in the passive film. An improvement on passivity of stainless steel 444 has also been reported by Doh *et al*. (2003) to be mainly attributed to the substitution of chromium oxide by molybdenum oxide in the

passive film. It was reported that, as the passivation time increases, the molybdenum oxide in the passive film increases, which aids a better passivity of the film even as the oxidation of the chromium oxide decreased the passivity. The addition of molybdenum could diminish the breakdown of passivity of 444 (Clayton and Lu, 1986; Olsson, 1995; Qvarfort, 1998). It has also been reported that molybdenum has similar corrosion effects on 316 (Mottu *et al*., 2005; Pardo *et al*., 2008).

The presence of titanium and niobium in the 444 stainless steel could be contributing to its outstanding pitting and crevice resistance as compared with 316 stainless steels. Titanium and niobium has been reported to be effective alloying elements for improving the corrosion resistance of ferritic stainless steel (Abdel *et al*., 2006; Van Warmelo *et al*., 2007). The effectiveness of niobium and titanium on improving the corrosion resistance of ferritic steel were attributed to their ferrite stabilization effects (Mantel, 2000; Van Warmelo *et al*., 2007). According to Alonso-Falleiros and Wolynec (1998), they could act as stabilizing elements of carbon and nitrogen, by forming carbides and nitrites preferentially to those of chromium, thus avoiding intergranular corrosion.

Considering the austenitic and ferritic nature of 316 and 444, the nickel-chromium-molybdenum balance, the different alloying elements, other mechanical properties, their production cost, etc, a need for a comparative study of their corrosion properties in various acidic media applications is very imperative.

1.3 AIM AND OBJECTIVES

The primary aim of this research work is to compare the general corrosion behavior of 444 ferritic stainless steel with that of 316 austenitic stainless steel and to determine the suitability of 444 in environments where 316 is typically and mostly applied. The aim could be achieve through the following objectives:

- To study and compare the electrochemical behavior of 444 ferritic and 316 austenitic stainless steels in HCl, H_2SO_4 and $H_2SO_4 + Cl^-$
- Investigate the types and stability of various passive films formed in different media.

1.4 RESEARCH QUESTIONS

- How will alloys 316 and 444 behave in similar and different environments?
- Will these alloys passivate in the similar manner in similar environments?
- What type(s) of passive films will form on these alloys in chloride, sulphate, and chloride-sulphate environments?
- How stable will the different passive films be?

1.5 HYPOTHESIS

The Cr-Mo-Nb-Ti ferritic stainless steel type 444 has been reported to have similar or even superior pitting and crevice corrosion to the austenitic type 316 Cr-Ni-Mo stainless steel. Therefore it can be deduced that the same is true for general corrosion.

1.6 SCOPE OF STUDY

In order to compare the general corrosion resistance of 444 ferritic stainless steel with that of 316 austenitic stainless steel in environments where 316 finds industrial applications, this study will involve: weight loss tests, electrochemical measurements (open circuit potential measurement, cyclic potentiodynamic polarization scans and chronoamperometry), scanning electron microscopy, Raman spectroscopy and X-ray diffraction analysis.

1.7 EXPECTED CONTRIBUTION TO KNOWLEDGE

The research study on the comparison of corrosion behaviour of 444 ferritic and 316 austenitic stainless steels in acidic chloride media is expected to provide information on:

- The comparative corrosion behavior of 444 and 316 stainless steel in chloride, sulphate and in both media.
- The types of passive films formed by 316 and 444 stainless steels in these media
- The behavior of different types of passive films formed by the alloys.

1.8 STRUCTURE OF THE DISSERTAION

To achieve the objectives of this study, a literature review of the basic concepts on the previous and on-going work was carried out in **Chapter Two** where the general corrosion behaviour of stainless steels, passivity of stainless steels as well as the effect of alloying elements was outlined. **Chapter Three** gives a presentation of the materials, equipment used in the research, and experimental methodology adopted for achieving the set objectives of this research. These included weight loss tests, electrochemical measurements (open circuit potential measurement, cyclic potentiodynamic polarization scans and chronoamperometry), Scanning Electron Microscopy (SEM), Optical Microscopy, Raman spectroscopy and X-ray Diffractometry analysis. Detailed results of the as-received materials which were characterized based on the material composition and microstructures, the investigations on the corrosion behaviour of 444 ferritic and 316 austenitic stainless steels in acidic chloride media and the corrosion products characterization are given in **Chapter Four, Chapter Five and Chapter Six.** The conclusion and recommendations for future work are presented in **Chapter Seven** and lastly, a list of references is given.

CHAPTER TWO

2.0 LITERATURE REVIEW

2.1 INTRODUCTION TO STAINLESS STEEL

Stainless steel was discovered more or less around 1913 by researchers in Britain and Germany (Beddoes and Parr, 1999; Karlsson, 2004). In Britain, Harry Brearley of Sheffield found that steel that had been alloyed with a sufficiently high level of chromium was not susceptible to attack from etching acids or moisture. According to Karlsson (2004), the first true stainless steel was melted on the 13th August 1913, in Sheffield, on the initiative of Harry Brearley. This first stainless steel was martensitic with 0.24% carbon and 12.8% chromium. Within a year of Brearley's discovery, Strauss & Maurer in Germany developed the first austenitic grades while experimenting with nickel additions.

Almost simultaneously, Dansitzen in the United States, who studied alloys similar to those that Brearley was investigating, but with lower carbon contents, discovered the ferritic stainless steels. From these inventions, just before World War 1, the martensitic, ferritic and austenitic stainless steel groups were developed. Beddoes and Parr (1999) mentioned that the first chromium alloy steel produced in Sweden was in 1924 and the first 18-8 (18% chromium, 8% nickel) austenitic grade was introduced the following year. While Brearley is given credit by most for the invention of stainless steel, French scientist Leon Gillet had documented the constitution of stainless steel already in 1904. Although Gillet noted the composition and properties of his alloy mix, he never recognized the corrosive resistance of the material. In 1911 Philip Monnartz of Germany published the first detailed work on the corrosion resistance of stainless steel. In 1912, two Germans at the Krupp Iron Works, Eduard Maurer and Benno Strauss, patented the first austenitic stainless steel with a 21% chromium and 7% nickel combination. Brearley patented the first martensitic stainless in 1913 (Beddoes and Gordon, 1999).

Stainless steel is a light material with a specific stiffness equal to that of light alloys; high strength grades provide a unique combination of strength, fatigue resistance, ease of forming, and ease of joining (Nethercot and Gardener, 2002). Stainless steels normally have excellent corrosion resistance in oxidizing acid media, but they are

very prone to corrosion in reducing acids such as HCl and H_2SO_4. It is well known that the corrosion resistance of virtually all stainless steels against non-oxidizing acids can be remarkably increased by alloying with nobler metals (Varga *et al*., 1997). The stainless character occurs when the concentration of chromium exceeds about 12 wt%. However, even this is not adequate to resist corrosion in acids such as HCl or H_2SO_4; higher chromium concentrations and the judicious use of other alloying elements such as molybdenum, nickel and nitrogen is then needed to ensure a robust material.

Properties of stainless steel include structural efficiency, corrosion resistance, easy maintenance, high ductility, high cryogenic toughness, and high work hardening rate, improved fire resistance, as well as a pleasing appearance. Increasing competitive prices could add to its advantages over other forms of steels. According to Nethercot and Gardener (2002), the excellent corrosion resistance of stainless steel in many atmosphere result from its ability to protect itself from its environment by forming a thin passive film on the surface which gives it a pleasing and aesthetic appearance. Stainless steels may be grouped into families based on their metallurgical microstructure. The microstructure may be composed of the stable phases of austenite or ferrite, a "duplex" mix of these two, martensite or a hardened structure containing precipitated micro-constituents (Leffler, 2005).

The effect of alloying elements on the formation of austenite and ferrite have been widely studied (Lula, 1986). The illustration shown in Figure 2.1 has been developed to show the maximum amount of ferrite (F), austenite (A) and martensite (M) that can be expected in the microstructure of stainless steels at room temperature in nickel and chromium equivalents (Peckner and Bernstein, 1977; Lula, 1986). The chromium and nickel equivalents have been determined with the most common ferrite and austenite forming elements as given in Equations 1 and 2 respectively.

Chromium equivalents = %Cr + 2 (%Si) + 1.5 (%Mo) + 5 (%V) + 5.5 (%Al) + 1.75 (%Nb) + 1.5 (%Ti) + 0.75 (%W) ..... (1)

Nickel equivalents = % Ni +% Co + 0.5 (%Mn) + 0.3 (%Cu) + 30 (% C) +25 (% N) …… (2)

The values in equations 1 and 2 above are in weight percentage. The austenite forming elements contribute towards the nickel equivalents while the ferrite forming elements contribute towards the chromium equivalents (Peckner and Bernstein, 1977).

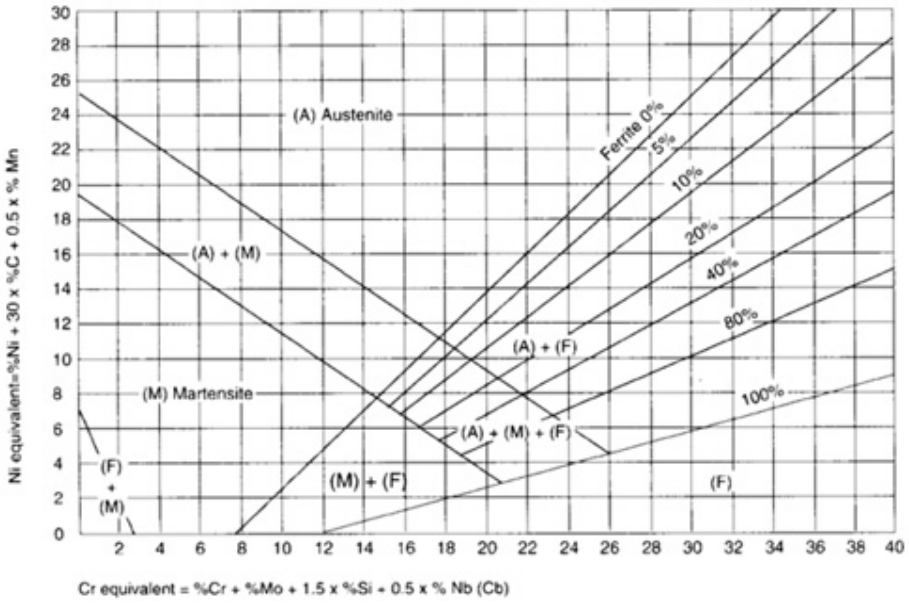

Figure 2.1: Schaeffler diagram *(Schaeffler , 1949).*

Several works had been published on the corrosion behavior of various types of stainless steels; the corrosion behavior of ferritic stainless steels has mainly been studied in aqueous solutions of inorganic acids or salts (Sekine *et al.,* 1991). The comparative study of surface properties of austenitic stainless steels in sulfuric and hydrochloric acid solutions was described by Varga *et al.* in 1997, corrosion resistance of dissimilar welds between ferritic stainless steel with high corrosion resistance and austenitic stainless steels (using types 304, 316 and 444 as the specimen) by Jun'ichi *et al.* (2001), and the effect of manganese, nitrogen and molybdenum on the corrosion resistance of a low nickel (<2wt%) austenitic stainless steels (201 and 304) by Muwila (2006). Likewise, Davies (1983) conducted a study on the effect of vanadium and other elements on the mechanical properties and corrosion resistance of ferritic stainless steels (444 and 316 included) in H_2SO_4, $FeCl_3$ and NaCl, while the electrochemical formation of highly pitting resistant passive films on a biomedical grade 316LVM stainless steel surface is described in another study by Shahryari *et al.* (2008). Asami and Hashimoto (2003) also studied the importance

of initial surface film in the degradation of stainless steels (444 and 316 included) by atmospheric exposure. Takada *et al.* (2007) examined the corrosion behavior of those types of stainless steel composing the dental magnetic attachments, and also investigated the galvanic corrosion of the stainless steels when in contact with the dental precious alloys for root caps in 0.9% NaCl at 37^{o}C.

Sekine *et al.* (1987a and 1987b) studied the corrosion behavior of ferritic 430 and 444 stainless steels in formic and acetic acids, paying attention to the concentration and temperature of acids. Sekine and Okano (1989) as well as Sekine *et al.* (1990), reported the corrosion of ferritic stainless steels in oxalic acids and discussed the mechanism of corrosion and the relationship between corrosion and stability of metal complexes formed. Sekine *et al.* (1990) also reviewed the factors affecting corrosion of steels in various organic solvents and later in 1991 studied the corrosion behavior of various ferritic stainless steels, namely types 410L, 430, 434, 444 and XM27 in boiling acetic acid solutions. So far, no literature could be found on a comparison of the corrosion behaviour of 444 ferritic and 316 austenitic stainless steels in acidic chloride media.

2.1.1 Austenitic stainless steels

Austenitic, or non-magnetic stainless steels, are classified in the 200 and 300 series of which 304 is the most common (Kotecki and Armao, 2003; Schweitzer, 2006). Their chromium composition varies from 16% to 30% and 2% to 20% nickel for enhanced surface quality, formability and increased corrosion and wear resistance, and they are non- hardenable by heat treatment (Ak Steel, 2008). Austenitic stainless steels are the most popular grades of stainless produced due to their excellent formability and corrosion resistance. All austenitic steels are non-magnetic in the annealed condition. (Depending on the composition, mainly the nickel content, austenitics do become slightly magnetic when cold worked).

Austenitic stainless steel grades include: Type 201, Nitronic 30, 301, 304, 305, 309S, 316, 316L, and 321(Schweitzer, 2006). These types of stainless steel find applications in automotive trim, cookware, food and beverage equipment, processing equipment, architectural applications such as roofing and cladding, roofing and gutters, doors and

windows, balustrades, benches, heat exchangers, ovens and chemical tanks and a variety of industrial applications(Aalco, 2004; Ak Steel, 2008).

By adding elements such as molybdenum, titanium or copper, the properties of these steels can be modified. The principal alloying elements are sometimes reflected in the name of the steel. Austenitic stainless steels were developed for use in both mild and severe corrosive conditions. According to Pardo *et al*. (2008), the high corrosion resistance of these steels is primarily due to the oxide layer formed on its surface. Many studies have revealed that the passive films formed on austenitic stainless steels, exposed to aqueous solutions, are a mixture of iron and chromium oxides with hydroxides and water-containing compounds in the outermost region of the film and chromium oxide at the metal–film interface (Marcus and Olefjord, 1988; Haupt and Strehblow, 1995; Maurice *et al*., 1996; Abreu *et al*., 2004). Schweitzer (2006) observed that the passive film formed on austenitic stainless steel could be duplex in nature consisting of an inner barrier oxide film and outer deposit of hydroxide or salt film. Table 2.1 shows nominal compositions of austenitic stainless steels.

Table 2.1: Nominal compositions of austenitic stainless steels *(Kotecki and Armao, 2003).*

Type	UNS Number	Composition - Percent *							Other
		C	Mn	Si	Cr	Ni	P	S	
201	S20100	0.15	5.5-7.5	1.00	16.0-18.0	3.5-5.5	0.06	0.03	0.25 N
202	S20200	0.15	7.5-10.0	1.00	17.0-19.0	4.0-6.0	0.06	0.03	0.25 N
205	S20500	0.12-0.25	14.0-15.5	1.00	16.5-18.0	1.0-1.75	0.06	0.03	0.32-0.40 N
216	S21600	0.08	7.5-9.0	1.00	17.5-22.0	5.0-7.0	0.045	0.03	2.0-3.0 Mo; 0.25-0.5 N
301	S30100	0.15	2.00	1.00	16.0-18.0	6.0-8.0	0.045	0.03	
302	S30200	0.15	2.00	1.00	17.0-19.0	8.0-10.0	0.045	0.03	
302B	S30215	0.15	2.00	2.0-3.0	17.0-19.0	8.0-10.0	0.045	0.03	
303**	S30300	0.15	2.00	1.00	17.0-19.0	8.0-10.0	0.20	0.15 min.	0.6 Mo
303Se**	S30323	0.15	2.00	1.00	17.0-19.0	8.0-10.0	0.20	0.06	0.15 min. Se
304	S30400	0.08	2.00	1.00	18.0-20.0	8.0-10.5	0.045	0.03	
304H	S30409	0.04-0.10	2.00	1.00	18.0-20.0	8.0-10.5	0.045	0.03	
304L	S30403	0.03	2.00	1.00	18.0-20.0	8.0-12.0	0.045	0.03	
304LN	S30453	0.03	2.00	1.00	18.0-20.0	8.0-10.5	0.045	0.03	0.10-0.15 N
S30430	S30430	0.08	2.00	1.00	17.0-19.0	8.0-10.0	0.045	0.03	3.0-4.0 Cu
304N	S30451	0.08	2.00	1.00	18.0-20.0	8.0-10.5	0.045	0.03	0.10-0.16 N
304HN	S30452	0.04-0.10	2.00	1.00	18.0-20.0	8.0-10.5	0.045	0.03	0.10-0.16 N
305	S30500	0.12	2.00	1.00	17.0-19.0	10.5-13.0	0.045	0.03	
308	S30800	0.08	2.00	1.00	19.0-21.0	10.0-12.0	0.045	0.03	
308L		0.03	2.00	1.00	19.0-21.0	10.0-12.0	0.045	0.03	
309	S30900	0.20	2.00	1.00	22.0-24.0	12.0-15.0	0.045	0.03	
309S	S30908	0.08	2.00	1.00	22.0-24.0	12.0-15.0	0.045	0.03	
309S Cb	S30940	0.08	2.00	1.00	22.0-24.0	12.0-15.0	0.045	0.03	8 x %C - Nb(Cb)
309 Cb + Ta		0.08	2.00	1.00	22.0-24.0	12.0-15.0	0.045	0.03	8 x %C (Nb(Cb) + Ta)
310	S31000	0.25	2.00	1.50	24.0-26.0	19.0-22.0	0.045	0.03	
310S	S31008	0.08	2.00	1.50	24.0-26.0	19.0-22.0	0.045	0.03	
312		0.15	2.00	1.00	30.0 nom.	9.0 nom.	0.045	0.03	
254SMo	S31254	0.020	1.00	0.80	19.5-20.5	17.50-18.5	0.03	0.010	6.00-6.50Mo; 0.18-0.22N; Cu=0.5-1.00
314	S31400	0.25	2.00	1.5-3.0	23.0-26.0	19.0-22.0	0.045	0.03	
316	S31600	0.08	2.00	1.00	16.0-18.0	10.0-14.0	0.045	0.03	2.0-3.0 Mo
316F**	S31620	0.08	2.00	1.00	16.0-18.0	10.0-14.0	0.20	0.10 min.	1.75-2.5 Mo
316H	S31609	0.04-0.10	2.00	1.00	16.0-18.0	10.0-14.0	0.045	0.03	2.0-3.0 Mo
316L	S31603	0.03	2.00	1.00	16.0-18.0	10.0-14.0	0.045	0.03	2.0-3.0 Mo
316LN	S31653	0.03	2.00	1.00	16.0-18.0	10.0-14.0	0.045	0.03	2.0-3.0 Mo; 0.10-0.30 N
316N	S31651	0.08	2.00	1.00	16.0-18.0	10.0-14.0	0.045	0.03	2.0-3.0 Mo; 0.10-0.16 N
317	S31700	0.08	2.00	1.00	18.0-20.0	11.0-15.0	0.045	0.03	3.0-4.0 Mo
317L	S31703	0.03	2.00	1.00	18.0-20.0	11.0-15.0	0.045	0.03	3.0-4.0 Mo
317M	S31725	0.03	2.00	1.00	18.0-20.0	12.0-16.0	0.045	0.03	4.0-5.0 Mo
321	S32100	0.08	2.00	1.00	17.0-19.0	9.0-12.0	0.045	0.03	5 x %C min. Ti
321H	S32109	0.04-0.10	2.00	1.00	17.0-19.0	9.0-12.0	0.045	0.03	5 x %C min. Ti
329	S32900	0.10	2.00	1.00	25.0-30.0	3.0-6.0	0.045	0.03	1.0-2.0 Mo
330	N08330	0.08	2.00	0.75-1.5	17.0-20.0	34.0-37.0	0.04	0.03	
AL6-XN	N80367	0.030	2.00	1.00	20.0-22.0	23.5-25.5	0.04	0.03	6.00-7.00Mo; 0.18-0.25N; Cu=0.75
330HC		0.40	1.50	1.25	19.0 nom.	35.0 nom.			
332		0.04	1.00	0.50	21.5 nom.	32.0 nom.	0.045	0.03	
347	S34700	0.08	2.00	1.00	17.0-19.0	9.0-13.0	0.045	0.03	10 x %C min. Nb(Cb) +Ta
347H	S34709	0.04-0.10	2.00	1.00	17.0-19.0	9.0-13.0	0.045	0.03	10 x %C min. Nb(Cb) + Ta
348	S34800	0.08	2.00	1.00	17.0-19.0	9.0-13.0	0.045	0.03	0.2 Cu; 10 x %C min. Nb(Cb) + Ta(c)
348H	S34809	0.04-0.10	2.00	1.00	17.0-19.0	9.0-13.0	0.045	0.03	0.2 Cu; 10 x %C min. Nb(Cb) + Ta
384	S38400	0.08	2.00	1.00	15.0-17.0	17.0-19.0	0.045	0.03	
Nitronic 32	S24100	0.10	12.0	0.50	18.0	1.6			0.35 N
Nitronic 33	S24000	0.06	13.0	0.5	18.0	3.0			0.30 N
Nitronic 40	S21900	0.08	8.0-10.0	1.00	18.0-20.0	5.0-7.0	0.06	0.03	0.15-0.40 N
Nitronic 50	S20910	0.06	4.0-6.0	1.00	20.5-23.5	11.5-13.5	0.04	0.03	1.5-3.0 Mo; 0.2-0.4 N; 0.1-0.3 Cb; 0.1-0.3 V
Nitronic 60	S21800	0.10	7.0-9.0	3.5-4.5	16.0-18.0	8.0-9.0	0.04	0.03	1.5-3.0 Mo; 0.2-0.4 N;

Type 316 is an austenitic chromium nickel stainless steel containing molybdenum, and has a density of 7.99 g/cm^3 (Allegheny Ludlum, 1999). The addition of molybdenum increases its general corrosion resistance, improves its resistance to pitting from chloride ion solutions, and provides increased strength at elevated temperatures (Davis, 1994; Jargelius-Petterson and Pound, 1998; Pardo *et al*., 2008). According to AK Steel (2007b), its properties are similar to those of type 304 except that this alloy is somewhat stronger at elevated temperatures. Its corrosion resistance is improved, particularly against sulfuric, hydrochloric, acetic, formic and tartaric acids; acid sulfates and alkaline chlorides. The corrosion behavior of 316 stainless steel in both dilute HCl solution and SO_4^{2-} containing dilute HCl solution are similar, and SO_4^{2-} ions could have some inhibitive effect on the corrosion (Li *et al*., 2003).

2.1.2 Ferritic stainless steels

Ferritic stainless steels contain a minimum of 10.5% and a maximum of 30% chromium (Kotecki and Armao, 2003). This group of steels includes the more common types 405, 409, 430, 442 and 446 (Kotecki and Armao, 2003; Schweitzer, 2006; Gilet, 1998). According to Gilet (1998), well-known standard ferritic grades 409, 410 and 430 are readily available all over the world. They have broad application potential in numerous fields and are very successful and important in applications including washing-machine drums, automotive exhaust systems, automotive trim, computer floppy disk hubs, material handling equipment etc. More recently-developed ferritic grades, such as 439 and 441 meet an even broader range of requirements. They can be formed to more complex shapes and joined using most conventional joining methods, including welding.

Ferritic stainless steels display a high corrosion resistance in many environments (Truman and Crawshaw, 1968; Dundas and Bond, 1978). However, when these steels are cooled from the temperature range 900°C - 1150°C, the high diffusion rate of carbon and nitrogen in these alloys could induce a fast intergranular precipitation of chromium carbides and nitrides, making them susceptible to intergranular corrosion (Dundas and Bond, 1978). An alternative to prevent this is to add a stabilizing element of carbon and nitrogen, such as niobium or titanium, which forms carbides and nitrites preferentially to those of chromium, thereby improving its resistance to intergranular corrosion (Demo, 1977; Van Warmelo *et al*., 2007).

The concept of ferritic stainless steels was rapidly established in the 1920s, but the compositions manufactured were generally used only in heat-resisting applications (Cortie, 1993). An advantage that the ferritics enjoy over the austenitic grades is a virtual immunity to chloride-induced stress corrosion cracking, thus making them, for example, the super-ferritic alloys, a material of choice for desalination plants and cooling circuits of coastal power stations (Armitage, 1985). Type 444 is a material of choice for moderately corrosive applications where the austenitics exhibit stress-corrosion cracking (Redmond, 1984). Other advantages include their lower price, the stable pricing structure which could be due to them not containing substantial amounts of nickel, which is an expensive element whose price fluctuates according to its availability on world markets and economic factors influencing trading conditions, their easier machinability, and their better deep-drawing properties (Cortie, 1993). Table 2.2 below shows nominal compositions of ferritic stainless steels.

Table 2.2: Nominal compositions of ferritic stainless steels *(Kotecki and Armao, 2003).*

Type	UNS Number	Composition - Percent *							Other
		C	Mn	Si	Cr	Ni	P	S	
405	S40500	0.08	1.00	1.00	11.5-14.5		0.04	0.03	0.10-0.30 Al
409	S40900	0.08	1.00	1.00	10.5-11.75		0.045	0.045	6 x %C min. Ti
429	S42900	0.12	1.00	1.00	14.0-16.0		0.04	0.03	
430	S43000	0.12	1.00	1.00	16.0-18.0		0.04	0.03	
430F**	S43020	0.12	1.25	1.00	16.0-18.0		0.06	0.15 min.	0.06 Mo
430FSe**	S43023	0.12	1.25	1.00	16.0-18.0		0.06	0.06	0.15 min. Se
430Ti	S43036	0.10	1.00	1.00	16.0-19.5	0.75	0.04	0.03	5 x %C - Ti min.
434	S43400	0.12	1.00	1.00	16.0-18.0		0.04	0.03	0.75-1.25 Mo
436	S43600	0.12	1.00	1.00	16.0-18.0		0.04	0.03	0.75-1.25 Mo; 5 x %C min. Nb(Cb) + Ta
442	S44200	0.20	1.00	1.00	18.0-23.0		0.04	0.03	
444	S44400	0.025	1.00	1.00	17.5-19.5	1.00	0.04	0.03	1.75-2.5 Mo, 0.035 N 0.2 + 4 (%C + %N); (Ti +Nb(Cb))
446	S44600	0.20	1.50	1.00	23.0-27.0		0.04	0.03	0.25 N
18-2FM**	S18200	0.08	2.50	1.00	17.5-19.5		0.04	0.15 min.	
18SR		0.04	0.3	1.00	18.0				2.0 Al; 0.4 Ti
26-1 (E-Brite)	S44625	0.01	0.40	0.40	25.0-27.5	0.50	0.02	0.02	0.75-1.5 Mo; 0.015N; 0.2 Cu; 0.5 (Ni+Cu)
26-1Ti	S44626	0.06	0.75	0.75	25.0-27.0	0.5	0.04	0.02	0.75-1.5 Mo; 0.04 N; 0.2 Cu; 0.2-1.0 Ti
29-4	S44700	0.01	0.30	0.20	28.0-30.0	0.15	0.025	0.02	3.5-4.2 Mo
29-4-2	S44800	0.01	0.30	0.20	28.0-30.0	2.0-2.5	0.025	0.02	3.5-4.2 Mo
Monit	S44635	0.25	1.00	0.75	24.5-26.0	3.5-4.5	0.04	0.03	3.5-4.5 Mo; 0.3-0.6 (Ti + Nb(Cb))
Sea-cure/ Sc-1	S44660	0.025	1.00	0.75	25.0-27.0	1.5-3.5	0.04	0.03	2.5-3.5 Mo; 0.2 + 4 (%C + %N) (Ti + Nb(Cb))

The type 444 is a low-carbon, low nitrogen, ferritic stainless steel that provides pitting and crevice corrosion resistance superior to most ferritic stainless steels (AK Steel, 2007a). Every application requiring superior corrosion resistance and resistance to

chloride stress corrosion cracking is ideal for this alloy. Current uses include food processing, brewery and wine-making equipment; hot-water tanks, heat exchanger tubing and automotive components (AK Steel, 2007a). The type 444 ferritic stainless steel has received attention as a potential material for use in medicine, because it does not contain much nickel (Chiba *et al*., 1997). Type 444 relies on a passive film to resist corrosion, but exhibits rather high corrosion rates when activated. It is resistance to very dilute H_2SO_4 at boiling temperature but corrodes rapidly at higher concentrations (Schweitzer, 2006). According to Schweitzer (2006), the corrosion resistance of 444 is generally considered equal to that of type 304. Its corrosion resistance to localized corrosion is at least equal to that of austenitic grade 316 (Gilet, 1998). According to Dowling *et al.* (1999), corrosion studies on a welded 444 stainless steel demonstrated that dual stabilization with low individual concentrations of titanium and niobium may possibly provide optimum corrosion resistance.

Type 444 ferritic stainless steel when immersed in a non-aqueous solution is liable to corrode without forming the stable passive film composed mostly of chromic ions as cations, since under de-aerated conditions the oxygen source for formation of the passive film is only water. Hence in the non-aqueous solution, the stable passive film cannot be formed because of a deficiency in the oxygen source (Sekine *et al.,* 1991). Type 444 ferritic stainless steel when immersed in a non-aqueous solution is liable to corrode without forming the stable passive film composing mostly of chromic ion as cations. Under de-aerated conditions the oxygen source for formation of the passive film is only water. Hence in the non-aqueous solution, the stable passive film cannot be formed because of a deficiency in the oxygen source (Sekine *et al.,* 1991). Type 444 stainless steel corrodes more in the non-aqueous solution in comparison with in aqueous solutions. According to Sekine *et al.* (1991), corrosion of type 444 ferritic stainless steel would not be severe in aqueous acetic acid solution because the passivity of stainless steel could be enhanced with increasing chromium and molybdenum content as compared to 410L, 430, 434, and XM27.

2.2 CORROSION BEHAVIOR OF STAINLESS STEELS

2.2.1 General corrosion behavior

The general electrochemical behavior of stainless steels can be described by a polarization curve. A hypothetical polarization curve of stainless steel showing active-

passive behavior (Curve 1) and a pseudo-passive behavior (Curve 2) is presented in Figure 2.2. It shows that stainless steels corrode in the active region, which exists at potentials below the passivation potential (E_{pp}). In the active-passive region represented by AB for a passivating system, current increases with potential until the passivation potential, E_{pp}, is reached. When the maximum current, i.e. the critical current density (i_{crit}) is reached, the current density drops to a very low value, called the passive current density ($i_{passive}$), and the passivation (formation of the protective film Cr_2O_3 layer) is initiated. i_{crit} represents the point of maximum anodic dissolution. During passivation the metal still corrodes but at a significantly lower rate. If the potential is increased even more, then a passive-transpassive transition is observed at the transpassive potential, $E_{transpassive}$ or $E_{pit.}$ When the transpassive region is reached, the metal starts to corrode at a high rate again. In the pseudo-passive system, the current does not decrease with increasing potential, but increases beyond point B to C where the current remains constant or increases only slightly. Usually it is difficult to define unambiguously the values for i_{crit}, E_{pp}, and $E_{transpassive}$ from this behavior.

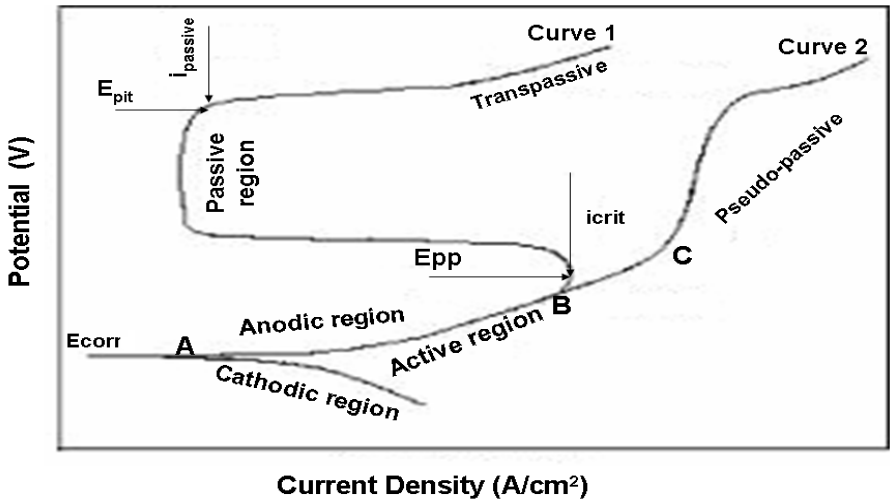

Figure 2.2: Hypothetical polarization curve of stainless steel showing active-passive behavior (Curve 1) and a pseudo-passive behavior (Curve 2) *(Viramontes-Gamboa et al., 2007).*

The potential value of E_{pit} depends on the corrodent. In chloride free aqueous sulphuric acid solution E_{pit} represents the point of oxygen evolution by the electrolysis of water and is called E_t (representing the beginning of transpassive behavior). In

chloride solutions, however, this point represents the breakdown of the passive film due to pit formation and is called E_{pit}. E_{corr} is the corrosion potential and is the point at which the total rate of all the anodic reactions equals the rate of all the cathodic reactions. The current density at E_{corr} is called the corrosion current density, i_{corr} which is a measure of corrosion rate since it is directly proportional to metal dissolution (Peckner and Berstein, 1977; Jones, 1996). The value of i_{corr} cannot be measured directly, but with the use of a counter electrode, reference electrode and a potentiostat, it can be determined (Jones, 1996). The corrosion rate can be determined by using Tafel extrapolation or polarization resistance.

The excellent corrosion resistance of stainless steels has been attributed to their ability to form very thin and stable oxide film of chromium oxide (Cr_2O_3) which protects them against most corrosive environments (Peckner and Bernstein, 1977; Sedriks, 1986). Hashimoto *et al*. (1979b) reported that Cr-O-OH could be formed in place of chromium oxide, which has better protective properties than the chromium oxide.

2.2.2 Pitting corrosion

Stainless steels depend on passive films for corrosion resistance. Unfortunately, they can suffer dangerous localized corrosion in the form of pitting and crevice corrosion when local breakdown of the protective passive film occurs under particular structural and environmental conditions (Cvijović and Radenković, 2006). This makes localized corrosion resistance a very crucial and important factor in stainless steel applications. The most significant environmental condition which influences the pitting corrosion behavior of stainless steels is the chloride ion concentration (Fielder and Johns, 1989). According to Siow *et al*. (2001), the main factor influencing the pitting resistance of stainless steels in halide solutions is the composition and the alloying elements.

A theoretical way of comparing the pitting corrosion resistance of various types of stainless steels, based on their chemical compositions, is the "Pitting Resistance Equivalent Number (PREN)". The PREN is useful for ranking and comparing the different grades. Actual or specified range compositions can be used and usually involve chromium, molybdenum and nitrogen in the calculations (British Stainless Steel Association, 2007). The PREN typically takes the form.

PREN = Cr + m Mo + n N

Where 'm' and 'n' are the factors for molybdenum and nitrogen

These are 'linear' formulas, where the molybdenum and nitrogen levels are 'weighted' to take account of their strong influence on pitting corrosion resistance. The most commonly used version of the formula is

PREN = Cr + 3.3Mo + 16N

Some formulas weigh nitrogen more, with factors of 27 or 30. As the actual nitrogen levels are quite modest in most stainless steels, and this does not have a dramatic effect on ranking. Tungsten is also included in the molybdenum-rating factor to acknowledge its effect on pitting resistance in the tungsten bearing super-duplex types (1.4501).

A modified formula is then used:

PREN = Cr + 3.3(Mo +0.5W) + 16N

Hence, attempts are continually being made to enhance the performance of stainless steel by designing grades with higher PRE values. Many studies appear to have been carried out to document the magnitude of the improvement in pitting corrosion resistance resulting from chromium, molybdenum and nitrogen additions (Cvijović and Radenković, 2006). According to the report given by the British Stainless Steel Association (2007), nitrogen ranges are not specified in standards such as BS EN 10088-1 for all but specific grades, such as 1.4311 (304LN) and 1.4406 (316LN) austenitics. Grades with a PREN of 40 or more are known as 'super' austenitic or 'super' duplex types; depending on which basic family they belong to. Nickel content is not considered in the formula, since in most applications it plays no role in resistance to pitting corrosion (Gilet, 1998).

2.2.3 Crevice corrosion

Crevice corrosion occurs as the name implies, in any confined spaces caused by component design or joints. In environments containing chlorides, crevices such as those found at flange joints are therefore the most critical places for corrosion

(Pickering, 1989; Nilsson, 2006). The influence of capillary forces in narrow crevices is significant and it is thus almost impossible to avoid the penetration of liquid into a crevice (Cunat, 2002). Oxygen and other oxidants are consumed for the maintenance of the passive layer in the crevice just as at the unshielded surface. The supply of new oxidants is restricted in the stagnant solution inside the crevices and the transportation of oxygen to the crevice is limited (Rosenfeld and Danilov, 1967). This restricts the reaction with oxygen while the dissolving of the metal continues and leads to an excess of metal ions in the crevice. These small amounts of dissolved metal ions and the migration of chloride ions into the crevice cause a decrease of the solution's pH inside the crevice (Pickering, 1989). Crevice corrosion may in some cases look similar to pitting corrosion but are usually wider and often similar in shape to the crevice former due to the larger anodic area (Leffler, 2005). Crevice corrosion takes place under similar conditions as pitting corrosion. The resistance of stainless steels to crevice corrosion increases with increasing the contents of chromium, molybdenum and nitrogen (Leffler, 2005).

2.3 CORROSION RESISTANCE OF STAINLESS STEELS

Stainless steels consists primarily of iron, carbon, chromium, nickel and other alloying elements at varying concentrations, depending on the desired applications. Each of the alloying elements has a specific effect on the properties of the stainless steel. The combined effect of all the alloying elements, and to some extent the impurities determines the property profile of different stainless steel grades (Leffler, 2005). A material's properties are strongly dependent on microstructure. Alloying elements affects microstructure, which in turn significantly influences the overall corrosion behavior of the alloy. The effect of the alloying elements differs in some aspects between the hardenable and the non-hardenable stainless steels. Chromium, molybdenum and nitrogen are the alloying elements that increase the resistance of stainless steels to both pitting and crevice corrosion.

2.3.1 Passivity

Several definitions have been given with regard to passivity. Fontana (1986) defined passivity as the loss of chemical reactivity experienced by certain metals and alloys under particular environmental conditions. According to Uhlig and Revie (1985), a

metal is passive if it substantially resists corrosion in a given environment resulting from marked anodic polarization. The passivity phenomenon is extremely important since it is the basic mechanism in the corrosion resistance of stainless steels, and involves the formation in fine barrier layer on alloy surface of the order of 1.0 to 2.0 nm thick, which reduces the corrosion rate to negligible levels (Cunat, 2002). Alloys which usually exhibit passivity include nickel, chromium, titanium, and iron in oxidizing environments, stainless steels and numerous others. Passivity affects the kinetics of the corrosion process because it produces a passive film that acts as a barrier to attack of the metal surface by the environment. Passivation reduces the corrosion rate of stainless steels. The passive layer or film adheres strongly to the metal substrate and prevents virtually all contact between the alloy and the surrounding medium (Cunat, 2002).

The passive films of stainless steels are very thin, being 1-5 nm thick, and are generally described as hydrous oxides, which are mostly enriched primarily with chromium, silicon, and molybdenum and are naturally free of pores (Wallen and Olsson,1977; Davies,1983). The nature of passive film formed on stainless steels depends on the underlying metal, and will have different properties in areas where the surface is homogeneous. Furthermore, the type of film varies according the potential applied (Davies, 1983). For passivation to occur and remain stable there is a threshold chromium content above which passivity can occur and below which it is impossible. According to Cunat (2002), the Fe-Cr alloy must have a minimum chromium content of about 11 weight per cent, and passivity increases fairly rapidly with increasing chromium content up to about 17%.

2.3.2 Passivity breakdown

The stability of passive films may be weakened considerably locally. The breakdown processes are brought about by the chemical alteration of the passive film or the environment so that the film becomes unable to effectively prevent destructive local attack (Kruger and Rhyme, 1982). Breakdown of passivity either due to mechanical damage or due to chemical attack often leads to localized corrosion in the form of pitting corrosion, crevice corrosion and stress corrosion cracking (Hoar and Jacob, 1967; Qui, 1998; Qiu, 2002). Chloride ions can be a problem because of their specific effect, which can lead to pitting corrosion. For a given system defined by an alloy

composition, microstructure, surface condition, and specific corrosion medium at a given temperature, pitting may appear above a certain potential that is effective for evaluating the resistance of stainless steel to pitting corrosion (Cunat, 2002). The breakdown of passivity according to Kruger (2000) initiates the most damaging kinds of corrosion, the localized corrosion, pitting corrosion, crevice corrosion, intergranular and stress corrosion.

2.3.3 Forms of film formed on stainless steels

There are two types of passive film, the primary and the secondary film. The primary film is stable only within a few mV of the primary activation potential; its formation or destruction is a reversible process (Davies, 1983). The thickness of the primary film at the primary activation potential is less than the equivalent of one atom to each surface metal atom. The secondary film which is formed slowly at more positive potentials grows to a thickness greater than 1 nm and with increasing potential and sufficient time it becomes very resistant to reduction (Davies, 1983). The passive film has been analysed by Auger and X-ray photoelectron spectroscopy in an examination by Lumsden and Staehle (1972) on molybdenum containing ferritic stainless steels in H_2SO_4, NaCl, and NaOH. It shows that the improve corrosion resistance obtained by the addition of molybdenum could not be explained by its enrichment in the protective film.

2.3.4 Stability of passive films form on stainless steels

The stability of passive films plays a vital role in the pitting corrosion resistance of stainless steels and passive alloys. The stability of passivation depends on the predominant cathodic process (hydrogen evolution, reduction of oxygen and reduction of metal ions). Fast and effective repassivation of locally activated metal surfaces only occurs if a stable passive film is formed (Bohni, 2000). Understanding the stability of passive films with respect to localized corrosion, requires knowledge of the behavior of naturally grown as well as synthetic prepared thin oxide films (Sugimoto *et al*. 1993; Tanaka *et al*., 1995). According to Pyun and Oriani (1989), hydrogen may enter into the passivating oxide film as a proton due to the ionic bonding character of the passive film and changes the electrochemical properties of passive film i.e the average valence state of the cations in the passive film. Hydrogen

may also change the electric structure, and increase the dielectric constant and capacitance of passive film (Li *et al*., 2003).

In some electrolytic solutions, generally those containing halogen ions such as chlorides, the stability of the passive film may be considerably reduced (Davies, 1983). The halogen ions reduce the potential range of the passive region, particularly by lowering the breakdown potential as a result of penetration and destruction of the passive film by the halogen ions. The service reliability of stainless steels and alloys is predominantly determined by the chemical stability of a passive film on their surfaces, and the thickness, composition and structure of such films are all influenced by the alloy composition and the nature of the environments they are exposed to (Qui, 2002). The protective passive film is never completely perfect but always contains microscopic defects, which usually do not affect the corrosion resistance. However, if there are halogenides such as chlorides present in the environment, these can break down the passive film locally and prevent the reformation of a new film (Leffler, 2005). A surface analysis study on passive films formed on different grades of stainless steels under different conditions by Qui (2002) showed that chromium can be significantly enriched in the surface film whereas nickel may not be present in the oxidized state. Davies (1983) discovered that the passive characteristics of the 18% chromium stainless steels in 1N H_2SO_4 could be little improved by alloying with vanadium.

In order to have a basis for understanding the behavior of the stainless steel (considering two types of stainless steel used for this study) and their different passive films, a brief overview of the important alloying elements and their corresponding effects on the structure and corrosion properties is given below.

2.4 EFFECT OF ALLOYING ELEMENTS ON THE CORROSION RESISTANCE OF STAINLESS STEELS

2.4.1 Effects of chromium on the corrosion resistance of stainless steels

Chromium is the most important alloying element in stainless steels and the element that gives stainless steels their basic corrosion resistance (Leffler, 2005). In most environments, chromium has the ability to form a stable and passive oxide film on the

surfaces of stainless steels that protects it from further corrosion. The effects of chromium on the passivity behavior of iron–chromium alloys (stainless steels) have been widely studied for a long time due to their technological importance. Monypenny (1951) reported that the minimum concentration of chromium needed for passivity depend on the type of acid, its concentration and the temperature of operation. It was noted by Monypenny (1951); Streicher (2000) that an increase in the concentration of chromium required to produce passivity can lead to a reduction in corrosion rate.

Many reports have accredited the high degree of corrosion resistance in Fe–Cr alloy systems to chromium enrichment in surface films (Holliday and Frankenthal, 1972; Okada *et al*., 1975; Olefjord, and Fischmeister, 1975; Asami *et al*., 1976). Besides Fe–Cr alloy systems, it was found that chromium enrichment in surface film is important for the corrosion resistance of alloys containing chromium such as Co–Cr alloys, Nb–Cr alloys, Ta–Cr alloys, Mo–Cr alloys, Ti–Cr alloys etc. (Naka *et al*., 1978; Hashimoto *et al*., 1979b; Kim *et al*., 1993; Park *et al*., 1995; Li *et al*., 1997). According to Leffler (2005), chromium increases the resistance of stainless steels to high temperature oxidation by the formation of a chromia (Cr_2O_3) scale on the metal surface. It was also reported that if the oxide forms a continuous layer on the surface it will stop or slow down the oxidation process and protect the metal. However, chromium contents needed to obtain a continuous protective chromia layer should be above 18%. According to Asami and Hashimoto (2003), the corrosion resistance of chromium containing alloys may be due to the passive films composed primarily of either Cr-oxide or oxyhydroxides, or both.

2.4.2 Effects of nickel on the corrosion resistance of stainless steels

Nickel content could also accelerate the formation of the films, which can be very stable, passive and could increase stainless steel resistance to corrosion. Abreu *et al*. (2006) reported that the presence of nickel promotes the formation of thinner and more protecting passive films. According to Streicher (2000), in both oxidizing and reducing acids, nickel additions may actually increase the corrosion rate of Fe-Cr alloys. Only when the chromium content exceeds 16%, is there a rapid reduction in corrosion. According to Kish *et al*. (2000 and 2004), nickel atoms in the stainless steel could promote the reduction of sulphuric acid molecules in concentrated sulphuric

acid and anodically dissolve with the formation of a nickel sulphide deposit. Nickel could promote the formation of nickel sulphide during the passivation induction stage, which depolarizes the cathodic reduction of undissociated sulphuric acid (through an increase in surface area) to a level that provides the current required to stabilize the passive chromium-rich oxide film. In a chloride environment, nickel could form a stable passive nickel oxide layer (Jiangzhou and Wang, 2001; Singh and Singh, 2002; Abd El Aal, 2003; Munoz *et al*., 2006).

Studies of the effects of nickel on the passivating tendency (Binder, 1946; Chernova and Tomashov, 1965), and the pitting resistance of ferritic stainless steels (Lizlovs and Bond, 1969) indicated that nickel could improve atmospheric corrosion resistance. Chernova and Tomashov (1965) recorded that 0.5% nickel increased the tendency of 25% chromium to become passive in 1N H_2SO_4 at room temperature. Binder (1946) also recorded that nickel increases the tendency of chromium to passivate. According to Lizlovs and Bond (1969), an addition of up to 1% nickel to 18Cr-2Mo-0.03C steels could depress the critical current density in 0.1N HCl to the point where the active region is displayed. An increase in nickel contents from 0.11% to 0.62% could result in complete suppression of the active region, indicating that nickel promotes passivation (Snape, 1977). Nickel could modify the properties of the corresponding passive films formed on the stainless steel surface, and the air formed films could show dielectric behavior with associated resistance value proportional to the nickel content in the alloy (Abreu *et al*., 2006).

2.4.3 Effects of molybdenum on the corrosion resistance of stainless steels

Molybdenum is considered as one of the principal alloying elements in stainless steels and its beneficial effect on corrosion resistance has been most thoroughly investigated. Horvarth and Uhlig (1968) studied the beneficial effect of chromium and molybdenum in stainless steels and reported that pitting potential tends to increase with increase in chromium contents > 20wt%, while molybdenum is effective at minor concentrations of 2-6wt%, but only in the presence of chromium. It was observed (Davis, 1994; Jargelius-Petterson and Pound, 1998) that molybdenum enhances the resistance to pitting corrosion and expands the passive region in sulphuric acid, making types 316 and 317 suitable for 90 wt.% H_2SO_4 at ambient temperature. Explanations with regards to the strong influence of molybdenum on the

pitting resistance of stainless steels (Sakashita and Sato, 1977; Ogawa *et al*., 1978; Hashimoto *et al*., 1979a; Newman, 1985) suggested that molybdenum could be absorbed on the surface as molybdate or acts by blocking active surface sites, inhibiting active metal dissolution and finally repassivate through protective film formation.

Several observations have thus been made to identify the presence and nature of molybdenum as dissolved species, a component of the passive film and/or element in the metallic matrix. Sugimoto and Sawada (1976) observed that a molybdenum addition to austenitic stainless steels allows the formation of a passive film consisting of a solid solution of Mo^{6+} in a chromium oxyhydroxide network, which reduces the corrosion current density in the active region for acidic solutions. However, Ogawa *et al*. (1978) suggested that molybdenum could first dissolve from the substrate into the solution, and then oxidizes to molybdate. Hashimoto *et al*. (1979a) proposed that the main effect of molybdenum is to decrease the rate of dissolution in active zones by the formation and preservation of molybdenum oxyhydroxide or molybdates (MoO_4^{2-}) at these sites. The presence of MoO_4^{2-} has been detected in the passive films formed on molybdenum bearing alloys in acidic solutions (Lu and Clayton, 1985; Brooks *et al*., 1986; Clayton and Lu, 1986). Clayton and Lu (1986) reported that molybdenum additions could aid the development and stability of an amorphous passive film which further provides resistance against $C1^-$ ion attack and subsequent pitting by eliminating the substrate-film epitaxy. Regarding the oxidation state of molybdenum in the passive layer, Carson and Graham (1977) reported that the corrosion rate in sulphuric acid solutions at 20^0C could be reduced by increasing the molybdenum content and the beneficial effect of increasing molybdenum is still quite marked at 50% H_2SO_4.

Contrary to the reported presence of molybdenum oxyhydroxide or molybdates within the passive films, Kozhevnikov *et al*. (1983) observed that no molybdenum oxides could be formed at the passive potential regions in HCl and H_2SO_4 solutions. It has also been reported that MoO_2 is stable only in neutral or weakly acidic conditions (Szklarska-Smialowska, 1986; Tan *et al*., 1995).

In addition to the contrary opposing views on the presence of molybdenum oxyhydroxide or molybdates within the passive films, theories including the enrichment of molybdenum in the metallic state in the alloy layer just below the passive film (Szklarska-Smialowska, 1986; Tan *et al*., 1995), enrichment of chromium in the oxide layer by the selective dissolution of molybdenum (Habazaki *et al*., 1992; Tan *et al*., 1995), thickening of the passive film and stabilization of the chromium oxides by the presence of Mo^{6+} (Leygraf *et al.,* 1979; Ihrzo *et al.,* 1986) have been proposed. It has also been proposed that molybdenum could form a protective film of MoO_2 or a similar hydrated product, since molybdenum remained passive at lower pH values than other elements (Yang *et al*., 1984; Hashimoto *et al*., 2007).

2.4.4 Effects of titanium and niobium on the corrosion resistance of stainless steels

Titanium and niobium (columbium) are strong ferrite formers and strong carbide formers, which could lower the effective carbon content, thereby promoting a ferritic structure of stainless steel and also improve its corrosion resistance (Leffler, 2005). In austenitic steels they are added to increase the resistance to intergranular corrosion and could increase its mechanical properties at high temperatures. Titanium and niobium has been reported to be effective alloying elements for improving the corrosion resistance of ferritic stainless steels (Abdel *et al*., 2006; Van Warmelo *et al*., 2007).

The effectiveness of niobium and titanium on improving the corrosion resistance of ferritic stainless steels is attributed to their ferrite stabilization effects (Van Warmelo *et al*., 2007). According to Alonso-Falleiros and Wolynec (1998), titanium and niobium could act as a stabilizing element of carbon and nitrogen by forming carbides and nitrites preferentially to those of chromium, thus avoiding intergranular corrosion. These two alloying elements are added to ferritic stainless steels as stabilizers to combine with carbon and so prevent the precipitation of chromium carbide which leads to chromium depletion adjacent to the grain boundaries and hence susceptibility to intergranular corrosion (Demo and Bond,1975). According to Alonso-Falleiros and Wolynec (1998), niobium increases the corrosion rate through the depolarization of the cathodic reaction, and decreases the corrosion rate through polarization increase of

the anodic reaction. The depolarization effect is based on the fact that both the corrosion potential and the corrosion rate increase simultaneously with time, while the polarization effect is a consequence of the protection delivered by the corrosion product. This will hinder the access of electrolyte to the metal i.e., it could decrease the exposed area.

2.4.5 Effects of nitrogen on the corrosion resistance of stainless steels

Nitrogen is an austenite former which could promote an austenitic structure of stainless steel, increases its resistance to localized corrosion, especially in combination with molybdenum (Leffler, 2005). Nitrogen is found to improve the corrosion resistance of molybdenum free austenitic stainless steels, and is beneficial in the development of passivity in sulphuric acid (Gross, 1980). The effect of nitrogen on the corrosion resistance of austenitic stainless steels is attributed to its homogenizing effects on microstructure, through the elimination of the delta ferrite and stabilization of the austenitic microstructure (Jargelius-Petterson, 1996). Nitrogen can also improve the resistance to grain boundary corrosion. This is because nitrogen can diffuse faster than the carbon to the grain boundaries so that chromium nitride is formed rather than chromium carbide precipitates (Turan, 1991).

Nitrogen could however have serious effects on the corrosion resistance of stainless steels in different media (Levey, 1995). According to Pehlke and Elllorr (1960); Iorio *et al.* (1994), alloys containing nitrogen tend to cause form porosity due to nitrogen coming out of solution during solidification. If the solubility limit of the nitrogen in the microstructure is exceeded, then chromium nitride precipitates will form in the matrix and these are detrimental to the corrosion properties of the stainless steel because they form chromium-depleted zones in the matrix which are susceptible to pitting attack (Levey, 1995).

2.5 CORROSION MEASUREMENT

Corrosion measurement is the quantitative method by which the effectiveness of corrosion control and prevention techniques can be evaluated and provides feedback to enable corrosion control and prevention methods to be optimized. It is meant to predict compatibility of a material before it is used in an environment and to aid in

understanding why a material-environmental interaction could occur. The measurement of corrosion and the action to remedy high corrosion rates permits the most cost effective plant operation to be achieved, while reducing the life-cycle costs associated with the operation. Corrosion measurement could employ a variety of techniques to determine the corrosiveness of the environment and the extent of metal loss. These techniques can be broadly classified as destructive or non-destructive (Berger, 1982; Rigaud, 2000). A measurement is said to be destructive if it alters the corrosion process during the measuring process (e.g. potentiodynamic polarization) or if the material is physically removed from the environment (e.g. weight loss measurement). Non-destructive techniques, including linear polarization resistance, electrochemical impedance spectroscopy, and electrochemical noise, could be used to make repeated measurements at different time intervals. For the purpose of this study, the destructive evaluation technique is briefly reviewed.

2.5.1 Weight loss technique

The weight loss technique which involves exposing a specimen of material to the corroding environment for a given duration and then removing the specimen for weighing is the best known and the simplest of all corrosion measurement techniques. The weight loss or gain is taken over the period of exposure, and later expressed as a corrosion rate. The determination of weight loss of a material in a corrosion experiment has been one of the common methods used to calculate corrosion rates (Berger, 1982; Rigaud, 2000). The weight loss technique is used so as to enable the corrosion rate measurements to be done without disturbing the plant operation (Malik *et al.,* 1994). The advantage of the weight loss technique is that the corrosion which has actually occurred can be observed on the sample. Moreover, this technique allows a visual examination, physical measurements and the chemical analysis of the corrosion products.

Corrosion coupons can be mounted in different configurations to study different types of corrosion mechanisms, such as crevice corrosion, galvanic attack and stress corrosion. Coupons, which are test specimens of the material of interest, are carefully cleaned, weighed and measured before being assembled on the corrosion test probes (Malik *et al*., 1994; Sharma *et al*., 2001). During assembly, the coupons are arranged such that they are electrically insulated from the corrosion probe so as to avoid

galvanic attack. After a prescribed period of exposure, the corrosion probe is disassembled and the corrosion coupons are chemically cleansed, weighed and measured (Malik *et al*., 1994). Assuming uniform corrosion takes place over the entire surface of the coupon, the corrosion rate is calculated from the weight loss, time

$$MPY = 534\frac{W}{AtD}$$

of exposure and original exposed surface area of the material by the following formula (Malik *et al.,* 1994):

Where:

MPY = mils per year

W = weight loss, mg

A = area of specimen, in^2

t = exposure time, hr

D = density of specimen, g/cm^3

OR

According to *He (2002)*

$$R_{corr} = 10^4 \, ML/ (\rho.A.t)$$

Where R_{corr} = μm/y

ML = mass loss, g

A= area of specimen, cm^2

t = time of exposure, yr

ρ = density of specimen, g/cm^3

2.5.2 Electrochemical techniques

Aqueous corrosion reactions are electrochemical in nature; therefore, they can be easily studied using electrochemical techniques (Moran, 1999; Andrews, 2005). Electrochemical techniques could provide a feasible alternative for rapid prediction or evaluation of alloy corrosion. It could be done to predict corrosion of a material in a plant operation or in the laboratory and its application in evaluating alloy corrosion arises from its relative ease of implementation requiring instrumentation that is

comparatively economical while being completely mechanized. A large number of electrochemical techniques used for corrosion measurements exist. These include, amongst others, open circuit potential measurement, potentiodynamic polarization, cyclic potentiodynamic polarization scans (especially for predicting localized corrosion), chronoampometry, linear polarization resistance, electrochemical impedance spectroscopy, and electrochemical noise etc (Moran, 1999; Silverman, 2000; Andrews, 2005).

2.5.2.1 *Potentiodynamic polarization method*

The potential difference across an open circuit cell (ΔE_n) could be determined thermodynamically. When a device which generates current (I) is applied, the voltmeter will read a value, (ΔE) which is different from (ΔE_n). If I is positive then ΔE will be larger i.e more positive than (ΔE_n) and so E will be more positive than E_n. On the other hand, negative current flow through the cell could result in a reductive electrode reaction at the working electrode and thus causing a negative shift in the electrode potential. This shift is called polarization (Oldham and Myland, 1994; Jones, 1996; Enos and Scribner, 1997). Polarization has ohmic polarization which reflects the resistance of the whole cell. The activation polarization effect arises at different locations in the cell and it has its origin at the electrode interface. When a reference electrode is introduced into the cell, the polarization could be reduced (Van Orden, 1998; Andrews, 2005).

The cyclic potentiodynamic polarization technique for corrosion studies was introduced in the 1960s and refined especially during the 1970s into a simple technique for routine use (Enos and Scribner, 1997; Silverman, 2000). It is useful for the prediction of the corrosion property of the self passivating alloys prone to localized corrosion. According to Silverman (1998; 2000), the technique is based on the idea that corrosion could be predicted by observing the response to a controlled upset from steady-state behavior; this may perhaps be created by application of voltage or current. Voltage could ramp in a cyclic manner from the corrosion potential and the characteristics of the current generated during the cycle are used to predict possible behavior at the corrosion potential. The voltage applied between a working electrode and the counter electrode could ramp at a continuous, slow rate relative to a reference electrode using a potentiostat. The voltage is increased in the anodic

direction (forward scan) and could be reversed at some chosen current or voltage. The potential at which the scan started is usually the corrosion potential measured when the corrosion process reaches steady-state. According to Silverman (1998; 2000), the polarization scan should not be used to estimate the general corrosion rate; meaning that such estimation could actually require the assumption of a mechanism and the curve fitting of the scan that could probably describe the mechanism over a potential range.

2.5.2.2 *Electrochemical cell*

The electrochemical cell is made up of a flask suitable for a conventional three-electrode system, comprising the working electrode, a reference electrode, counter electrode with a lid that has five holes for the reference electrode, working electrode, counter electrode, temperature measurement and an aeration/de-aeration, gas purger.

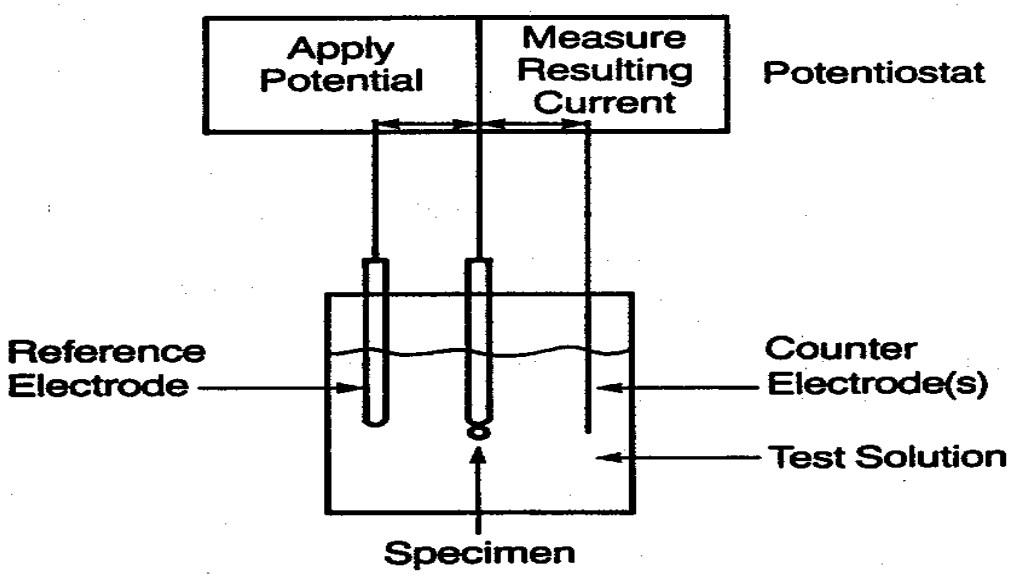

Figure 2.3: Schematic diagram of a potentiodynamic polarization set up (after Jones, 1996).

A potentiostat is usually used for electrochemical measurements. It is generally connected to the three electrodes as shown in the Figure 2.3 above and then to a computer which has relevant software. The potentiostat when started automatically varies the potential at a steady rate between two preset potentials which generates

current through the cell. The current supplied goes into the working electrode through the counter electrode. The potential of the working electrode could thereby be measured with respect to the reference electrode. Data logging of the potential and current could be done by the computer. The open circuit potential (E_{corr}), current density, Tafel slope and corrosion rate are usually obtained from this graph of the data obtained. A typical example is shown in Figure 2.4.

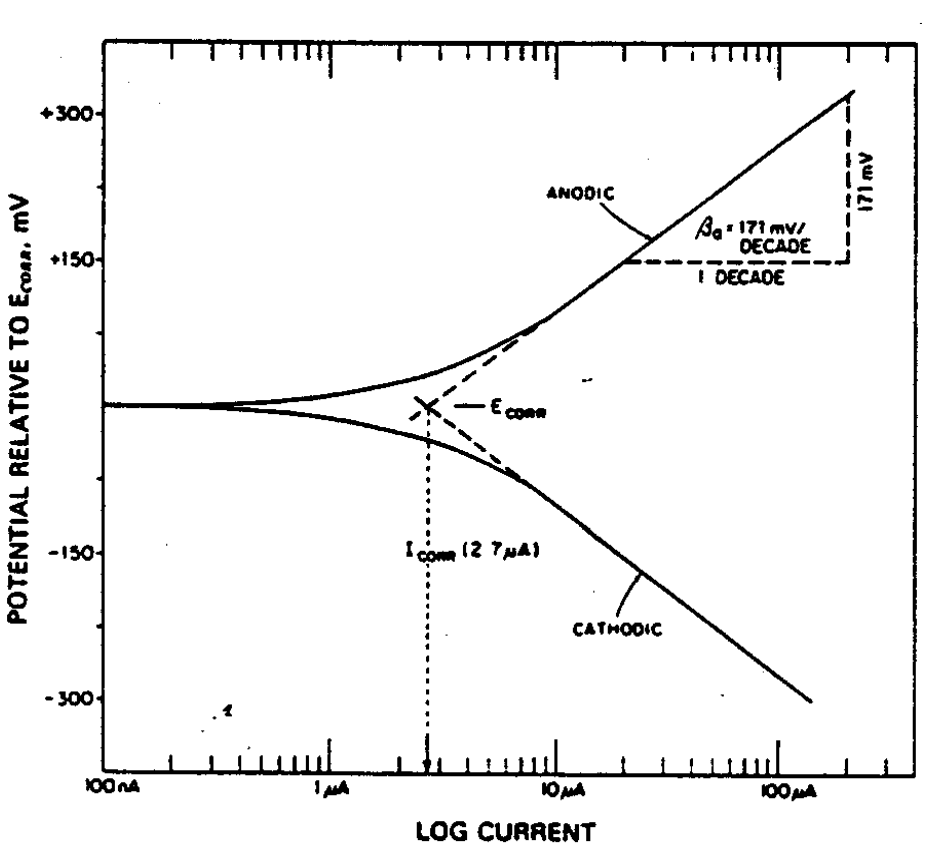

Figure 2.4: Typical Tafel plot from polarization experiment (ASTM G3-89).

CHAPTER THREE

3.0 MATERIALS AND EXPERIMENTAL PROCEDURE

3.1 MATERIALS

The stainless steels used for this study consist of 316 austenitic and 444 ferritic stainless steels. They were supplied by the South African Stainless Steel Development Association. The chemical compositions of the as-received steels are shown in Table 3.1.

3.1.1 Reagents

The following pure and analytical grade reagents purchased from Merck Chemical, Johannesburg were used: Sulphuric acid (98 vol% H_2SO_4) Hydrochloric acid (37 vol %) and Sodium chloride.

3.1.2 Equipment

Equipment used for this project work included: X-Ray Diffractometer (XRD), model Philips PW 1830 with a Cu-anode, X $^{//}$Pert PRO Diffractometer software by PAN-alytical; Scanning Electron Microscope (SEM) model JEOL 840, equipped with Energy-Dispersive X-ray analysis (EDX); Electrodes, Electronic Weighing Balance, Water Bath, Mechanical Stirrers, Autolab Potentiostat (PGSTAT30 computer controlled) with the General Purpose Electrochemical Software (GPES) version 4.9, Computer equipped with cards and software packages, Pyrex Glass, Conical Flasks (500 ml).

3.2 SAMPLE PREPARATION

3.2.1 Samples for microstructural and morphological examinations

Samples for microstructural and morphological examination were prepared by cutting samples into squares of 1.5 cm, and these were hot mounted in bakelite. After mounting, the samples were mechanically ground successively on 240, 320, 600 to 1000 grade silicon carbide papers. They were further polished using 1 to 6μm grades of diamond pastes to obtain a mirror-like surface. The surfaces were rinsed in distilled water and degreased with acetone. The samples were electro-etched with 10 % oxalic acid for about 5s to reveal the details of their microstructures for microstructural

examination and carbon coated for morphological analysis in order to make samples' surface conductive.

Table 3.1: Nominal chemical composition of 444 ferritic and 316 austenitic stainless steels.

Elements	**Compositions (mass %)**	
	444	316
C	0.012	0.029
S	0.006	0.040
P	0.022	0.026
Mn	0.450	1.520
Si	0.340	0.50
Ni	0.150	10.03
Cr	17.95	16.60
Mo	1.906	2.030
Ti	0.093	Nil
N	0.017	0.046
Co	0.020	0.090
Cu	0.090	0.160
B	NIL	0.0034
Fe	balance	balance

3.2.2 Samples for X-ray diffraction studies

Samples for X-Ray diffraction studies were cut similar to the samples for microstructural analysis. They were abraded on 1000-grit silicon carbide metallurgical

paper in accordance to ASTM-G59-97, degreased in acetone, and washed with distilled water to remove any contamination from the silicon carbide paper.

3.2.3 Samples for weight loss measurement

The samples for weight loss tests were prepared in accordance to the procedure recommended by ASTM G 1. The samples were cut to rectangular size of 2.5 cm by 1.5 cm. A hole of 5 mm diameter was drilled at one end of the samples, in which a string was attached for hanging them in the electrolytes. Before attaching strings to the samples, the samples were mechanically abraded with a series of emery papers up to 1000 grade. They were rinsed in acetone and distilled water to remove dirt, oils, and possible product formed on the surface of the samples.

3.2.4 Samples for electrochemical study

Samples for electrochemical analysis were cut similar to the samples for microstructural analysis. They were prepared by attaching an insulated copper wire to one of their faces using an aluminum conducting tape, and cold mounted in epoxy resin. The samples were abraded through 1000-grit silicon carbide metallurgical paper in accordance to ASTM-G59-97, degreased in acetone, and washed with distilled water.

3.3 EXPERIMENTAL PROCEDURES

3.3.1 Materials characterization

Scanning electron microscopy, X-ray diffractometry, Raman spectroscopy and optical microscopy techniques were used in the study of the microstructure and morphology of the samples before the samples were immersed in the corrosive solutions.

3.3.1.1 *Optical microscopy*

Optical microscopy was employed to conduct cross sectional analyses of the samples' surfaces. An Axiocam microscope installed with Axio vision 3.1 programs was used to study the cross sections of the samples.

3.3.1.2 *Raman spectroscopy*

Raman experiments were conducted using a SENTERRA dispersive Raman microscope. The instrument is calibrated using a silicon wafer. A 50X microscope was used to focus the 534 nm excitation laser beam. The laser power used on the samples was 5 mW. The spectra were recorded in the range of 50-1550 cm^{-1}. The acquisition time was 10 s. The OPUS^{TM} software package was used to carry data acquisition and manipulation.

3.3.1.3 *Scanning Electron Microscopy*

Morphological observations of the samples were carried out using a Scanning electron microscope model JEOL 840. At other points, a Phillips (XL30 SERIES) scanning electron microscope (SEM) equipped with a field emission gun operating between 5 and 30 kV was used to assess the microstructure of the polished samples. Elemental analysis was done using energy dispersive X-ray (EDX) analyser. The mirror-like polished samples were carbon coated before analysis in order to make samples' surfaces conductive.

3.3.1.4 *X-ray diffraction*

A Philip-PW 1710 XRD was used to identify the microstructure of the samples before exposure to corrosive environments. The XRD was set at 40 kV and 20 mV with copper K-alpha as anode. A scan with a step size of 0.02^{o} per minute was run from a starting position of 10^{o} up to 80^{o}. Expert High Score software was used to identify peaks in each of the spectra.

3.4 CORROSION STUDIES

3.4.1 Immersion tests

The samples attached to strings were fully immersed in 1 M and 0.1 M the solutions at room temperature after the initial weight had been recorded. The samples in 0.1 M solutions were removed every four days for a period of three months to measure the weight losses, while those in 1 M solutions were removed every day for 12 days to measure the changes in their weights, which was obtained after cleaning the surfaces of the samples. The electrolytes were changed before continuing with the subsequent test. Each test was carried out in duplicate and the mean weight losses were reported.

The mathematical formula by He (2002) was used to calculate the corrosion rates of the samples after the weight loss measurements, namely:

$$R_{corr} = 10^4 \, ML/ (\rho.A.t)$$

Where R_{corr} = μm/y

ML = mass loss, g

A= area of specimen, cm^2

t = time of exposure, yr

ρ = density of specimen, g/cm^3

3.4.2 Electrochemical studies

Electrochemical analysis was conducted using the potentiodynamic polarization technique according to ASTM G 3-89 and ASTM 5-94. The conventional three-electrode electrochemical cell system was used. The electrochemical cell was made of a 500 ml Pyrex glass conical flask suitable for the conventional three-electrode system. The cover of the cell had five holes for the reference electrode, working electrode, counter electrode, temperature measurement and aeration/de-aeration. The stainless steel samples were used as the working electrode, graphite rods as the counter electrodes and a silver/silver chloride 3 M KCl electrode as the reference electrode (SSE).

3.4.3 Electrochemical measurement

The electrochemical corrosion behaviour of the samples was measured using a cyclic potentiodynamic scan, open circuit corrosion potential measurements and employing the chronoamperometry technique. Electrochemical measurements were done using an Autolab potentiostat (PGSTAT30 computer controlled) with the General Purpose Electrochemical Software (GPES) package version 4.9. All the measurements were made at room temperature and varying concentrations of H_2SO_4, HCl, and H_2SO_4 + 3.5% NaCl. Solutions for the study were prepared from analytical grade reagents and distilled water. The samples used for this investigation were prepared as described in section 3.2.3. Solutions were replaced after each test run and samples were re-polished for the subsequent scans to remove any possible corrosion product that might have formed on the surface of the sample during the scanning. All the potentials reported were versus the SSE potentials.

3.4.3.1 Open circuit potential measurement

The variations in the open circuit potential values of the alloys were measured at zero applied current immediately after the immersion of the alloys in different media for up to about two hours.

3.4.3.2 Cyclic potentiodynamic polarization measurement

Cyclic polarization measurements were carried out to determine the corrosion rates, evaluate the passivity behavior, and to determine the pitting and repassivation behavior of the alloys. Before potentiodynamic polarization, the alloys were immersed in the electrolytes for suitable time to stabilize at the OCP. Cyclic polarization curves were measured at a scan rate of 2 mV/s starting from -250mV (with respect to the OCP) up to 1200mV before reversing.

3.4.3.3 Chronoamperometry technique

Chronoamperometric tests were carried out to further assess the pitting corrosion behavior of the alloys and to determine the stability of passive films formed in the different media. Chronoamperometric behavior was studied for about eight hours in different media at 0.2 V and 0.6 V applied potentials, both which were within the passivity regions obtained from the cyclic potentiodynamic polarization measurements. After each scan, the electrolytes were replaced with fresh electrolytes, while the samples were re-polished, rinsed in water and washed with acetone to remove the products that might have formed on the surface that could affect the subsequent measurements.

3.5 POST CORROSION STUDIES

Types and morphologies of possible pits on the surfaces of the corroded samples after chronoamperometric studies were examined using SEM. The nature of possible corroded products and the types of passive films were also determined using Raman spectroscopy and XRD.

CHAPTER FOUR

4.0 RESULTS AND DISCUSSION

This chapter covers the results obtained from the phase identification studies, microstructural and morphological studies of as-received alloy 316 and alloy 444 and their corrosion behaviour in 0.1 M and 1 M sulphuric acid, with detailed discussion.

4.1 WEIGHT LOSS TESTS

The corrosion behaviour of the alloys was first studied using weight loss measurements in 0.1 and 1 M sulphuric acid. The corrosion behaviour of the alloys in 0.1 M sulphuric acid solutions was studied for 92 days while their behaviour in a 1 M solution was assessed over a period of 12 days.

4.1.1 Corrosion kinetics of both alloys in 1 M sulphuric acid solution

The variation of the cumulative weight loss as a function of exposure time for alloy 316 and alloy 444 is shown in Table 4.1 and graphically represented in Figure 4.1. The corrosion rates of alloy 444 and alloy 316 as a function of time is shown in Figure 4.2a and 4.2b and is shown in Table 4.2. The cumulative weight loss patterns in the 1 M sulphuric acid solution was observed to be different from those obtained in 0.1 M solutions. Alloy 444 generally showed an increase in weight- with time of immersion in the 1 M sulphuric acid. However, a constant relationship was observed between the weight loss of alloy 316 and the time of immersion as the rate of weight loss was constant throughout the experiment. A comparison of alloy 444 and alloy 316 showed that alloy 316 is more corrosion resistant in sulphuric acid than alloy 444. The corrosion rates of both alloy 444 and alloy 316 were observed to generally decrease with immersion time. The presence of chromium and molybdenum could be responsible for the decrease in the corrosion rates of both alloys in sulphuric acid solution.

Table 4.1: Cumulative weight loss of alloy 444 and alloy 316 in 1 M sulphuric acid solution.

Time(days)	Cumulative weight loss (g/cm^2)	
	444	316
1	1.39×10^{-1}	2.67×10^{-4}
2	2.77×10^{-1}	2.67×10^{-4}
3	2.77×10^{-1}	2.67×10^{-4}
4	2.77×10^{-1}	2.67×10^{-4}
5	2.77×10^{-1}	2.67×10^{-4}
6	2.77×10^{-1}	2.67×10^{-4}
7	3.34×10^{-1}	2.67×10^{-4}
8	4.40×10^{-1}	2.67×10^{-4}
9	4.89×10^{-1}	2.67×10^{-4}
10	4.89×10^{-1}	2.67×10^{-4}
11	4.89×10^{-1}	2.67×10^{-4}
12	4.89×10^{-1}	2.67×10^{-4}

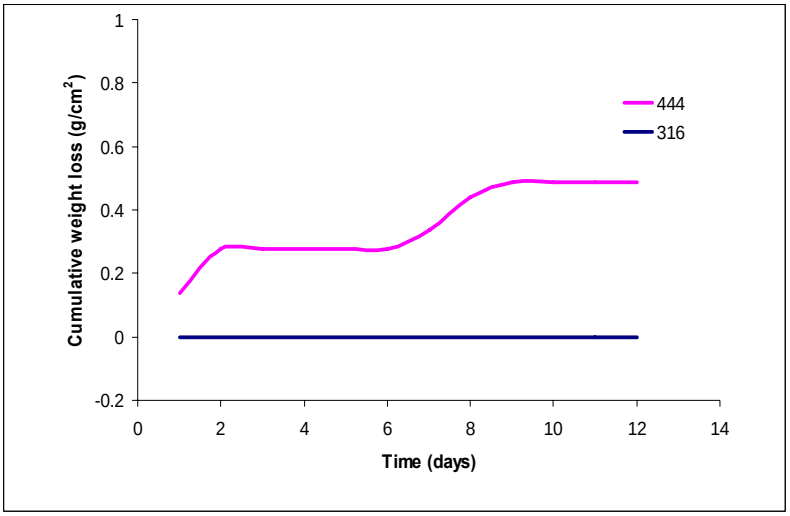

Figure 4.1: Cumulative weight loss of both alloys in 1 M sulphuric acid solution as a function of immersion time.

Table 4.2: Corrosion rates of alloy 444 and alloy 316 in 1 M sulphuric acid solution**.**

Time(days)	Corrosion rate (μm/yr)	
	444	316
1	6.53×10^{4}	1.22×10^{2}
2	6.53×10^{4}	6.09×10^{1}
3	4.35×10^{4}	4.06×10^{1}
4	3.26×10^{4}	3.05×10^{1}
5	2.61×10^{4}	2.44×10^{1}
6	2.17×10^{4}	2.03×10^{1}
7	2.26×10^{4}	1.74×10^{1}
8	2.59×10^{4}	1.52×10^{1}
9	2.54×10^{4}	1.35×10^{1}
10	2.29×10^{4}	1.22×10^{1}
11	2.08×10^{4}	1.11×10^{1}
12	1.91×10^{4}	1.02×10^{1}

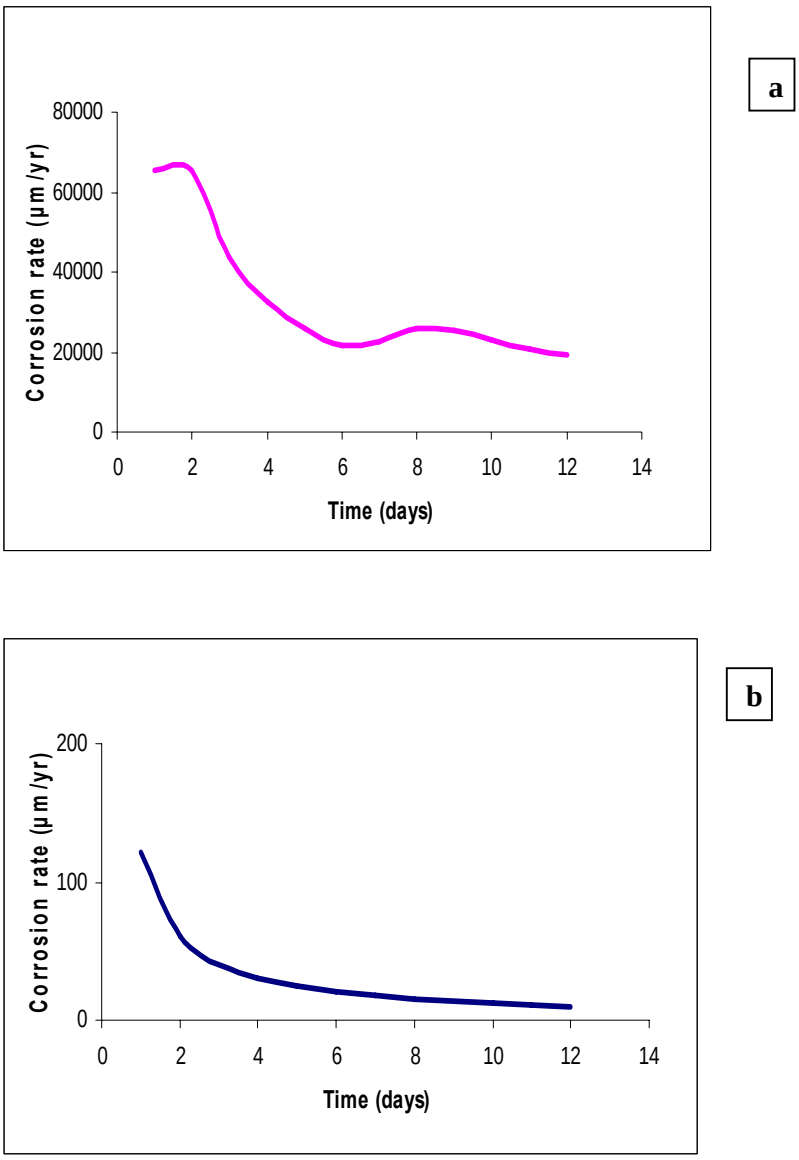

Figure 4.2: Corrosion rates of (a) alloy 444 (b) alloy 316 in 1 M sulphuric acid solution as a function of immersion time.

4.1.2 Corrosion behaviour of both alloys in 0.1 M sulphuric acid solution

Figures 4.3 and 4.4 show the corrosion rate (kinetics) curves of both alloys after their exposure to 0.1 M sulphuric acid solution for 92 days. The patterns observed for the cumulative weight loss versus immersion time for both alloys in 0.1 M sulphuric acid were closely related. There was a noticeable increase in the weight loss of both alloys in the first cycle of the test but no significant change was observed afterward up unto the end of the test. This may indicate that both alloys were in the passive state throughout the test. In all cases, alloy 316 exhibited lower weight loss in both 0.1 M

sulphuric acids compared to alloy 444. Alloy 444 displayed the highest weight loss in sulphuric acid solution compared to the other two solutions. The outcome of this phase of the investigation correlates with the results obtained from the electrochemical tests that were performed. The weight loss of alloy 316 in sulphuric acid and hydrochloric acid were observed to be similar. It was observed that the corrosion rates of both alloys in all the solutions initially increased followed by a steady state decrease with an increase in immersion time. A comparison of alloy 444 with alloy 316 in all the solutions showed that alloy 316 was more corrosion resistant than alloy 444. This is in agreement with the corrosion behaviour exhibited by alloys compose of higher molybdenum and nickel content.

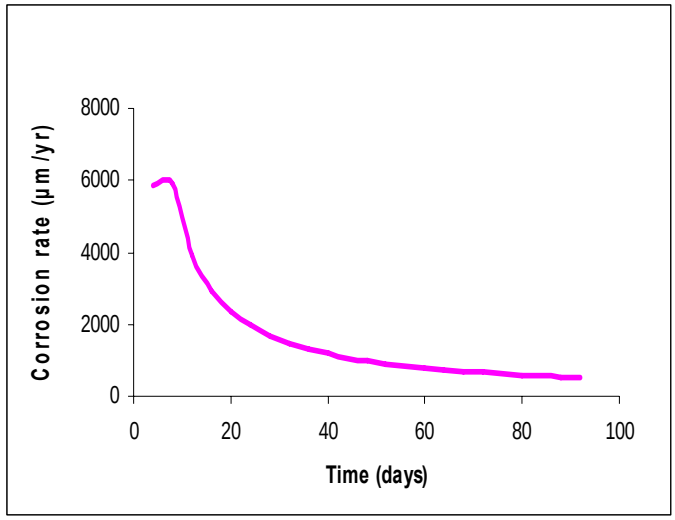

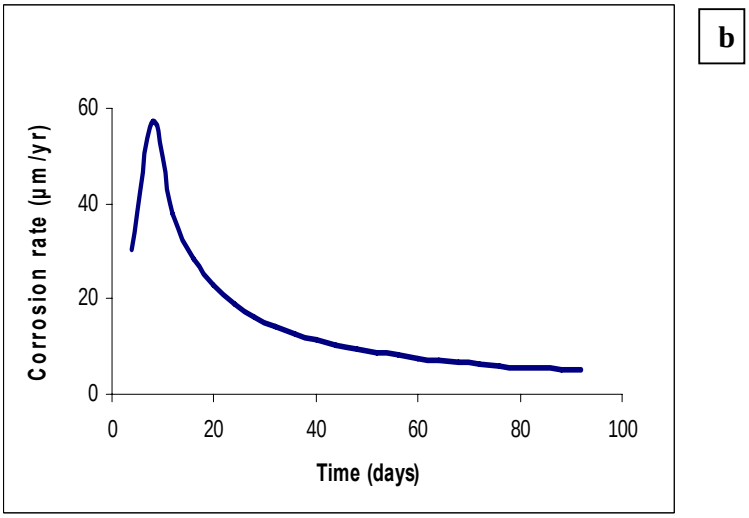

Figure 4.3: Corrosion rates of (a) alloy 444 (b) alloy 316 in 0.1 M sulphuric acid solution as a function of immersion time.

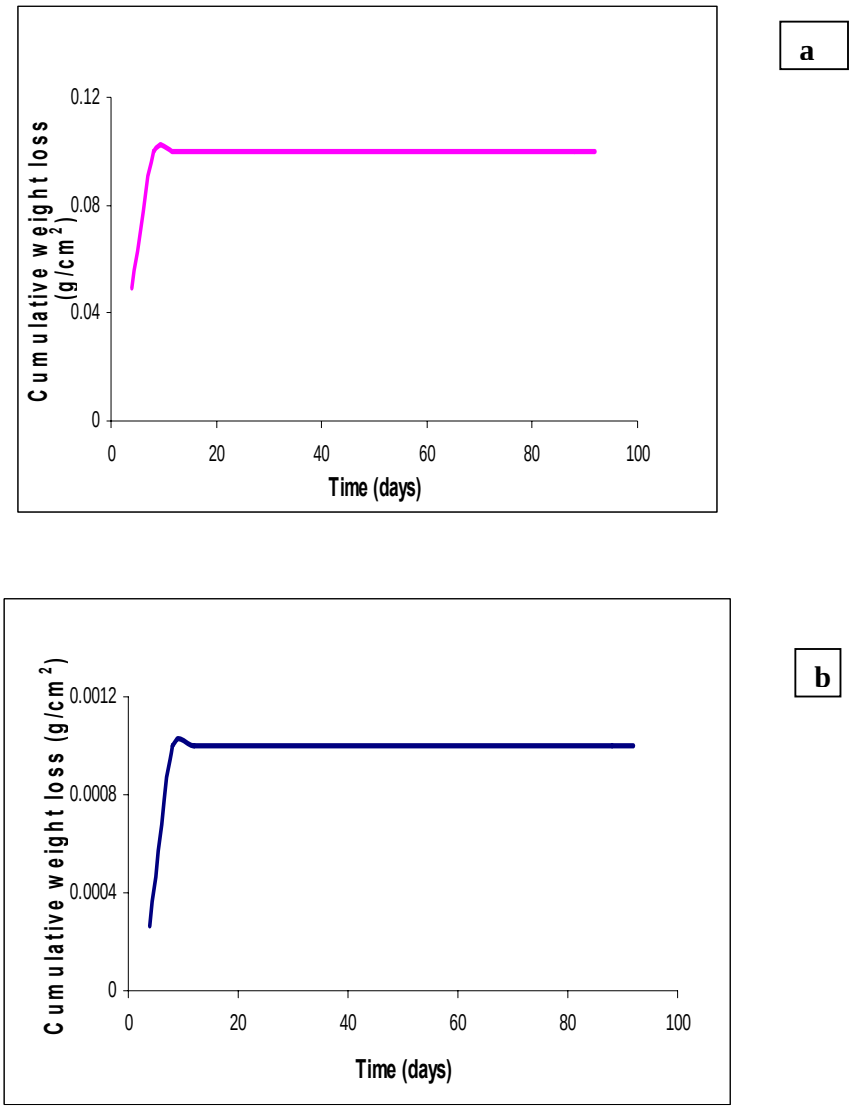

Figure 4.4: Cumulative weight loss of (a) alloy 444 (b) alloy 316 in 0.1 M sulphuric acid solution as a function of immersion time.

4.2 OPEN CIRCUIT CORROSION POTENTIAL VARIATIONS WITH TIME OF BOTH ALLOYS IN SULPHURIC ACID SOLUTION

A study on the reactivity of the alloys i.e. their tendencies to corrode in the different media with time was carried out using Open Circuit Potential (OCP) measurements. The variations in the OCP values of the alloys were studied at zero applied current immediately after the immersion of the alloys in the different media for two hours. The variation in open-circuit potential as a function of time for alloys 316 and 444

tested in 0.1 M and 1 M sulphuric acid solutions are presented in Figures 4.5 and 4.6. The potential was observed to generally shift toward positive values for alloy 316 in 0.1 M sulphuric acid solution. However, the potential values for alloy 444 in sulphuric acid solution decreased initially before increasing. This suggested that there was a breakdown in the film on the surface of alloy 444 in the initial stages, followed by the formation of a new passive film after dissolution. However, in 1 M sulphuric acid, both alloys generally showed a small and progressive increase in potential from negative values to more positive values with time. Alloy 316 showed the largest increase in OCP in the sulphuric acid solution.

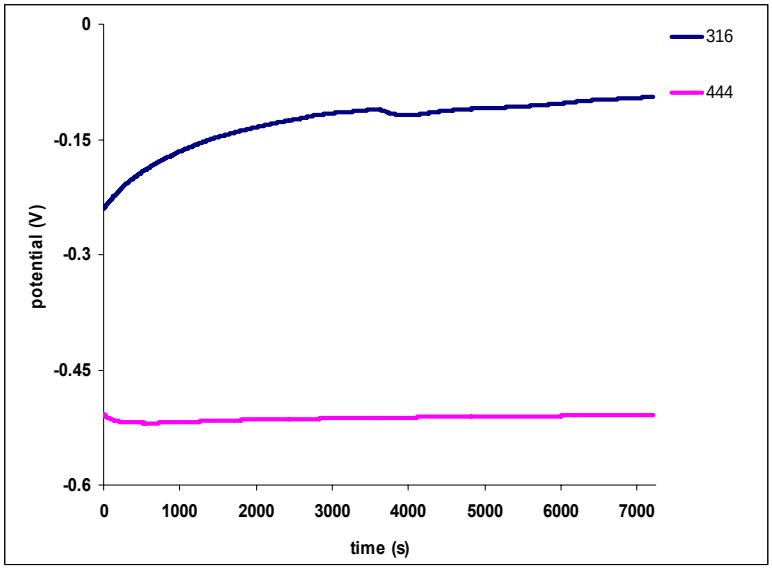

Figure 4.5: Open circuit potential of both alloys in 0.1 M sulphuric acid.

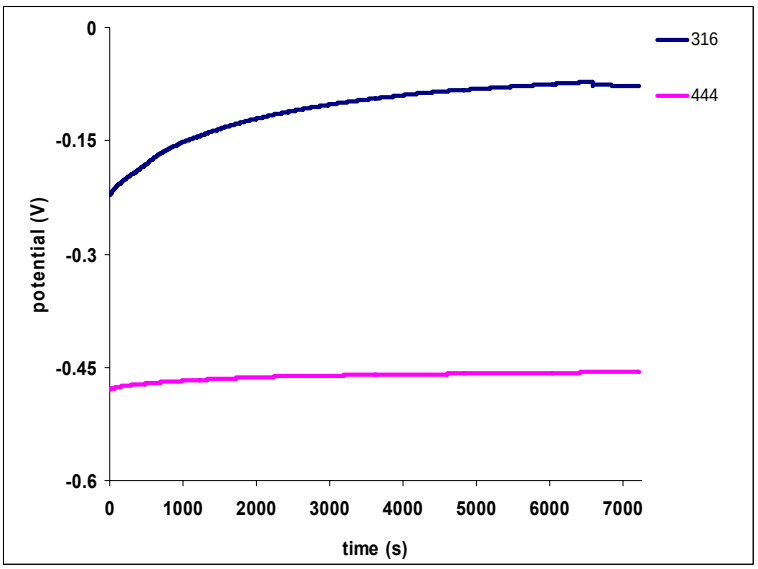

Figure 4.6: Open circuit potential of both alloys in 1 M sulphuric acid.

4.3 POTENTIODYNAMIC TESTS

Cyclic potentiodynamic polarization measurements were carried out to determine the corrosion rates, evaluate the passivity behavior, and to determine the pitting and repassivation behavior of the alloys in sulphuric acid solutions. The electrochemical data obtained from the potentiodynamic polarization scans in 0.1 M and 1 M sulphuric acid solutions for the 316 and 444 alloys are summarized in Table 4.3, while Figures 4.7 and 4.8 give the graphical representations of their responses to polarization. It is noticeable that both alloys display distinct and classical active to passive transition behavior during polarization from active to more noble potentials, with the 444 alloy having more pronounced features in this regard than the curves of the 316 alloy. In all the solutions investigated, the 316 alloy displayed a more noble corrosion potential than the 444 alloy, thus indicating a lower tendency to undergo corrosion. In the two chloride containing media the corrosion potential values remain very similar despite the increase in the concentrations of the solutions, while it tend to be slightly more anodic in the 1 M sulphuric acid solution compared to the 0.1 M one for both 316 and 444.

The critical current densities are substantially lower for the 316 alloy in comparison to the 444 alloy ones, with a two orders of magnitude difference. Alloy 444 displayed a larger passive range than alloy 316, regardless of the concentration of the sulphuric

acid solutions. The E_{tr} did not differ largely between the two alloy types in sulphuric acid solutions. The passive current densities of alloy 444 were greater than those of alloy 316 in both sulphuric acid solutions, and the difference between them becomes greater and more noticeable with an increase in the concentration of the H_2SO_4 solution from 0.1 M to 1 M. The same type of phenomenon is seen in the corrosion current densities, where the values from the 444 alloy are always greater than those from the 316 alloys. Consequently type 444 alloy displayed a lower corrosion resistance (and higher corrosion rate) than the type 316 alloy under all experimental conditions investigated. In both sulphuric acid solutions, the corrosion rates of the type 444 alloy were two orders of magnitude higher than those of the 316 alloys.

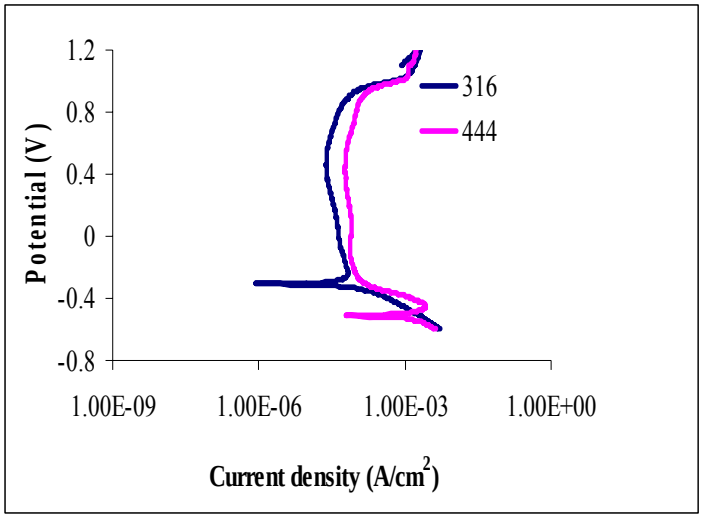

Figure 4.7: Cyclic potentiodynamic polarization curve of both alloys in 0.1 M sulphuric acid.

This same difference in corrosion rates between the two alloys is also seen in the 0.1 M hydrochloric acid solution, but in the 1 M solution they become of a similar magnitude. In the 0.1 M sulphuric acid solution containing added chloride ions, the corrosion rate of type 444 is similar to that of type 316, but as the concentration of the sulphuric acid solution increases and active corrosion sets in, there is again a marked difference between the resistances of alloy 316 compared to alloy 444. These results are in agreement with previous observations reported by Hashimoto (2007) who also

found that the presence of molybdenum in stainless steel (as in the 316 alloy), caused an increased corrosion resistance compared to alloys containing only chromium (such as the type 444 alloy). This is also well documented in most textbooks on corrosion. Similar results reported here were also found by Bojinov *et al.* (2001) during their investigations of the electrochemical behavior of pure Cr, Fe-Cr and Fe-Cr-Mo alloys in 1 M sulphuric acid solutions. It was observed that both alloys had similar molybdenum contents of 2.0 %, so it can be concluded that the higher nickel content of alloy 316 compared to alloy 444 increased its corrosion resistance to pitting. It was observed by Potgieter *et al.* (2008) that nickel could have a substantial effect in improving an alloy's general as well as pitting corrosion resistance.

Table 4.3: Corrosion data obtained from cyclic potentiodynamic curves of alloy 444 and alloy 316 in 0.1 M and 1 M sulphuric acid solutions.

Corrosion media	Alloy type	E_{corr} (V)	i_{corr}(A/cm^2)	I_{corr}(A)	i_{crit}(A/cm^2)	$i_{passive}$(A/cm^2)	Corrosion Rate (mm/yr)
0.1M H_2SO_4	444	-0.512	2.7E-5	6.2E-5	2.4E-3	3.1E-4	3.0E-1
	316	-0.307	3.8E-7	8.5E-7	8.8E-5	7.6E-5	4.0E-3
1M H_2SO_4	444	-0.473	2.1E-4	4.6E-4	8.4E-3	1.3E-4	2.2E+0
	316	-0.287	2.4E-6	5.3E-6	7.5E-5	1.2E-4	2.5E-2

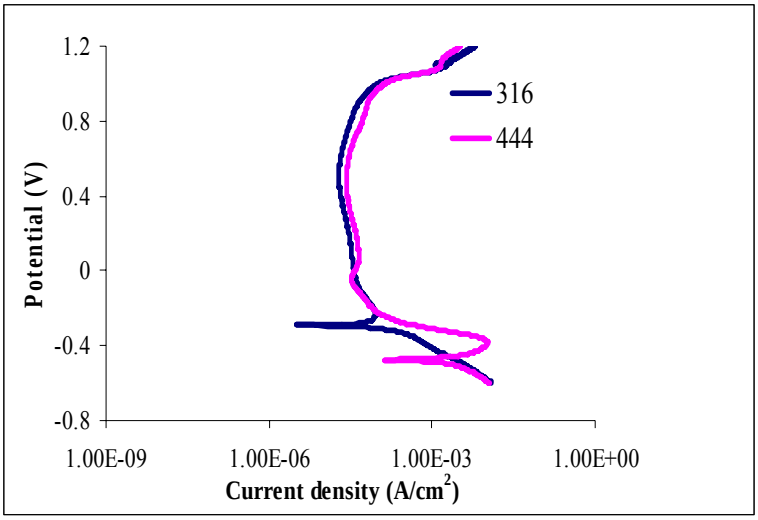

Figure 4.8: Cyclic potentiodynamic polarization curve of both alloys in 1 M sulphuric acid.

4.4 THE CORRELATION BETWEEN THE WEIGHT LOSS AND ELECTROCHEMICAL RESULTS

A comparison of the corrosion rates of alloy 444 and 316 determined by mass loss and polarization tests both at 0.1 M and 1 M concentrations is as shown in Figures 4.9 to 4.12. The value of the electrochemical determination of the corrosion rate, obtained through polarisation measurements for both alloys in both concentrations of sulphuric acid, were lower than the corrosion rate of the direct evaluation from mass loss data. In 0.1 M sulphuric acid, the corrosion rate of alloy 444 from the mass loss test is about six times higher that from electrochemical test. The corrosion rate of alloy 316 in mass loss test was two order magnitudes higher than in electrochemical test. The corrosion rates of alloy 316 in 1 M sulphuric acid of both tests were in the same range and magnitude. The corrosion rates of alloy 444 obtained in mass loss tests was in the same magnitude with those obtained in 1 M sulphuric acid for polarization tests. These lower corrosion rates in polarization tests compared to mass loss test could be due to the fact that there were controlled variables (time, current and voltage) during the polarisation test. Likewise, the alloys were immersed in test media during mass loss test for a longer period of time which could cause an increase in the corrosion rates, especially under conditions of active corrosion. Furthermore, mass loss tests are

different in nature from electrochemical ones and represent true thermodynamical equilibrium or non-steady state conditions.

The present results show that the electrochemical technique may possibly disguise the true behaviour of a corrosion process in this media. A similar observation was made by Rocchini and Enel (1995). The results show that electrochemical test can be used instead of long period mass loss tests, provided that steady state conditions have been reached and that these alloys passivate spontaneously under the conditions investigated. The error bars given on the figures shows the standard deviation of the alloys in the different media.

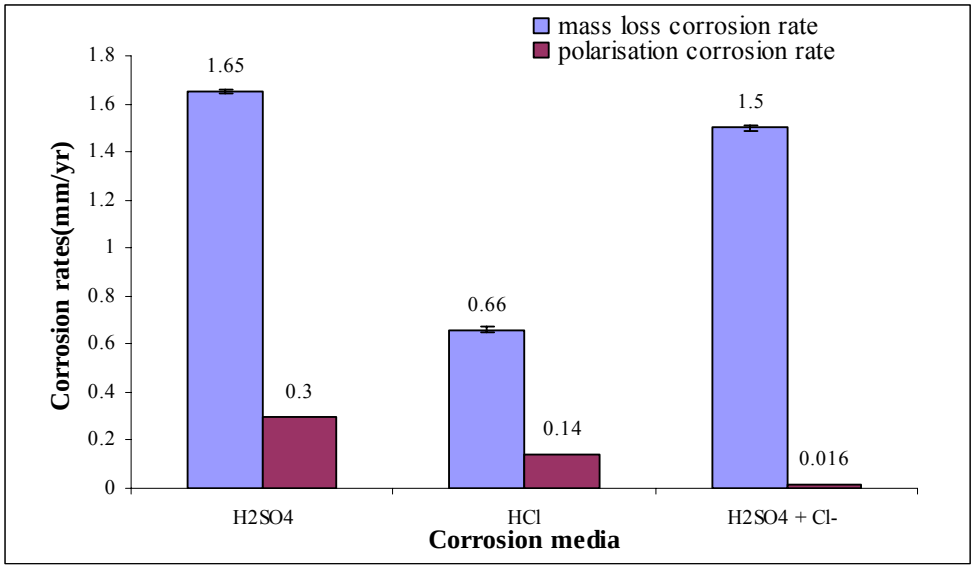

Figure 4.9: Comparison of the corrosion rates of alloy 444 for mass loss and polarization tests in 0.1 M solutions.

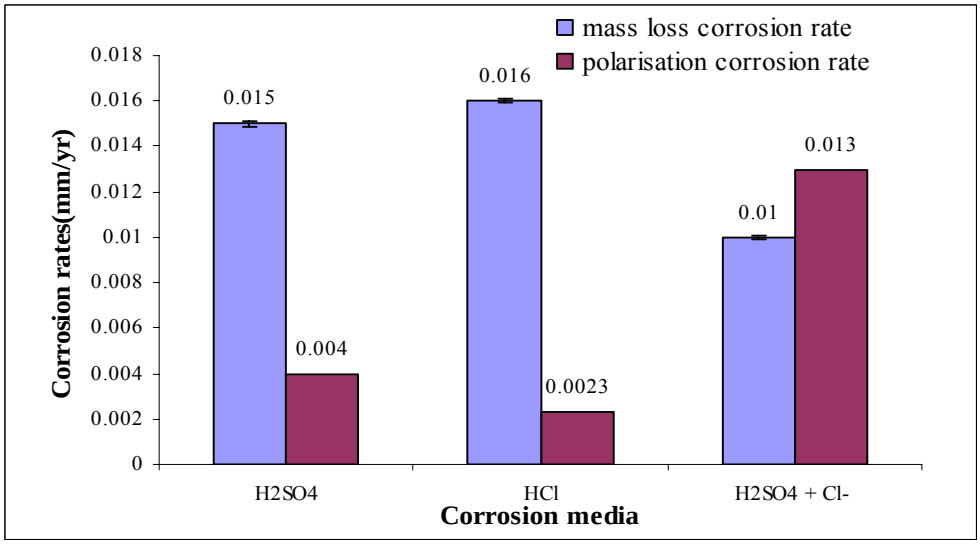

Figure 4.10: Comparison of the corrosion rates of alloy 316 for mass loss and polarization tests in 0.1 M solutions.

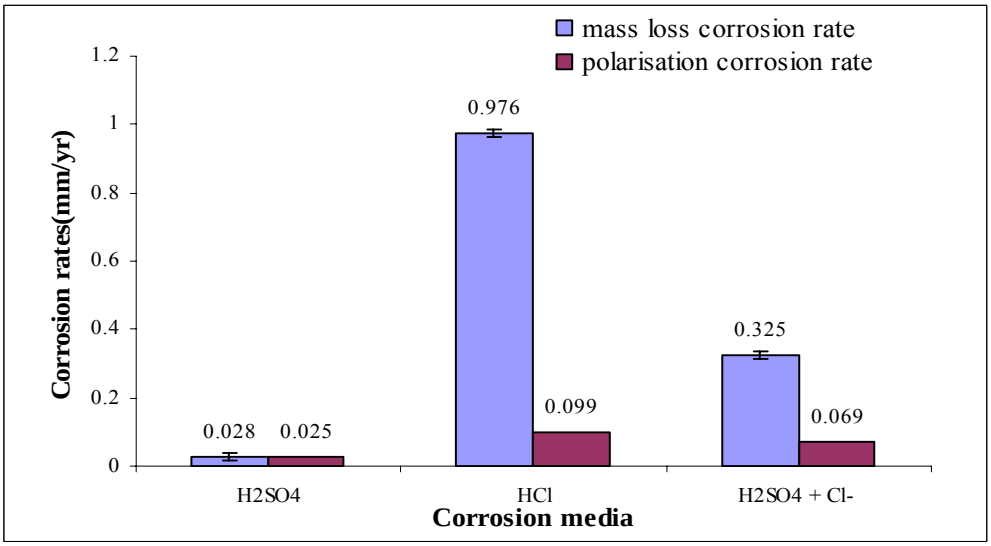

Figure 4.11: Comparison of the corrosion rates of alloy 316 for mass loss and polarization tests in 1 M solutions.

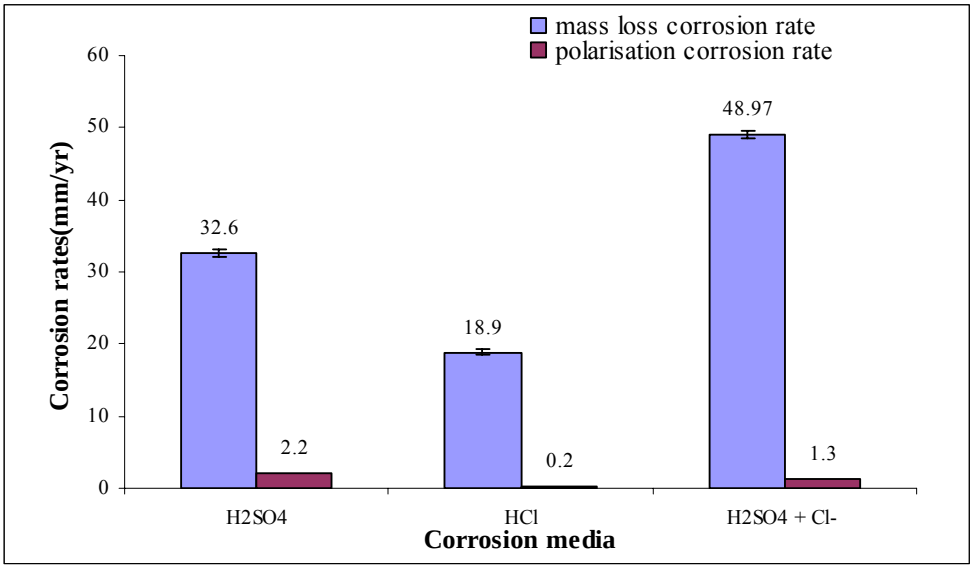

Figure 4.12: Comparison of the corrosion rates of alloy 444 for mass loss and polarization tests in 1 M solutions.

4.5 CHRONOAMPEROMETRIC STUDIES

Chronoamperometric tests were carried out to further assess the pitting corrosion behavior of the alloys and to determine the stability of passive films formed in the different media. Chronoamperometric behavior was studied for about eight hours in different media at 0.2 V and 0.6 V applied potentials, both which were within the passivity regions obtained from the cyclic potentiodynamic polarization measurements. Pitting corrosion is triggered by the susceptible spots formed on the surface of a metal. As a pit forms, the metal goes into solution and increases the flow of current. As the number of the active spots on the surface increases, the probability of the stable pits formation also increases (Shahryari *et al.*, 2008). Figures 4.13a and 4.13b show the chronoamperometry curves of the alloy 316 and 444 in the H_2SO_4 recorded at 0.2 V and 0.6 V respectively. There was a difference in the behaviour of the alloys in the solution at both potentials. At 0.6 V, no current spikes were observed on the curve recorded on the alloy 444 in H_2SO_4. Several current spikes, representing local dissolution of the passive film followed by its repassivation, are on the other hand visible on the curve for alloy 316. The observed current spikes on alloy 316 curves were observed to be quite sharp. The pitting potential region (between the OCP and pitting potential) could result in the formation of pits on the alloys' surfaces,

followed by their repassivation, which is in chronoamperometry manifested as a series of sharp current spikes. The propagation (growth) of the pit to form a critical-pit was not thermodynamically and kinetically favourable, and the pit eventually repassivates. On the other hand, at 0.2 V alloy 316 tends to form a stable film. Unlike at 0.6 V, alloy 444 exhibited more current spikes which indicated the local dissolution and the repassivation of the alloy at this potential. Therefore the passive film formed during polarisation is not yet stable and well established. The result showed that the passive currents of both alloys decreased with time before the stabilizing. This result is in agreement with the results reported by Shahryari *et al.* (2008).

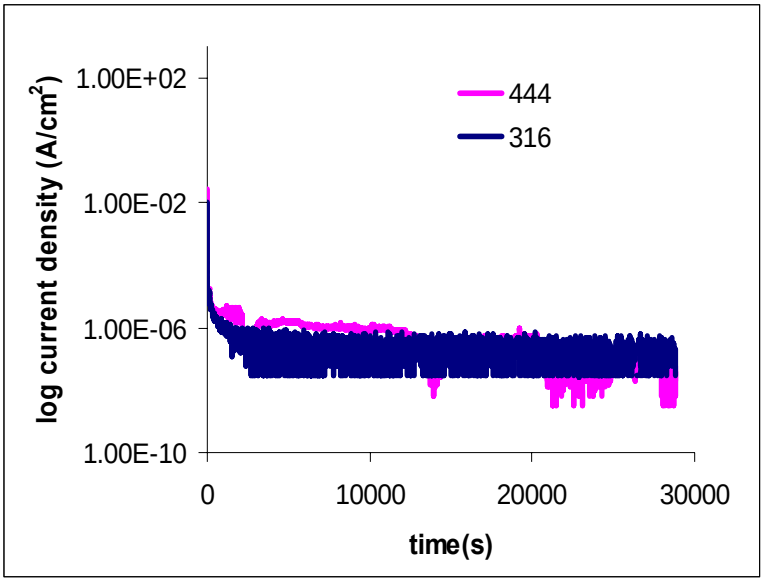

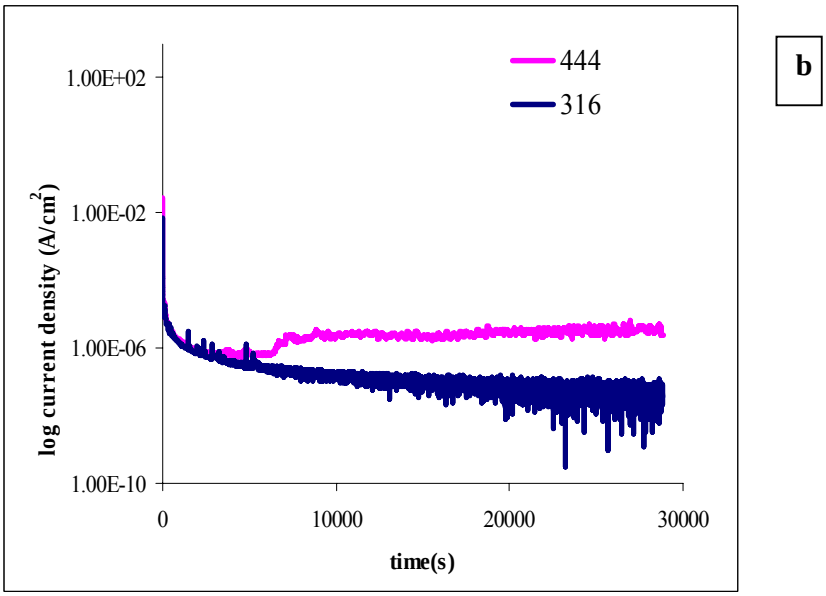

Figure 4.13: Chronoamperometry curves of the alloys 316 and 444 in 0.1 M sulphuric acid at (a) 0.2 V (b) 0.6 V.

The corrosion current of alloy 444 was observed to decrease from 0.03 A/cm^2 to 4.9x 10^{-7} A/cm^2 after 3498 seconds and was constant at this current density for about 3090 seconds before a slight increase was observed. However, despite the fact that it indicates a slight increase in the corrosion current, the passivity seems to remain stable and did not breakdown or goes into a pitting mode. A steady-state (localized)

dissolution of the film, characterized by high current density 0.002 A/cm^2 was reached after 26300 seconds. No current spikes could be observed on this curve. At 0.2 V, no current spike was observed on the alloy 316 curve. The result at 0.2 V showed that alloy 444 formed pits faster than alloy 316 but seems to form a more stable passive film than alloy 316. The SEM and optical microscopy showed that the pits formed on alloy 444 surfaces were shallower compared to those observed on alloy 316.

4.6 MATERIAL CHARACTERISATION

4.6.1 Microstructural studies of as-received alloy 316 and alloy 444

Figure 4.14 and 4.15 show the optical micrographs of the as-received 444 ferritic and 316 austenitic stainless steel samples respectively at different magnifications. The 316 sample appears to be a homogeneous, fine-grained microstructure with randomly spaced inclusions which could be carbides or nitrides of the stabilizing elements (titanium) in alloy 444 and (nickel) in alloy 316 resulted from the electro-etching. The grains of alloy 444 were observed to be coarser than those of alloy 316. The grains of the 444 steel displayed a polygon structure while those of 316 exhibited a triangular/trapezium structure. Both samples were found to have inclusions that were randomly dispersed on their surfaces. Inclusions were however more in the 444 ferritic stainless steel than in 316. The grain size of alloy 444 ranged between 80 to 100 microns, while those of 316 ranged between 20 to 30 microns.

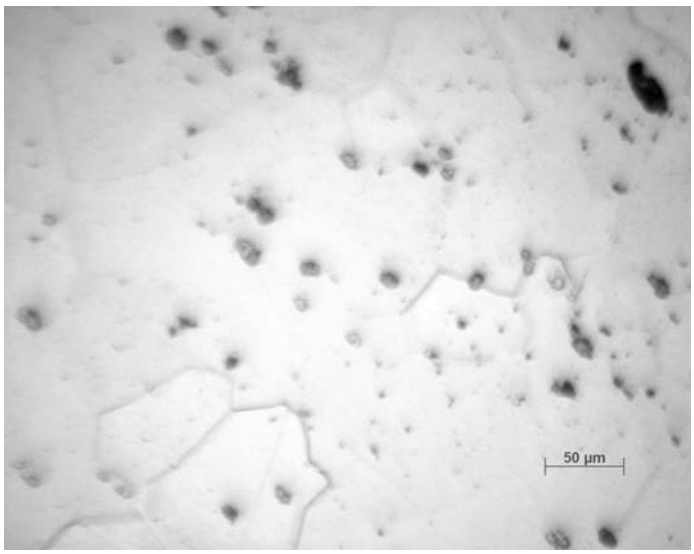

Figure 4.14: Optical image of the as-received alloy 444.

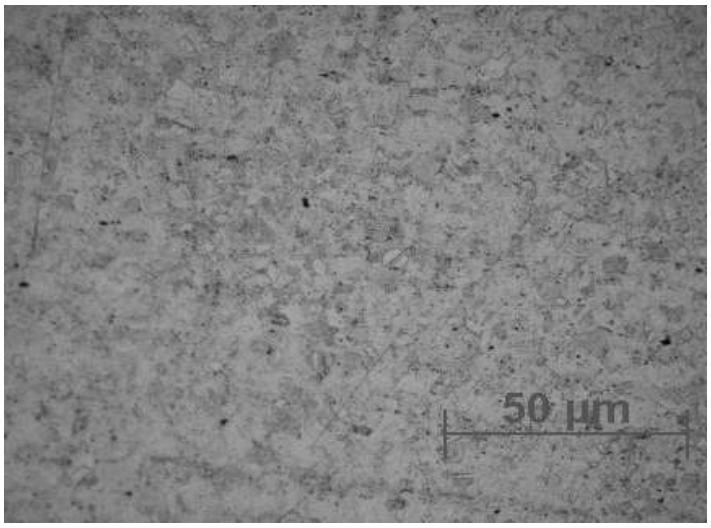

Figure 4.15: Optical image of the as-received alloy 316.

4.6.2 Microstructural studies of both alloys in 0.1 M sulphuric acid

Immersion tests were carried out to investigate the corrosion behaviour of alloys 316 and 444 in 0.1 M sulphuric acid. Figures 4.16 show the microstructures of both alloys after 92 days of exposure in 0.1 M sulphuric acid solution. The typical optical micrographs of the microstructures of alloy 316 and 444 alloy investigated in sulphuric acid for a period of 92 days are shown in Figure 4.16. It was apparent that both alloys showed randomly dispersed pits which are shallow in geometry. Figure 4.16 revealed that the microstructure of both alloys varied significantly after the corrosion test in all the studied solutions. A single morphology observed on alloy 316 was probably a scale. Alloy 444 displayed two major morphological features. More scales were formed on the surface of alloy 316 compared to the case for alloy 444.

The microstructure obtained for alloy 444 was similar to that obtained for the as-received sample of alloy 444. The grains were coarse and similar to those of the as-received alloy. The light region in the micrographs corresponds to the ferritic phase. Unlike alloy 444, the micrograph of alloy 316 did not show any grain feature or any distinct grain structure after the test.

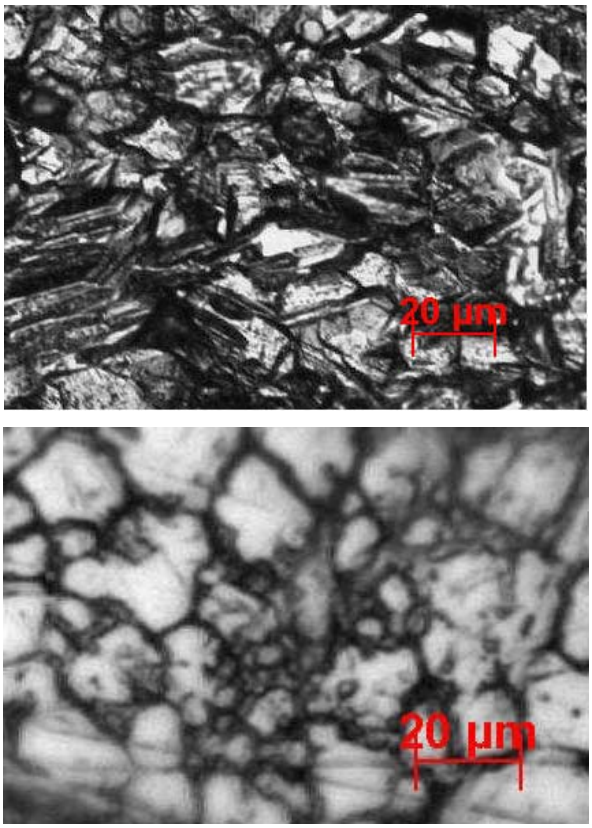

Figure 4.16: Typical optical microstructure of both alloys after immersion in 0.1 M sulphuric acid for 92 days (a) 444 (b) 316.

4.6.3 Morphological studies of as-received alloy 316 and alloy 444

The micrographs obtained from the SEM analysis of the as-received samples electro-etched in 10 % oxalic acid are shown in Figures 4.17 and 4.18. The micrographs showed the morphology of both alloys and give more details of the grain size and structure of the alloys. The micrographs were observed to be similar to those obtained from the optical microscope. Similar to the optical microscopic investigations, alloy 444 was observed to be coarser than alloy 316. The grain size of alloy 444 was between 40 to 50 µm, while in alloy 316 it varied between 15 to 20 µm. As observed in the optical micrographs, there are also more inclusions on the surface of alloy 444 than on alloy 316. Despite the similarities in the information obtained in the SEM and light microscopic studies, slight variations were also observed in the SEM studies. The numerical values in the grain sizes of the samples obtained from light microscopic studies were slightly higher than the SEM studies. SEM information is

usually more reliable than the optical microscopic ones. Nevertheless, the two studies confirmed a similar trend in the coarseness of 444 and 316.

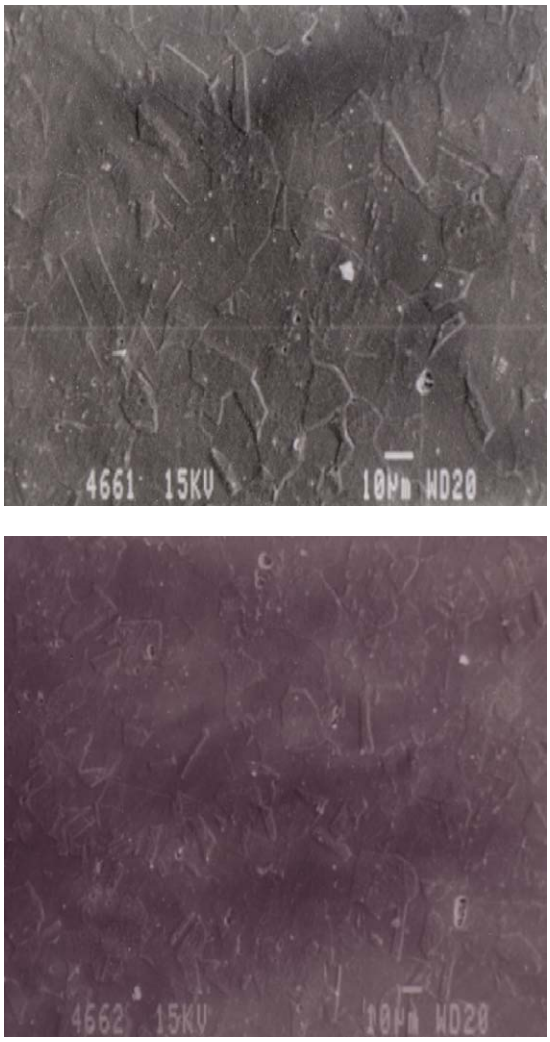

Figure 4.17: Secondary electron micrograph showing the microstructure of as-received alloy 316 at varying locations.

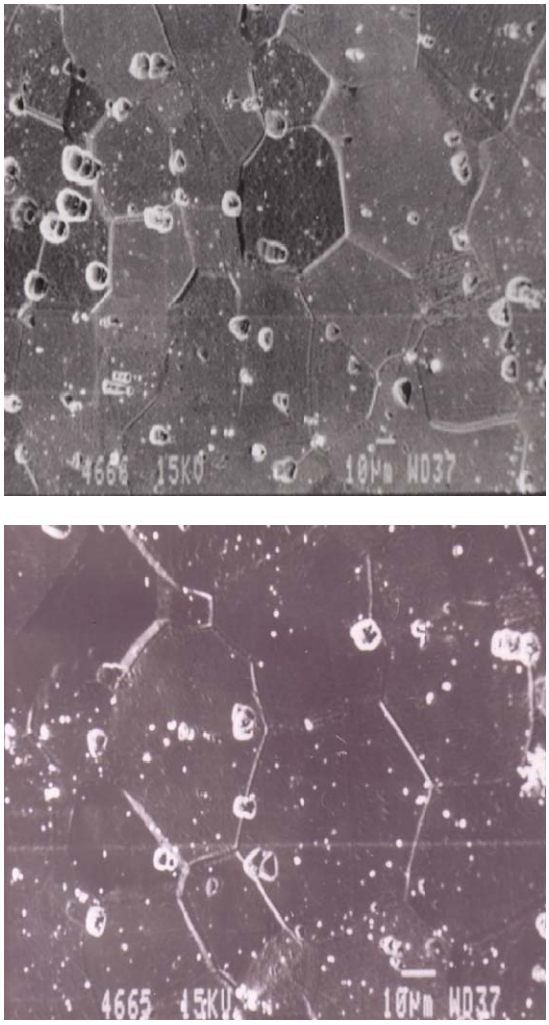

Figure 4.18: Secondary electron micrograph showing the microstructure of as-received alloy 444 and varying locations.

4.6.4 Morphological studies after immersion test

The morphology of the alloys are shown on the SEM micrographs and the EDX of the overall surface obtained after immersion of alloy 444 and alloy 316 in 0.1 M sulphuric acid are presented in Figure 4.19 and 4.20. The micrographs showed more details of the grain size and structure of the alloys. Alloy 444 was observed to be coarser than alloy 316 after the immersion in sulphuric acid. As observed in the optical micrographs, more pits and some parallel features which were probably due to corrosion were observed on the surface of alloy 444 than on alloy 316. The morphology of the as-received samples of alloy 444 and that of alloy 444 after

immersion tests show that there was no considerable variation in the grain appearances and observed sizes. However the morphology of alloy 316 as-received was different from that observed after corrosion. It was observed that the grain size of alloy 316 appeared coarser than that of the as-received sample of alloy 316. The EDX observed for both alloys in sulphuric acid is shown in Figures 4.19 and 4.20 and the main features are summarised in Tables 4.4 and 4.5.

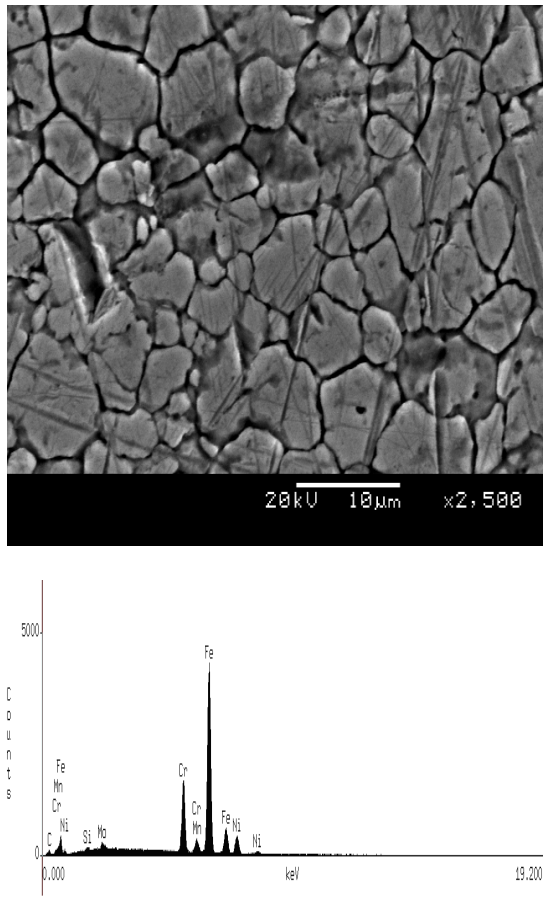

Figure 4.19: SEM/EDX of alloy 316 after immersion in 0.1 M sulphuric acid for 92 days.

Table 4.4: Summary of EDX obtained for alloy 316 in sulphuric acid for 92 days.

Element	Si	Cr	Mn	Ni	Mo	C	Fe
Wt %	0.4 ± 0.1	16.4 ± 0.2	1.8 ± 0.1	10.3 ± 0.45	1.5 ± 0.1	0.7 ± 0.1	68.9 ± 0.5

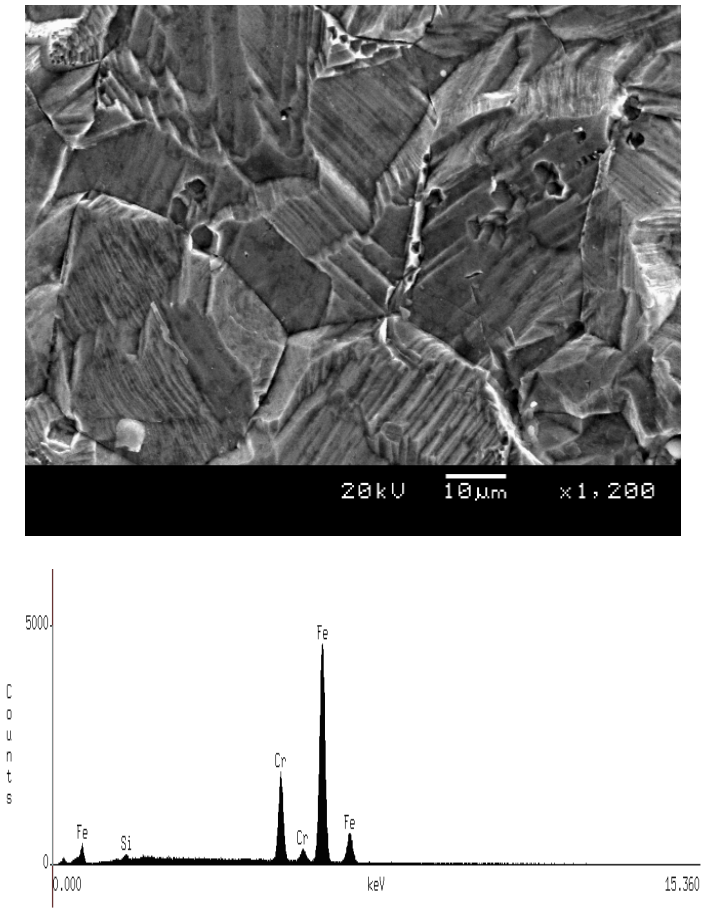

Figure 4.20: SEM/EDX of alloy 444 after immersion in 0.1 M sulphuric acid for 92 days.

Table 4.5: Summary of EDX obtained for alloy 316 in sulphuric acid for 92 days.

Element	Si	Cr	Fe
Wt %	0.6 ± 0.1	18.2 ± 0.2	78.8 ± 0.5

4.6.5 Morphological studies after polarisation test

An important consideration regarding corrosion resistance of the studied alloys is the structure and type of corrosion products that may form once active corrosion and passivation occurs. A preliminary survey of the relevant properties of possible oxides which may be formed was conducted using SEM/EDX. The corroded alloys were examined to determine the corrosion products formed on the alloys. EDX was taken to identify the components of corrosion products film formation on the stainless steels surfaces.

4.6.5.1 *Morphological studies of alloy 316 after corrosion in 0.1 M sulphuric acid*

Figure 4.21 shows the detail of corrosion products and films developed on the alloy 316 surface exposed to 0.1 M sulphuric acid at 0.6 V for 8 hrs. Pitting corrosion was observed on the surface of the alloy as indicated in Figures 4.21. The pits formed on the surface of alloy 316, were small and randomly dispersed all over the surface. From the micrograph, a matrix was observed, with pits formed on the surface of the alloy. In the first spectrum which represented the light phase, iron, chromium, nickel and manganese were observed. Other elements observed on this spectrum were carbon, and molybdenum. However, in the second spectrum, manganese was not observed. Other elements detected were molybdenum, carbon and silicon.

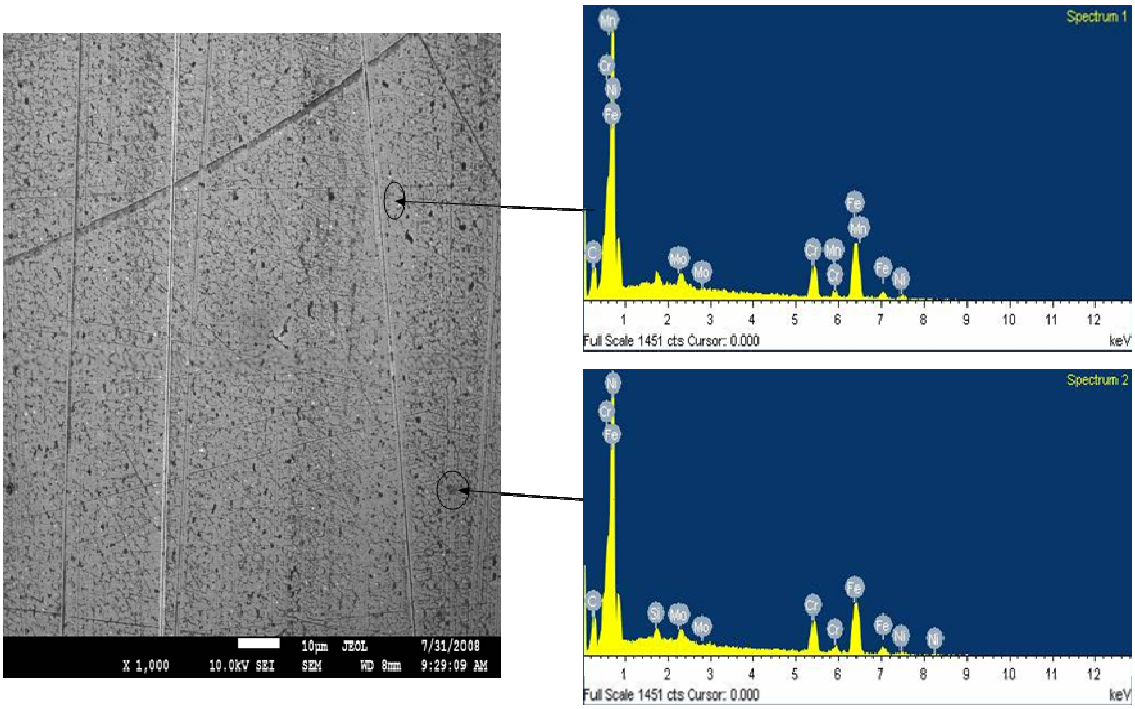

Figure 4.21: SEM scan obtained from the surface of alloy 316 after corrosion in 0.1 M sulphuric acid.

4.6.5.2 *Morphological studies of alloy 444 after corrosion in 0.1 M sulphuric acid*

The SEM micrograph of alloy 444 after corrosion in 0.1 M sulphuric acid is presented in Figure 4.22. The EDX analysis performed on the surface of the alloy 444 is also shown in Figure 4.22. This result shows two significant phases on the surface of alloy 444. The phases observed were a light and a dark phase as indicated on Figure 4.22.

The elements detected on the light phase were iron, chromium, oxygen, nickel, copper, carbon with trace of silicon. The elements detected on the dark phase were similar to the elements observed on the light phase.

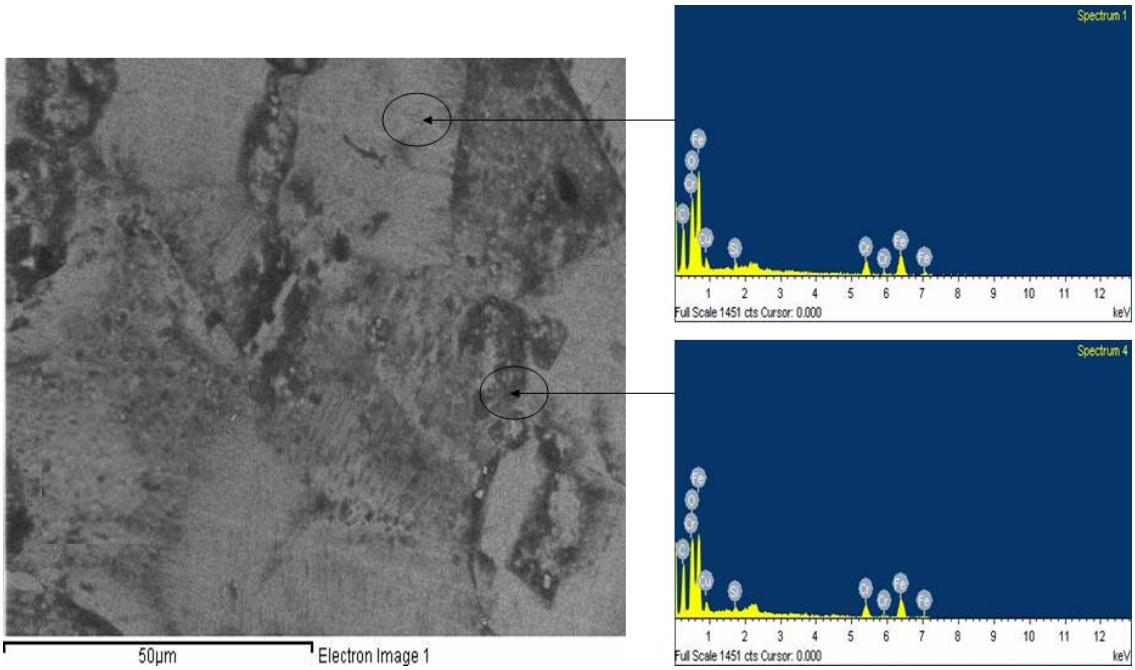

Figure 4.22: SEM scan obtained from the surface of alloy 444 after corrosion in 0.1 M sulphuric acid.

4.7 PHASE IDENTIFICATION STUDIES

4.7.1 X-ray diffraction of the as-received alloys

X-ray diffraction patterns obtained from the external surfaces of the as-received samples are presented in Figures 4.23 and 4.24. The major structures observed on alloy 444 observed to contain iron-chromium and small traces of silicon. On the other hand, the major structures observed to be on alloy 316 surfaces contain iron, chromium, nickel, carbon and some traces of silicon. There were no traces of molybdenum structure at all in the two alloys. Some of the structures in the alloys could not be identified by the X-ray diffractometer, as they did not give any diffraction peak (Kile and Eberl, 2000). The structure of alloy 316 was observed to have cubic austenite structure.

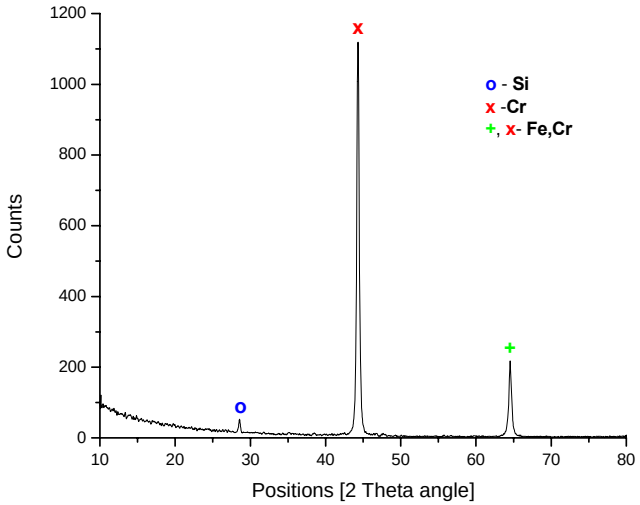

Figure 4.23: X-ray diffraction patterns of alloy 444 before corrosion (01-080-0018, 01-089-4055, and 00-035-1375).

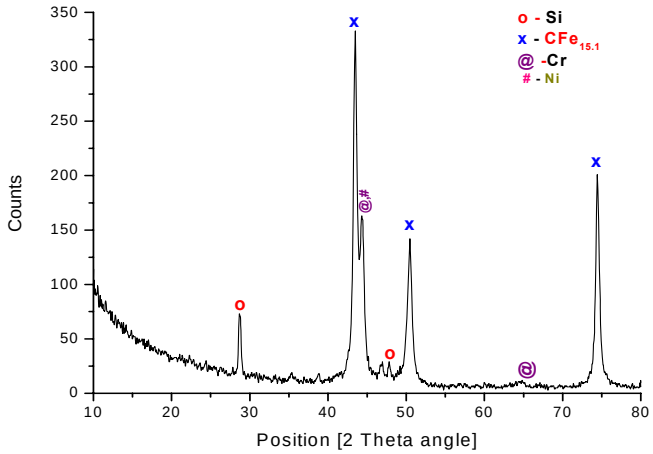

Figure 4.24: X-ray diffraction patterns of alloy 316 before corrosion (01-080-0018, 00-033-0945, 01-089-4055; 00-004-0850, 01-080-0018, 00-033-0945, 01-089-4055, and 00-033-0945).

4.7.2 X-ray diffraction of the corrosion products on both alloys after polarization

It is important to understand the structures of the corrosion products formed on alloys 444 and 316 used for this study. The various types of corrosion products on the samples were analysed using XRD. Representative XRD patterns of alloys 316 and

444 after exposure in sulphuric acid are presented in Figures 4.16 and 4.17. These patterns show the peaks from all the major phases present on the alloys' surfaces. Several points need to be considered in interpreting the XRD data. While analysis by XRD can be very accurate in quantifying major structures within a mixture, it is not very good at detecting constituents that are present in minor or trace amounts (less than about 2 percent) (Kile and Eberl, 2000; Olubambi *et al.,* 2008).

4.7.2.1 *Corrosion products on alloy 316 after polarization*

The major structures that were observed to be on the 316 alloy surfaces before its exposure in the difference media contained iron, chromium, nickel, carbon, and some traces of silicon as reported in section 4.7.1. The peaks were observed at 2θ positions of 28, 43.6, 44.6, 50.7 and 74.6 ^{0}. Some of the constituents of the alloy e.g. molybdenum, did not show up in structures found by the X-ray diffractometer. Thus, while small amounts of molybdenum, boron, copper and others may be expected to be present, such as minor constituents will not be evident on the XRD pattern.

Figure 4.25 shows the grazing angle incidence X-ray diffraction patterns generated from the corrosion products formed on the alloy 316 in sulphuric acid. The major peaks were observed at 2θ positions of 43.5, 50.5 and 74.5 ^{0}. It was observed that the peaks which occurred on the alloy at 2θ positions of 28 and 44 ^{0} before the corrosion test disappeared after the corrosion test. Likewise, the peaks' intensities of the as-received sample at the remaining 2θ positions of 43.6, 50.7 and 74.6 ^{0} respectively increased. This observation indicates that the peaks' heights increased after the corrosion studies in sulphuric acid. This observation indicated higher crystallinity of the corroded products which confirms the observation from the Raman spectra. Molybdenum and silicon were not observed as major peaks of the XRD patterns before the corrosion test, but were observed in all cases in the XRD patterns after the corrosion tests in sulphuric acid.

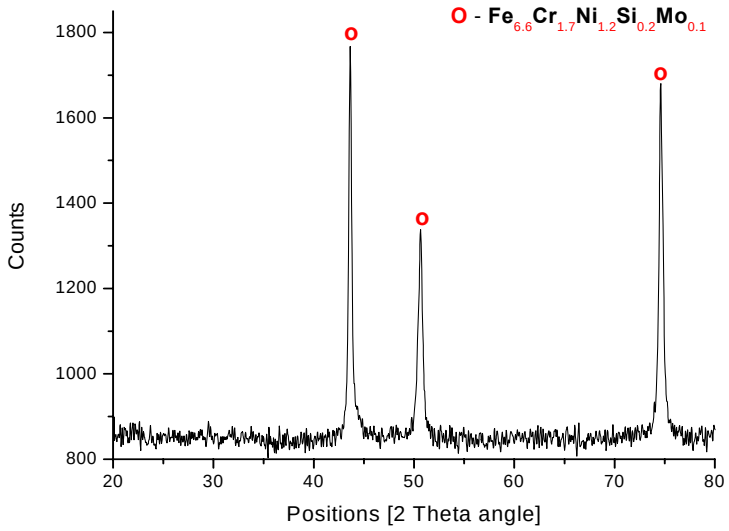

Figure 4.25: X-ray diffraction patterns of alloy 316 after corrosion in sulphuric acid (00-050-1293).

4.7.2.2 *Corrosion products on alloy 444 after polarization*

The XRD spectra obtained from the as-received alloy 444 and after corrosion in sulphuric acid are presented in Figures 4.23 and 4.26 respectively. Three peaks were observed from the XRD pattern of the as-received sample. The major structure observed on the surface of as-received alloy 444 was observed to be iron-chromium with a small trace of silicon. There were no traces of molybdenum at all on the as-received alloy. Some of the structures composed in the alloys could not be identified by the X-ray diffractometer, as they did not give any diffraction peak. Peaks' heights of 35.2, 1147.2 and 216.1 counts were observed at 2θ positions of 28.5, 44.5 and 64.5 ^{0} respectively on the as-received samples. However, peaks' heights of 463 and 473.7 counts were observed at 2θ positions of 44.5 and 64.5 ^{0} respectively on the alloy after the corrosion study in sulphuric acid. The result shows that the counts increased after the corrosion study. Looking at the XRD patterns obtained after the corrosion study, it was observed that the XRD patterns at 2θ positions of 44.5 and 64.5 ^{0} became smaller compared to the pattern obtained for the as-received sample. The iron-chromium was observed to be cubic ferrite structure.

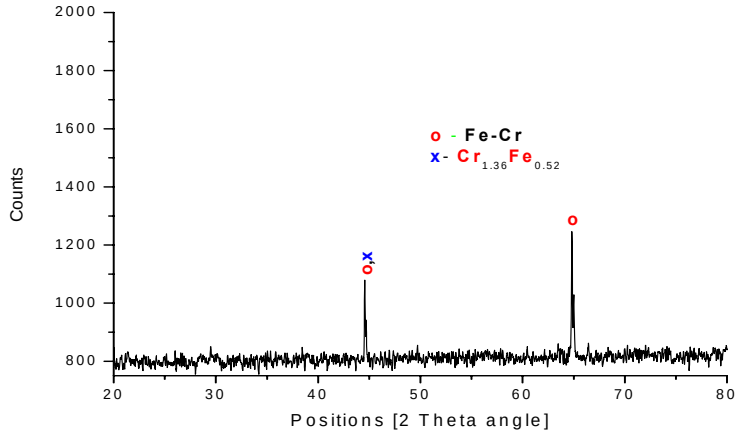

Figure 4.26: X-ray diffraction patterns of alloy 444 after corrosion in sulphuric acid (00-041-1224, and 00-034-0396).

4.8 RAMAN SPECTRA

4.8.1 Raman spectra of as-received alloy 316 and alloy 444

The Raman spectra of alloy 316 and alloy 444 prior to corrosion tests in sulphuric acid are shown in Figures 4.5 and 4.6 respectively. The image shown on the Raman spectroscopy figure shows the overall surface from which the study was made. The Raman spectra of both alloys show similar patterns. The alloy 316 Raman shift intensities were higher compared to that of alloy 444. The Raman spectrum of alloy 316 shows that the compounds of iron and molybdenum were predominant. However, alloy 444 shows compounds of titanium in two band widths at 906 cm^{-1} and 994 cm^{-1}. The summary of the Raman spectra of the alloys compared to other observations from other previous studies is shown in Table 4.6 and 4.7.

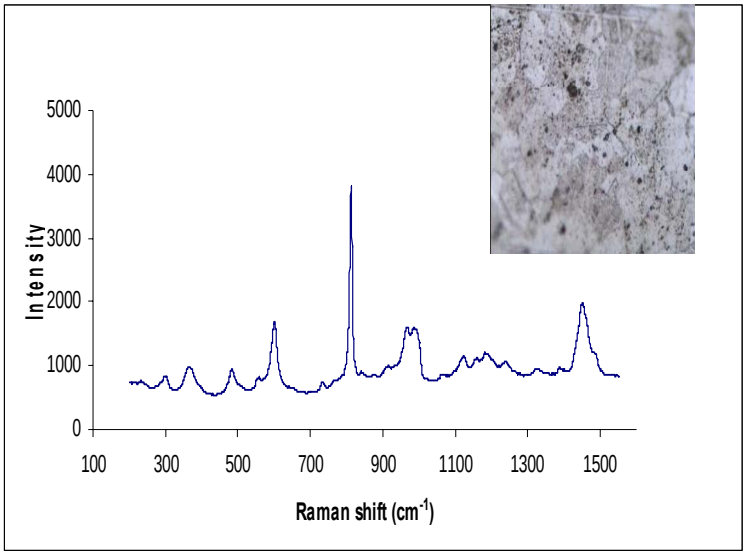

Figure 4.27: Raman spectrum and the image of the overall surface of as-received alloy 316.

Table 4.6: Summary of the Raman spectrum of as-received alloy 316.

Raman shift (cm^{-1}) from this study	**Reference (cm^{-1})**	**Probable corrosion product/compound**	**References**
876	870	$Mo_70_{24}^{6-}$	*Hart et al., 1976; Guevara-Lara et al., 2007*
300	300	Fe_2O_3	*McCarty and Boehme,1989; Gui and Devine, 1991;*
375	370	$Mo_80_{26}^{4-}$	*Hart et al., 1976; Guevara-Lara et al., 2007*
483	490	MoO_2	*Chang et al., 1992; Guevara-Lara et al., 2007*
601	600	NiO	*Chang et al., 1992; Guevara-Lara et al., 2007*
840	840	MoO_4	*Hart et al., 1976; McCarty and Boehme,1989; Guevara-Lara et al., 2007*
882	890	$Fe_2Cr_2O_4$	*McCarty and Boehme,1989; Gui and Devine, 1991*
893	890	$Fe_2Cr_2O_4$	*McCarty and Boehme,1989; Gui and Devine, 1991*
906	900	MoO	*Hart et al., 1976; Guevara-Lara et al., 2007*
967	960	MoO_3	*Hart et al., 1976; Guevara-Lara et al., 2007*
994	994	MoO_3	*Hart et al., 1976; Chang et al., 1992*
1240	1265	$FeCr_2O_4$	*McCarty and Boehme,1989; Gui and Devine, 1991*
1389	1381	$Fe_{0.4}Cr_{1.6}0_{0.3}$	*McCarty and Boehme,1989; Gui and Devine, 1991*
1450	1440	Fe_2O_3	*McCarty and Boehme,1989; Gui and Devine, 1991*

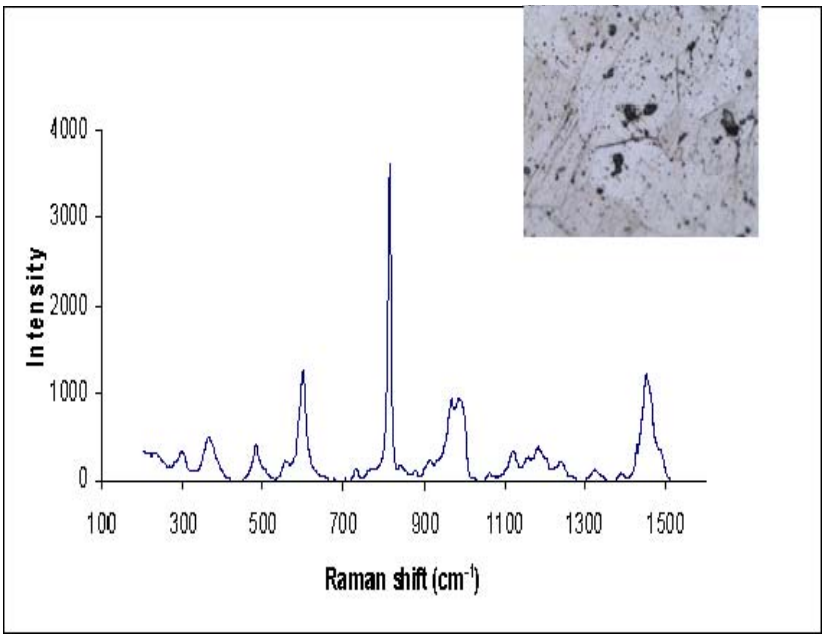

Figure 4.28: Raman spectrum and the image of the overall surface of as-received alloy 444.

Table 4.7: Summary of the Raman spectrum of as-received alloy 444.

Raman shift (cm^{-1}) from this study	**Reference (cm^{-1})**	**Probable corrosion product/compound**	**References**
876	870	$Mo_70_{24}^{6-}$	*Hart et al., 1976; Chang et al., 1992*
300	300	Fe_2O_3	*McCarty and Boehme,1989; Gui and Devine, 1991*
375	370	$Mo_80_{26}^{4-}$	*Hart et al., 1976; Chang et al., 1992*
483	490	MoO_2	*Hart et al., 1976; Guevara-Lara et al., 2007*
601	600	NiO	*Guevara-Lara et al., 2007*
840	840	MoO_4	*Hart et al., 1976; Guevara-Lara et al., 2007*
882	890	$Fe_2Cr_2O_4$	*McCarty and Boehme,1989; Gui and Devine, 1991*
893	890	$Fe_2Cr_2O_4$	*McCarty and Boehme,1989; Gui and Devine, 1991*
906	900-930	TiO_2	*Guevara-Lara et al., 2007*
967	960	MoO_3	*Hart et al., 1976; Guevara-Lara et al., 2007*
994	994	TiO_2	
1240	1265	$FeCr_2O_4$	*McCarty and Boehme,1989; Gui and Devine, 1991*
1389	1381	$Fe_{0.4}Cr_{1.6}0_{0.3}$	*McCarty and Boehme,1989; Gui and Devine, 1991*
1450	1440	Fe_2O_3	*McCarty and Boehme,1989; Gui and Devine, 1991*

4.8.2 Raman spectroscopy of corrosion products formed on both alloys in sulphuric acid solution

The Raman spectra of the corrosion products formed on the surfaces of alloy 316 and alloy 444 in sulphuric acid are shown in Figures 4.29 and 4.30 respectively. The micrographs next to the Raman spectra are the optical micrographs of the corroded surfaces of the investigated alloys. The Raman spectra of the corrosion products on the surface of alloy 316 and alloy 444 were observed within the 50-1550 cm^{-1} spectra range. Raman shifts for alloy 316 were observed at 316, 464, 645, 984, 1040 and 1278 cm^{-1}. The shifts for alloy 444 were observed at 963, 766.1, 766.2, 357, and 240 cm^{-1}. The observed shifts for both 316 and 444 were very similar to the observations which were reported earlier by Hart *et al.* (1976); Gui and Devine (1991); Vuurman and Wachs (1992); Chang *et al.* (1992); and Guevara-Lara *et al.* (2007). Amongst the peaks observed for alloy 444, two were very conspicuous, namely the bands at 963 and 766.1 cm^{-1}. A broad band was formed on alloy 444 spectrum at high intensity. This suggested the formation of an amorphous structure. A similar observation was made by Maledi (2007). The broad band was observed to have two minor peaks at 357 cm^{-1} and 240 cm^{-1}. The structure of the alloy 316 spectrum suggested that the corrosion products formed on its surface were crystalline in nature. Table 4.8 gives the summary of the Raman spectroscopy results obtained for alloy 316 and alloy 444 in sulphuric acid solution.

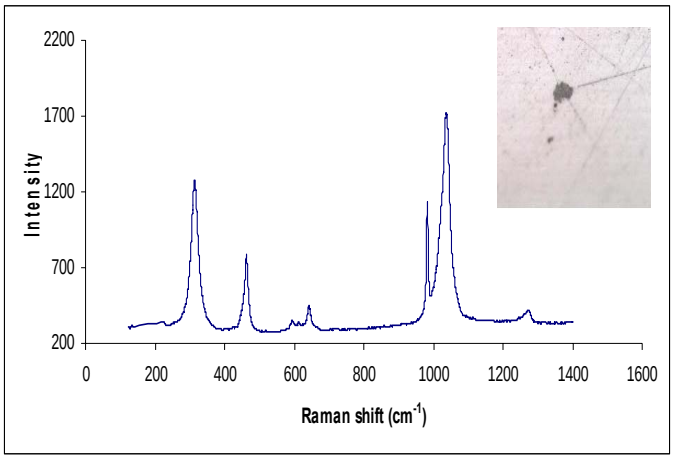

Figure 4.29: Raman spectrum and the image of the overall surface of alloy 316 tested in 0.1 M sulphuric acid.

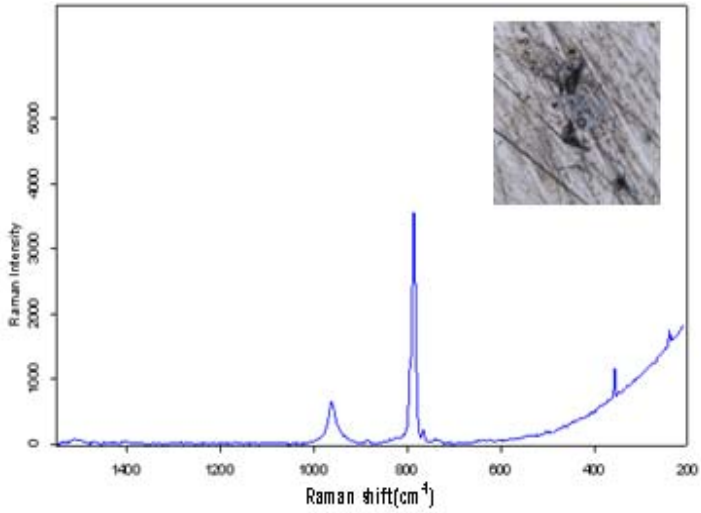

Figure 4.30: Raman spectrum and the image of the overall surface of alloy 444 tested in 0.1 M sulphuric acid.

Table 4.8: Summary of the Raman spectrum of the corrosion products formed on alloy 316 and alloy 444 tested in sulphuric acid.

Alloys	**Raman shift (cm^{-1}) from this study**	**References (cm^{-1})**	**Probable corrosion product/compound**	**References**
316	316	312	MoO_4	*Chang et al., 1992*
		317	Fe_3O_4	*McCarty and Boehme,1989; Gui and Devine, 1991*
		319	Fe_3O_4	*McCarty and Boehme,1989; Gui and Devine, 1991*
	464	460	$Fe(OH)_2$	*Gui and Devine, 1991*
		472	Fe_3O_4	*Gui and Devine, 1991*
	645	645	γ-Fe_2O_3	*Gui and Devine, 1991*
	984	984	MoO_3	*Chang et al., 1992*
	1040	1045	Al_2O_3	*Guevara-Lara et al., 2007*
	1277	1265	$FeCr_2O_4$	*Gui and Devine, 1991*
444	963	960	MoO_3	*Chang et al., 1992*
	766.1	760	NiO	*Guevara-Lara et al., 2007*
	766.2	760	NiO	*Guevara-Lara et al., 2007*
	357	350	$Mo_7O_{24}^{6-}$	*Chang et al., 1992*
	240	245	α-Fe_2O_3	*Gui and Devine, 1991*

4.9 THE CORRELATION BETWEEN ALL THE MICROSCOPY SURFACE ANALYSES TECHNIQUES.

The micrographs obtained from the SEM, Raman spectroscope and optical microscope both as-received and after corrosion studies was observed to be similar (Figures 4.18 to 4.21 and 4.22 to 4.30). SEM micrographs give more details of the surface of the alloys than optical micrographs. All the observations confirmed that alloy 444 was coarser than alloy 316. The morphology of the as-received samples of alloy 444 and that of alloy 444 after immersion test show that there was no considerable change in the appearance of the grain sizes. However, the morphology of alloy 316 as-received was different from that observed after corrosion. This could be due to the corrosion products that were formed on the surface of the alloy. The surface of alloy 316 showed that there were breakdown and repassivation as some pits were still observed. The results show that the film formed during passivation was uniform for both alloys but continuous only for alloy 444. The continuity in the film formed for alloy 444 was confirmed by the results obtained in immersion test, open-circuit potential and chronoamperometric tests. Though the corrosion products formed on alloy 444 were more stable and continuous than for alloy 316 as observed from the open circuit and chronoamperometry results, more pits were formed on the surface of alloy 444 compared to alloy 316. The reason for this is not clear and requires more investigation. It was observed (Davis, 1994; Jargelius-Petterson and Pound, 1998) that molybdenum enhances the resistance to pitting corrosion and expands the passive region in sulphuric acid, making types 316 and 317 suitable for 90 wt.% H_2SO_4 at ambient temperature. The presence of titanium coupled with molybdenum could add to the stability of film formed in alloy 444. Dowling *et al.* (1999) reported that dual stabilization of a welded 444 stainless steel with titanium and niobium may possibly provide optimum corrosion resistance.

CHAPTER FIVE

5.0 CORROSION BEHAVIUOR OF ALLOY 316 AND ALLOY 444 IN SULPHURIC ACID CONTAINING 3.5 % NaCl

The standard test of alloy 316 and alloy 444 in sulphate solution was studied in Chapter Four considering the effect of sulphate on the corrosion behaviour of the studied alloys. This Chapter covers the results obtained from the corrosion behaviour in 0.1 M and 1 M sulphuric acid containing 3.5 % NaCl, phase identification studies, microstructural and morphological studies of alloy 316 and alloy 444 with detailed discussion considering the effect of chloride addition.

5.1 WEIGHT LOSS TESTS

The corrosion behaviour of the alloys in 0.1 M sulphuric acid containing 3.5 % NaCl solutions was studied for 92 days while their behaviour in 1 M solution was assessed over a period of 12 days.

5.1.1 Corrosion kinetics of both alloys in 1 M sulphuric acid containing 3.5 % NaCl

The variation of the cumulative weight loss as a function of exposure time for alloy 316 and alloy 444 is shown in Table 5.1 and graphically represented in Figure 5.1. The corrosion rates of alloy 444 and alloy 316 as a function of time are shown in Figure 5.2a and 5.2b and are shown in Table 5.2. The cumulative weight loss patterns of both alloys in the 1 M sulphuric acid containing 3.5 % NaCl solution were observed to be different from those obtained in 1 M sulphuric acid solution. In both cases alloy 444 generally showed an increase in weight with the time of immersion. A linear relationship was observed between the weight loss of alloy 316 and the time of immersion when compared to alloy 444, although this may not be feasible on the figure. The linearity is seen on Table 5.1, the cumulative weight loss increased with the time of immersion. It was observed that the addition of 3.5 % NaCl increased the cumulative weight loss and the corrosion rates of both alloys as shown in the cumulative weight loss and corrosion rates curves. No significant changes were observed in the corrosion rates of alloy 316. However, the corrosion rates of alloy 444 were observed to generally decrease with immersion time.

Table 5.1: Cumulative weight loss of alloy 444 and alloy 316 in 1 M sulphuric acid containing 3.5 % NaCl.

Time(days)	Cumulative weight loss (g/cm^2)	
	444	316
1	1.01×10^{-1}	5.33×10^{-4}
2	3.03×10^{-1}	1.47×10^{-3}
3	4.03×10^{-1}	2.27×10^{-3}
4	4.37×10^{-1}	3.20×10^{-3}
5	5.47×10^{-1}	3.33×10^{-3}
6	6.67×10^{-1}	4.13×10^{-3}
7	0.714667	5.20×10^{-3}
8	7.36×10^{-1}	5.73×10^{-3}
9	8.00×10^{-1}	6.67×10^{-3}
10	8.80×10^{-1}	7.47×10^{-3}
11	9.15×10^{-1}	7.87×10^{-3}
12	9.20×10^{-1}	8.27×10^{-3}

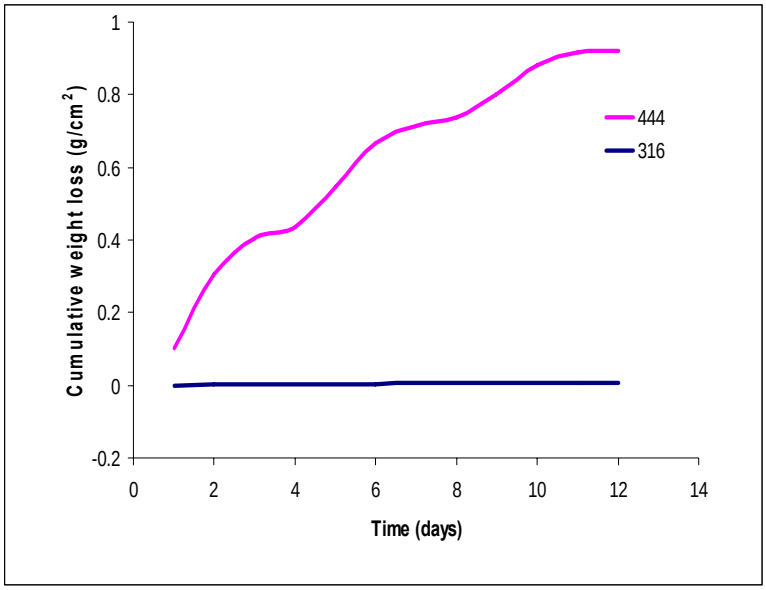

Figure 5.1: Cumulative weight loss of (a) alloy 444 (b) alloy 316 in 1 M sulphuric acid containing 3.5 % NaCl as a function of immersion time.

Table 5.2: Corrosion rates of alloy 444 and alloy 316 in 1 M sulphuric acid containing 3.5 % NaCl.

Time(days)	Corrosion rate (µm/yr)	
	444	316
1	4.77×10^{4}	2.43×10^{2}
2	7.14×10^{4}	3.35×10^{2}
3	6.32×10^{4}	3.45×10^{2}
4	5.15×10^{4}	3.65×10^{2}
5	5.15×10^{4}	3.05×10^{2}
6	5.23×10^{4}	3.15×10^{2}
7	4.81×10^{4}	3.39×10^{2}
8	4.33×10^{4}	3.27×10^{2}
9	4.19×10^{4}	3.38×10^{2}
10	4.14×10^{4}	3.41×10^{2}
11	3.92×10^{4}	3.27×10^{2}
12	3.61×10^{4}	3.15×10^{2}

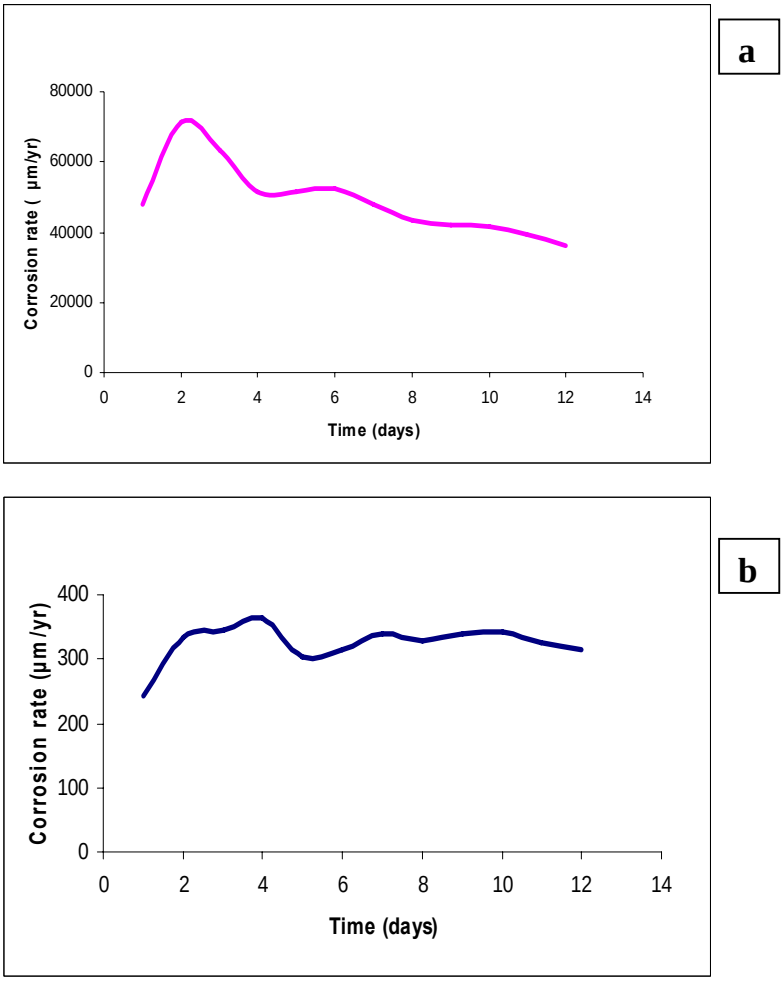

Figure 5.2: Corrosion rates of (a) alloy 444 (b) alloy 316 in 1 M sulphuric acid containing 3.5 % NaCl as a function of immersion time.

5.1.2 Corrosion behaviour of both alloys in 0.1 M sulphuric acid solution containing 3.5 % NaCl

The corrosion kinetics of the investigated alloys after their exposure to 0.1 M sulphuric acid solution containing 3.5 % sodium chloride for 92 days are shown in Figures 5.3 and 5.4. The patterns observed for the cumulative weight loss versus the immersion time for both alloys in this solution were closely related. There was a noticeable increase in the weight loss of both alloys in the first part of the test, but no significant change was observed afterwards up unto the end of the test. This may indicate that both alloys were in the passive state throughout the latter part of the tests.

In all cases, alloy 316 exhibited a lower weight loss in both 0.1 M concentrations of all the solutions compared to alloy 444. Alloy 316 displayed the lowest weight loss and corrosion rate in 0.1 M sulphuric acid solution containing 3.5 % NaCl compared to the other two solutions investigated. These results showed that at lower concentrations of sulphuric acid, when 3.5 % NaCl is added, the corrosion rate of both alloys decreased with time. It was observed that the corrosion rates of both alloys in all the solutions initially increased followed by a steady state decrease with an increase in immersion time.

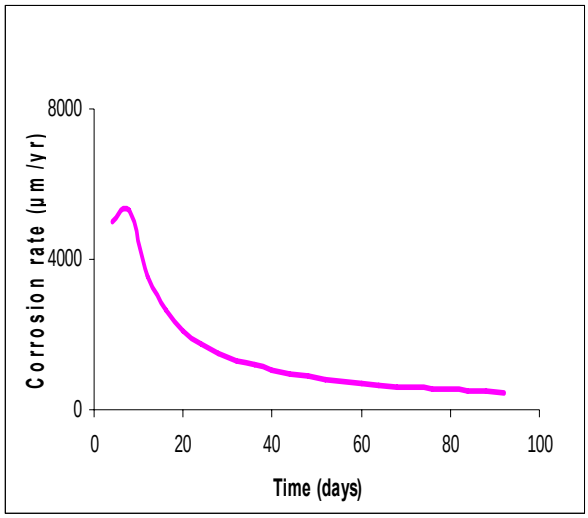

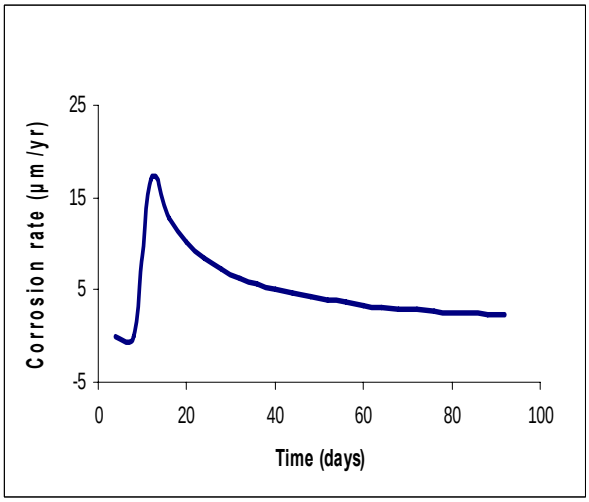

Figure 5.3: Corrosion rates of (a) alloy 444 (b) alloy 316 in 0.1 M sulphuric acid containing 3.5 % NaCl as a function of immersion time.

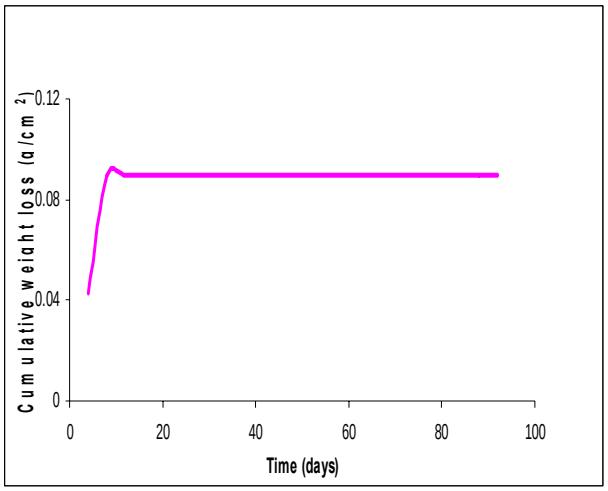

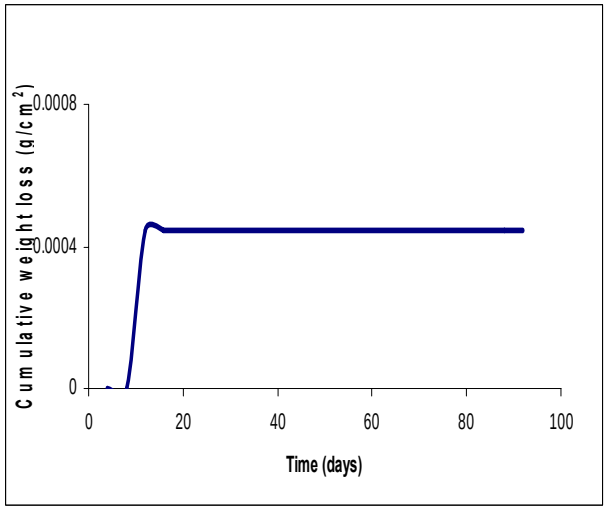

Figure 5.4: Cumulative weight loss of (a) alloy 444 (b) alloy 316 in 0.1 M sulphuric acid containing 3.5 % NaCl as a function of immersion time.

5.2 OPEN CIRCUIT CORROSION POTENTIAL VARIATIONS WITH TIME OF BOTH ALLOYS IN SULPHURIC ACID CONTAINING 3.5 % NaCl SOLUTION

The variation in open-circuit potential as a function of time for alloys 316 and 444 tested in 0.1 M and 1 M sulphuric acid solutions containing 3.5 % NaCl are presented in Figures 5.5 and 5.6. The potential values for alloy 444 in sulphuric acid solution containing 3.5 % sodium chloride solution decreased initially before increasing. This suggested that there was a breakdown in the film on the surface in the initial stages, followed by the formation of a new passive film. Alloy 316 showed a similar small and progressive increase in potential from negative values to more positive values with time in sulphuric acid containing 3.5 % NaCl. The OCP values for alloy 444 were relatively lower than that of the alloy 316 in this solution. The increase in the OCP values of alloy 316 in sulphuric acid solution was an order of magnitude more than the increase seen in sulphuric acid solution containing 3.5 % NaCl.

In 1 M sulphuric acid containing 3.5 % NaCl, the potential of alloy 444 was observed to increase steadily to more noble potentials. The potential of alloy 316 however, initially decreased, but later increased to a more noble potential. The largest OCP increase in sulphuric acid containing 3.5 % NaCl was observed for alloy 316. The OCP values for alloy 444 were always lower than that of the alloy 316 in all the solutions.

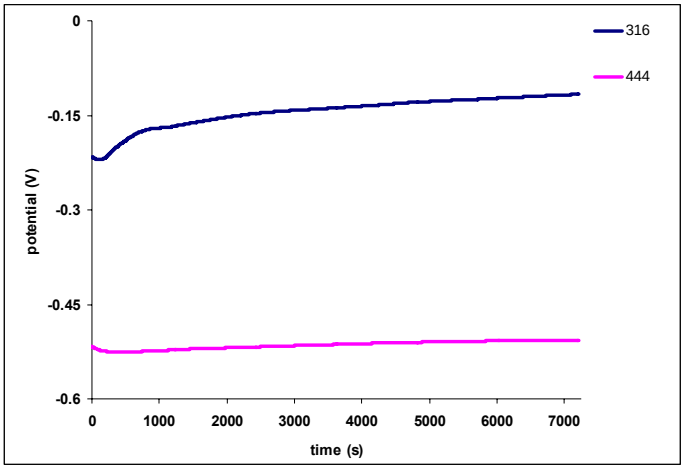

Figure 5.5: Open circuit potential of both alloys in 0.1 M H_2SO_4 + 3.5 %NaCl.

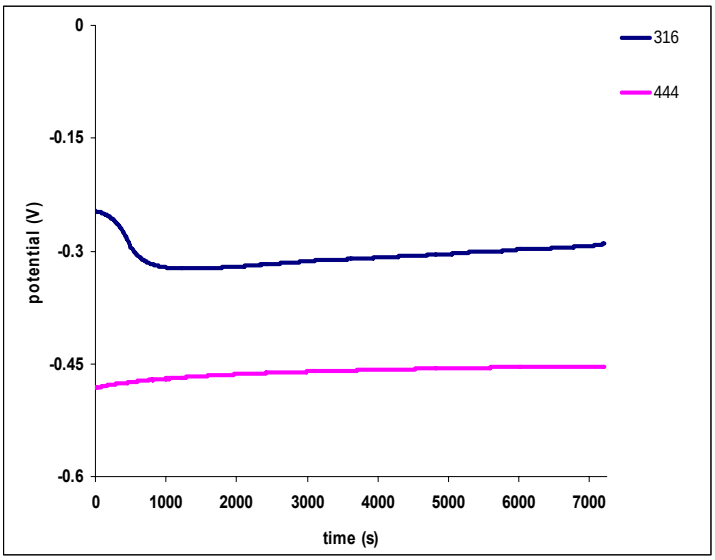

Figure 5.6: Open circuit potential of both alloys in 1 M H_2SO_4 + 3.5 %NaCl.

5.3 POTENTIODYNAMIC TESTS

Cyclic potentiodynamic polarization measurements were carried out to determine the corrosion rates, evaluate the passivity behavior, and to determine the pitting and repassivation behavior of the alloys in various solutions. The comparative corrosion behaviour of alloys 444 and 316 in 0.1 and 1 molar sulphuric acid solution containing 3.5 % NaCl is summarized in Table 5.3 and graphically represented in Figures 5.7 and 5.8. Both alloys were observed to display distinct active to passive transition regions in both solutions with the 444 alloy having more pronounced features in this regard than the curves of the 316 alloy. In all the solutions investigated, alloy 316 displayed a more noble corrosion potential than alloy 444, thus indicating a lower tendency to undergo corrosion. In the two chloride containing media, the corrosion potential values remain very similar despite the increase in the concentrations of the solutions. The passive current densities and the corrosion rates of alloys 444 and 316 were observed to be within the same range with similar magnitude in both solutions.

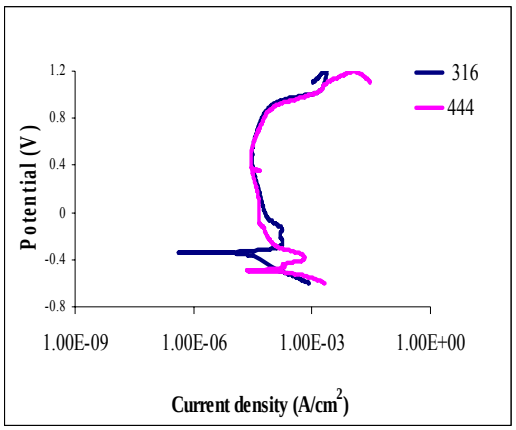

Figure 5.7: Cyclic potentiodynamic polarization curve of both alloys in 0.1 M H_2SO_4 + 3.5 %NaCl.

In the 1 M sulphuric acid solution containing 3.5 % NaCl, the corrosion current density of alloy 444 were two orders of magnitude higher than those of the 316 alloys. As the concentration of the sulphuric acid solution increases, and active corrosion sets in, there is a noticeable difference between corrosion resistance of alloy 316 compared to alloy 444. There was no noticeable difference in the i_{corr} and i_{crit} values between the SO_4^{2-} and Cl^- media. This may be possibly due to the insignificant difference in the extent of change of the oxide film on the steel surface by the electrolyte species.

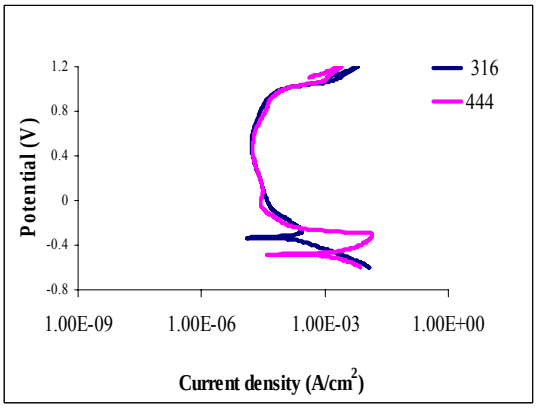

Figure 5.8: Cyclic potentiodynamic polarization curve of both alloys in 1 M H_2SO_4 +3.5 % NaCl.

Alloy 444 displayed the lowest corrosion rate in 0.1M sulphuric acid solution containing 3.5 % NaCl and the highest in the 0.1M sulphuric acid alone. At an increased concentration, alloy 444 was observed to be generally more resistant in

hydrochloric acid compared to sulphuric acid and sulphuric acid containing 3.5 % NaCl. In 0.1 M sulphuric acid solutions alloy 316 displayed a more noble corrosion potential as compared to the chloride containing solutions. Alloy 444, on the other hand, displayed a more noble potential in sulphuric acid solution containing 3.5 % NaCl as compared to hydrochloric acid.

At 1M concentration, alloy 316 displayed a higher corrosion rate in hydrochloric acid than in sulphuric acid. It was observed that both alloys generally exhibited higher corrosion resistance in hydrochloric acid compared to sulphuric acid solution. Similar observation made by Ameer *et al.* (2004) showed that the corrosion rate of the alloy tested was higher in the sulphate medium as compared with the chloride solution at comparable concentration. Betova *et al.* (2002) also reported that the rate of transpassive dissolution of highly alloyed stainless steels is the lowest in chloride solutions and the highest in sulphate electrolytes. According to Olefjord *et al.* (1985), the chloride ions can be incorporated into the passive film when a Mo-containing stainless steel was exposed in hydrochloric acid at various potentials in the active and passive ranges of the alloys. It is suggested that molybdenum can form strong soluble oxochloro-complexes, which thereby will decrease the free Cl^- ion concentration close to surface during passivation. The presence of an adequate amount of chromium is also indispensable for the improvement of pitting resistance (Sugimoto and Sawada, 1976).

Table 5.3: Corrosion data obtained from cyclic potentiodynamic curves of alloy 444 and alloy 316 in 0.1 M and 1 M sulphuric acid solutions.

Corrosion media	Alloy type	E_{corr} (V)	I_{corr} (A/cm^2)	i_{corr}(A)	i_{crit}(A/cm^2)	$I_{passive}$(A/cm^2)	Corrosion Rate (mm/yr)
0.1M H_2SO_4 + Cl^-	444	-0.428	1.4E-6	3.2E-6	5.3E-4	7.1E-4	1.6E-2
	316	-0.361	1.2E-6	2.7E-6	4.6E-5	1E-4	1.3E-2
1MH_2SO_4 + Cl^-	444	-0.49	1.2E-4	2.8E-4	1.2E-2	1.7E-4	1.3E+0
	316	-0.333	6.6E-6	1.5E-5	2.6E-4	1.7E-4	6.9E-2

5.4 THE CORRELATION BETWEEN THE WEIGHT LOSS AND ELECTROCHEMICAL RESULTS

A comparison of the corrosion rates of alloy 444 and 316 determined by mass loss and electrochemical tests both at 0.1 M and 1 M concentrations is as shown in Figures 4.9 to 4.12. The value of the corrosion rate obtained through polarization measurements for alloy 316 in 0.1 M sulphuric acid containing 3.5 % NaCl was slightly higher than the corrosion rate of the direct evaluation from mass loss data. The corrosion rates of alloy 316 in 1 M sulphuric acid containing 3.5 % NaCl from the polarization test were two order magnitudes lower than those obtained from the mass loss evaluations. The corrosion rate from mass loss measurements was higher than that of polarization measurements for alloy 444. In 0.1 molar sulphuric acid containing 3.5 % NaCl, the corrosion rate of alloy 444 calculated from the polarization test was about three times lower than that obtained from the mass loss test.

5.5 CHRONOAMPEROMETRIC STUDIES

Chronoamperometric tests were carried out to further assess the pitting corrosion behavior of the alloys and to determine stability of the passive films formed in the sulphuric acid containing 3.5 % NaCl solutions. Chronoamperometric behavior was studied for about eight hours at 0.2 V and 0.6 V applied potentials, both which were within the passivity regions obtained from the cyclic potentiodynamic polarization measurements.

The chronoamperometry curves for alloys 316 and 444 in sulphuric acid containing 3.5 % sodium chloride at 0.2 V and 0.6 V are represented in Figures 5.9a and 5.9b respectively. Current spikes were completely absent in the chronoamperometry curves of both alloys in the chloride containing solution at 0.6 V and for alloy 444 at 0.2 V. This indicated that stable films were formed on the surface of both alloys. The recorded passive current density for alloy 316 at 0.6 V was noted to decrease sharply before reaching a stable value after about 810 seconds and then increased slightly but remain stable after about 10000 seconds, and no current spikes were formed. The passive current density for the alloy 444 first started to decrease due to the initial passivation of the surface. After approximately 612 seconds, it suddenly started to

increase as a result of the localized dissolution (pitting) of the passive film. A steady-state (localized) dissolution of the film, characterized by high current density of 0.002 A/cm^2 was reached after 26300 seconds. No current spikes could be observed on this curve. At 0.2 V, no current spike was observed on the alloy 444 curve, but some current spikes were observed on the alloy 316 curve. The result at 0.2 V showed that alloy 444 seems to form a more stable passive film than alloy 316.

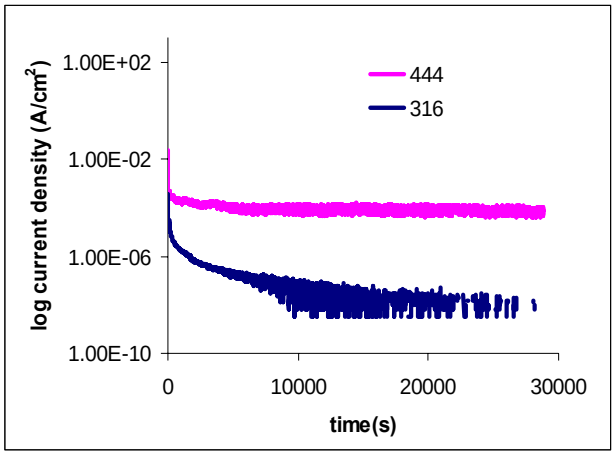

a

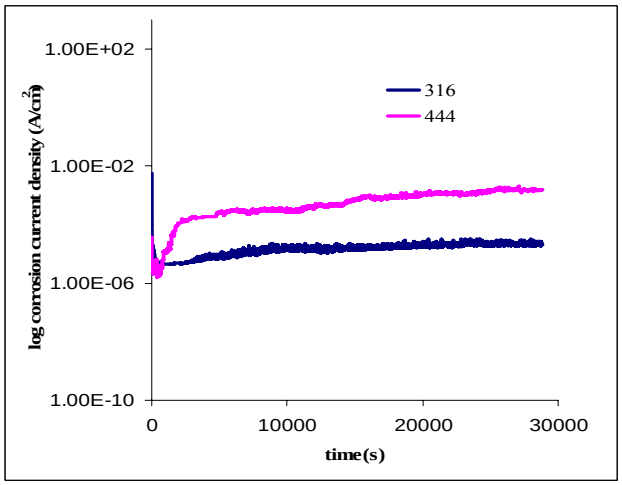

b

Figure 5.9: Chronoamperometry curves of the alloys 316 and 444 in 0.1 M H_2SO_4 + Cl^- at (a) 0.2 V (b) 0.6 V.

5.6 Microstructural studies of both alloys in 0.1 M sulphuric acid containing 3.5 % NaCl

Similar to the optical micrographs observed for alloy 316 in sulphuric acid, the optical micrograph of alloy 316 showed randomly dispersed pits in sulphuric acid containing 3.5 % NaCl as shown in Figure 5.10. Alloy 444 was observed to form pits in the grains rather than on the grain boundaries. The microstructure of alloy 316 after immersion in sulphuric acid containing 3.5 % NaCl did not show much similarity with the as-received sample. However, alloy 444 showed some similarity in its grain sizes and it seems that no alterations occurred.

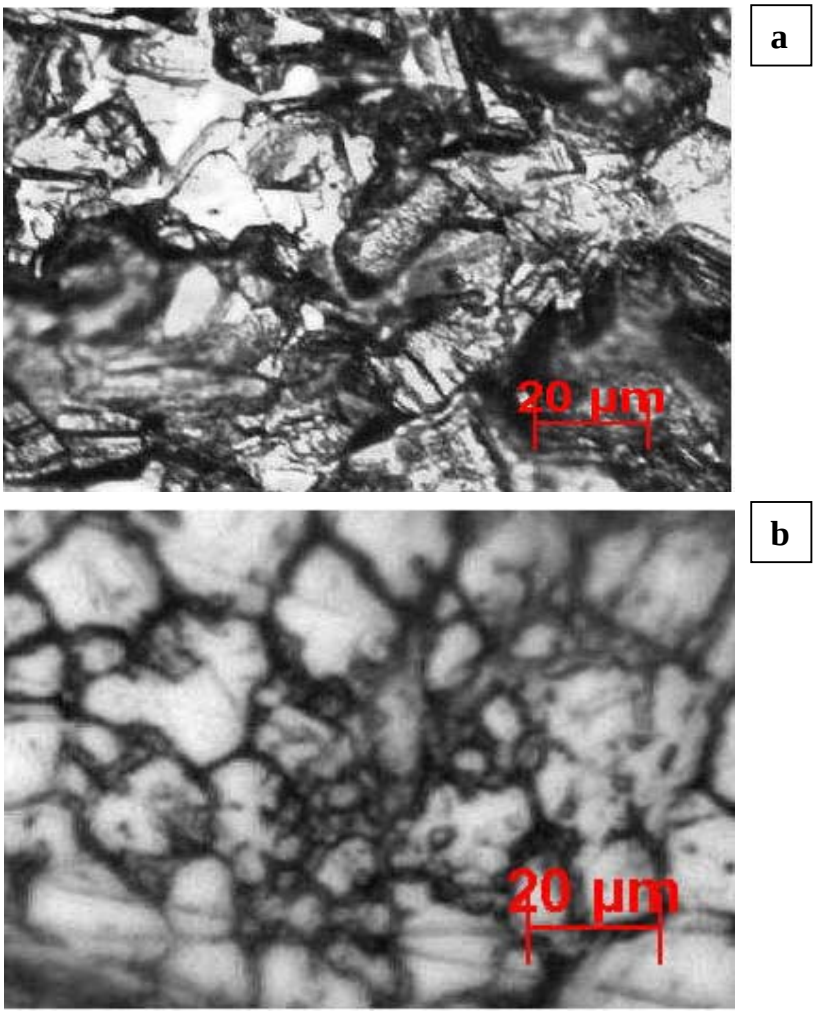

Figure 5.10: Typical optical microstructure of both alloys after immersion in 0.1 M sulphuric acid containing 3.5 %NaCl for 92 days (a) 444 (b) 316.

5.6.1 Morphological studies of both alloys after immersion test in sulphuric acid containing 3.5 % NaCl solution

The micrographs obtained from the SEM study of the overall surface of both alloys after immersion in sulphuric acid containing 3.5 % NaCl solution for 92 days is shown in Figures 5.11 and 5.12. The micrographs show the morphology of the alloys. Randomly dispersed pits were observed on the surface of alloy 316. The pits of alloy 444 were observed to form in the grains rather than on the grain boundaries. Parallel features were observed on the surface of alloy 444 which could result from corrosion of the alloy. The EDX line profiles of the alloys are shown in Figures 5.11 and 5.12 and are summarised in Tables 5.4 and 5.5. The EDX obtained for each of the alloys were similar in all the solutions with slight differences in the composition of the elements.

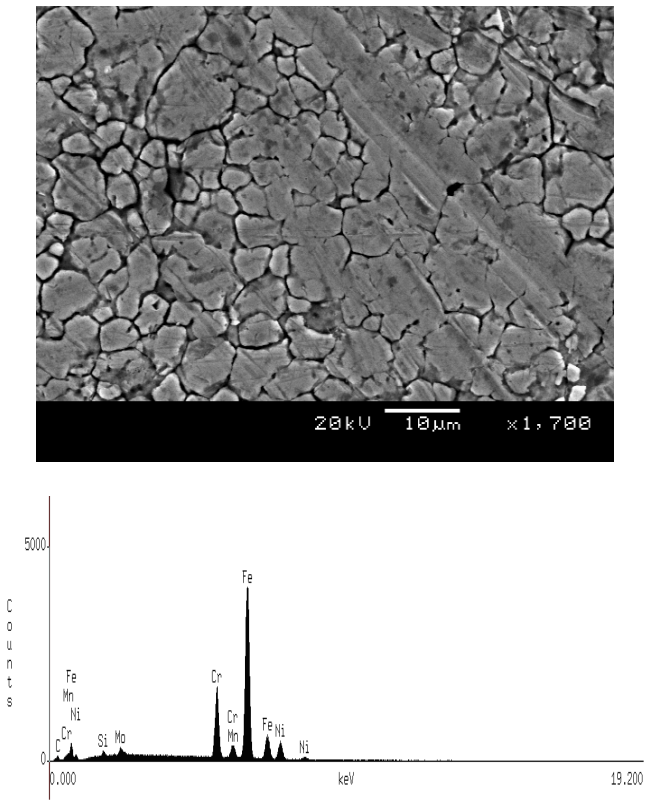

Figure 5.11: SEM/EDX of alloy 316 after immersion in 0.1 M sulphuric acid containing 3.5 % NaCl for 92 days.

Table 5.4: Summary of EDX obtained for alloy 316 in sulphuric acid containing 3.5 % NaCl for 92 days.

Element	Si	Cr	Mn	Ni	Mo	C	Fe
Wt %	0.4 ± 0.1	16.4 ± 0.2	1.8 ± 0.2	10.3 ± 0.4	1.5 ± 0.3	0.7 ± 0.1	68.9 ± 0.5

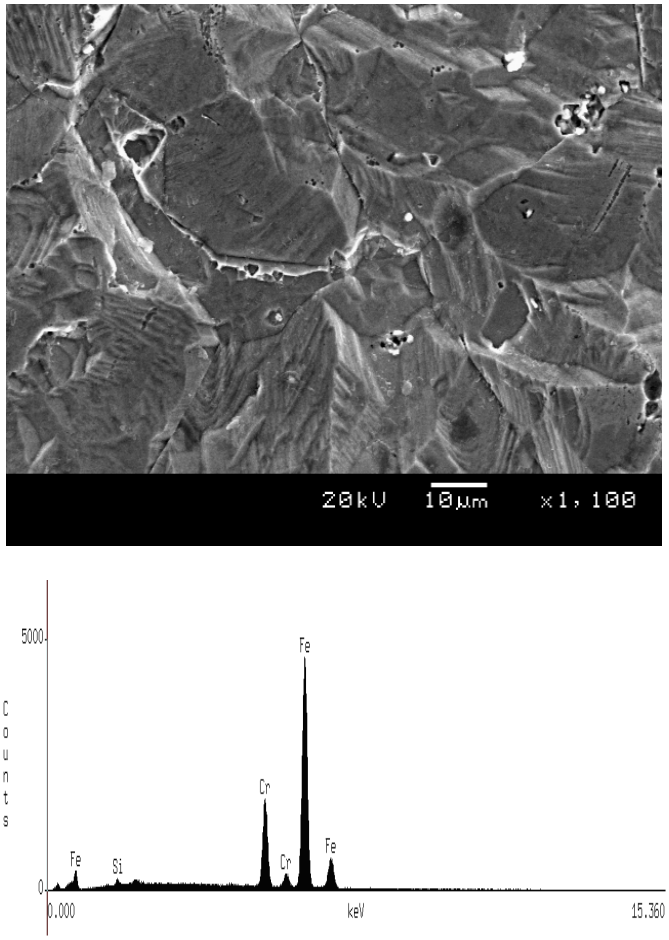

Figure 5.12: SEM/EDX of alloy 444 after immersion in 0.1 M sulphuric acid containing 3.5 % NaCl for 92 days.

Table 5.5: Summary of EDX obtained for alloy 444 in sulphuric acid containing 3.5 % NaCl for 92 days.

Element	Si	Cr	Fe
Wt %	0.6 ± 0.1	18.2 ± 0.2	78.8 ± 0.5

5.6.2 Morphological studies after polarisation test

An important consideration regarding corrosion resistance of the studied alloys is the structure and type of corrosion products that may form once active corrosion or passivation occurs. Based on the alloy compositions of the materials considered, a preliminary survey of the relevant properties of possible oxides which may be formed was conducted using SEM/EDX. The corroded alloys were examined to determine the corrosion products formed on the alloys. EDX was taken to verify the mechanism of corrosion products film formation on stainless steel surface.

5.6.3 Morphological studies of alloy 316 after corrosion in sulphuric acid containing 3.5 % NaCl solution

The micrograph obtained from the SEM study of alloy 316 after corrosion in sulphuric acid containing 3.5 % NaCl is shown in Figure 5.13. The EDX line profiles from the corrosion products on the alloy indicated the presence of iron, chromium, manganese, nickel, oxygen, carbon and aluminium and a trace of titanium which could be a contaminant. However, on the main surface of the alloy, carbon, chromium, silicon, nickel and iron were observed. The presence of oxygen and carbon was an indication of oxides and carbides formation on the surface of the alloy. The possible oxides could be chromium oxide, iron oxide, aluminum oxide, nickel oxide and silicon oxides. The Raman spectra of alloy 316 after corrosion confirmed the presence of nickel oxide in the corrosion products. On the other hand, chromium carbide could be present on the main surface and in the corrosion products. Although molybdenum and nitrogen were not observed in both spectra, Raman spectra showed the presence of molybdenum oxides.

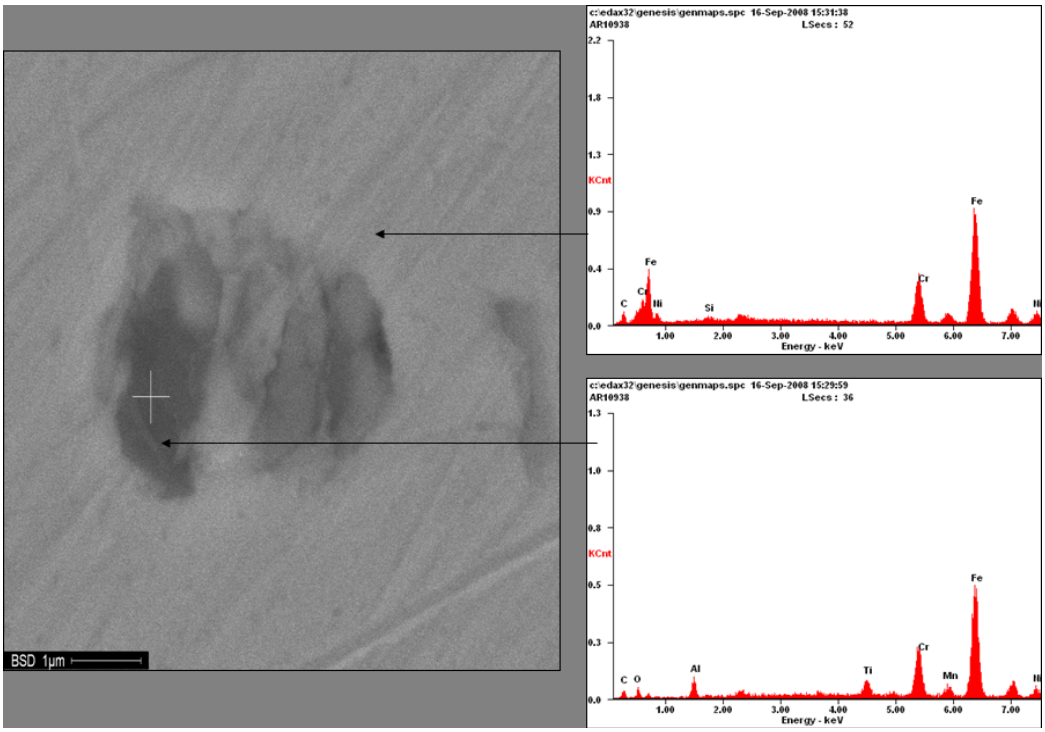

Figure 5.13: SEM scan obtained from the surface of alloy 316 after corrosion in sulphuric acid containing 3.5 % NaCl.

5.6.5 Morphological studies of alloy 444 after corrosion in sulphuric acid containing 3.5 % NaCl solution

The corroded alloy 444 exposed to sulphuric acid containing 3.5 % NaCl was studied by SEM and analysed with EDX, as is shown in Figure 5.14. Three spectra were recorded on the surface of the alloy. Pits were observed on the surface of the alloy containing some corrosion products. In the pits, titanium, iron, chromium, aluminum, chlorine, oxygen, carbon, silicon and manganese were the elements observed. The presence of oxygen and carbon indicated the possible formation of oxides and carbides. The peak of carbon in the results was observed to be high. However, from the compositions of the alloy, there was a little carbon. This high carbon content could be from the carbon used in coating the alloy prior to the SEM study. The elements observed in the corrosion products were carbon, oxygen, silicon, chromium, molybdenum, chlorine, titanium and iron. However, on the main surface of the alloy, only four elements were observed. These elements were carbon, iron, silicon and chromium, with iron being the most prominent.

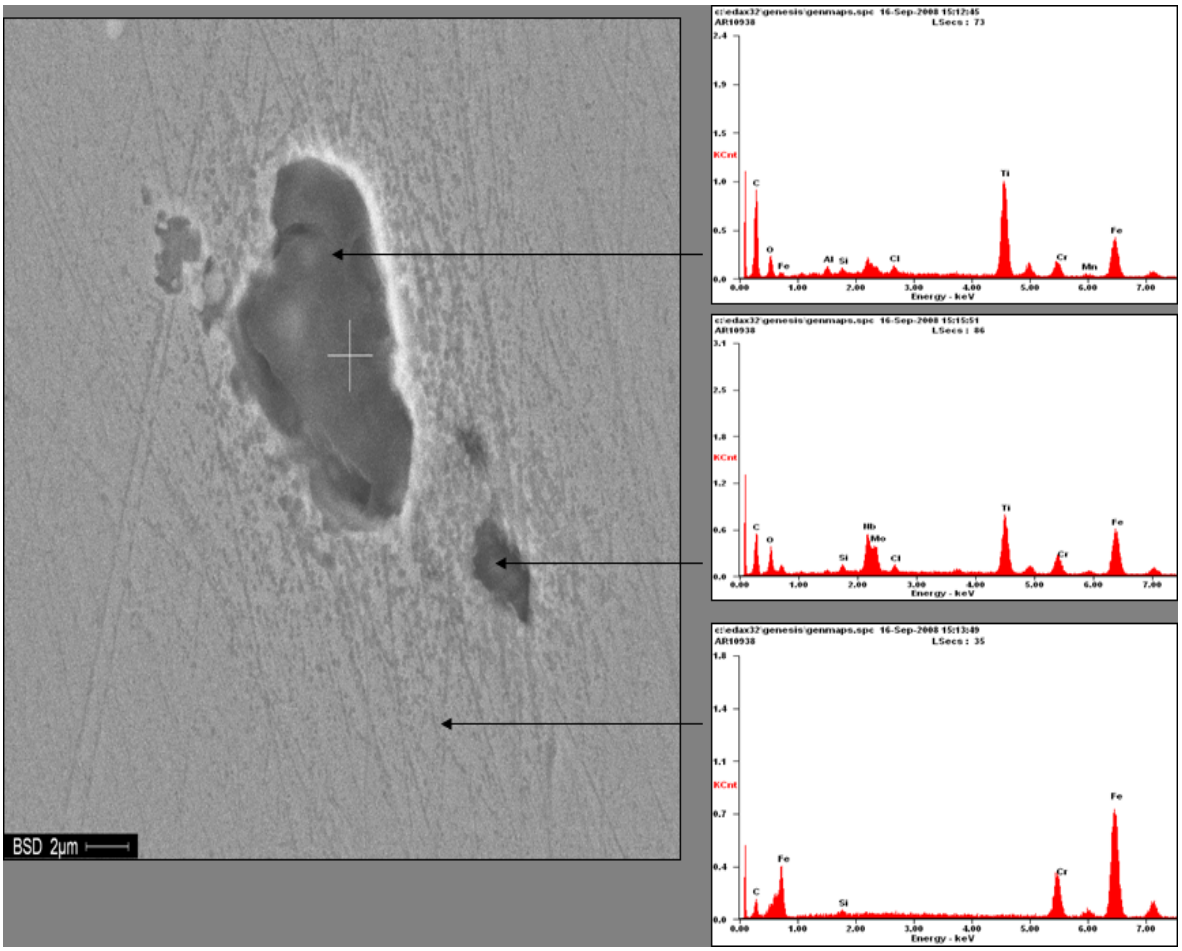

Figure 5.14: SEM scan obtained from the surface of alloy 444 after corrosion in sulphuric acid containing 3.5 % sodium chloride.

5.7 PHASE IDENTIFICATION STUDIES

5.7.1 X-ray diffraction of the corrosion products on alloy 316 after polarization

The XRD patterns obtained from the surface of the as-received alloy 316 and after the corrosion studies in sulphuric acid containing 3.5 % NaCl are presented in Figures 4.24 and 5.15 respectively. A comparative study of the two patterns indicated some changes that occurred after the test. Peaks at 2θ positions 28 and 44.6 ^{0} were not observed on the XRD pattern obtained from alloy 316 after the corrosion test. In Figure 5.15 peaks' heights were observed to be 2080, 1683, and 5443 counts at 2θ positions of 43.6, 50.7 and 74.6 ^{0} respectively. The result shows that the peaks' heights increased after corrosion. XRD patterns obtained after the corrosion of alloy 316 in sulphuric acid and sulphuric acid containing 3.5 % NaCl shows that the

chloride addition did not have any specific effect on the corrosion process. However, the addition of chloride to sulphuric acid solution increased the peak heights of the alloy.

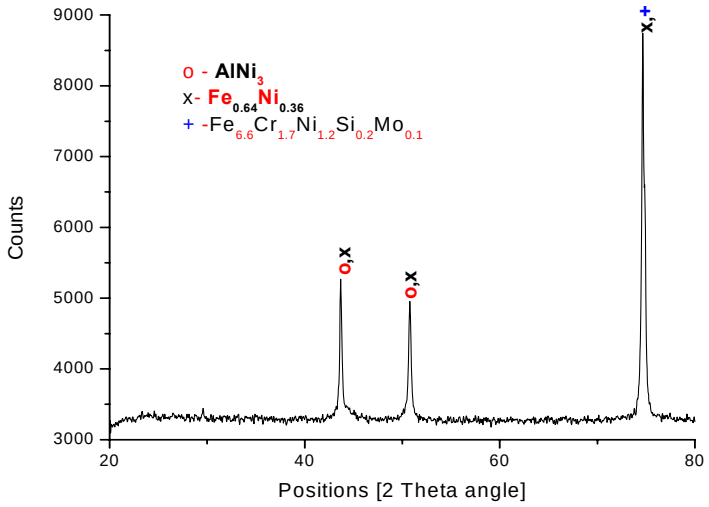

Figure 5.15: X-ray diffraction patterns of alloy 316 after corrosion in sulphuric acid containing 3.5 % NaCl (00-050-1293, 00-047-1405 and 00-050-1293).

5.7.2 X-ray diffraction of the corrosion products on alloy 444 after polarization

The details of the phase constituents present on the surface of alloy 444 after the corrosion test in sulphuric acid containing 3.5 % NaCl solution is presented in figure 5.16. Figures 4.23 and 5.16 show the XRD patterns of alloy 444 as-received and after its exposure to sulphuric acid containing 3.5 % NaCl. The peaks were observed at 2θ positions of 44.5 and 64.5 ^{0}. The peaks' heights observed at these angles were 15859.6 and 864.3 counts respectively. The XRD spectra show that iron and chromium were the elements mostly making up the structures observed on the alloy surface after corrosion. The results show that the as-received sample and the alloy after the corrosion test virtually constituted the same structures but in different ratios.

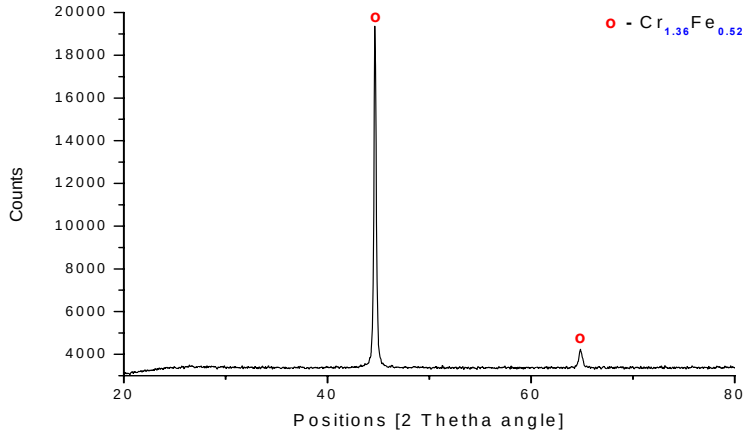

Figure 5.16: X-ray diffraction patterns of alloy 444 after corrosion in sulphuric acid containing 3.5 % NaCl (00-041-1224).

5.8 RAMAN SPECTRA

5.8.1 Raman spectra of corrosion products formed on alloys in sulphuric acid solution containing 3.5 % NaCl

The Raman spectra of alloy 444 and alloy 316 after corrosion in sulphuric acid containing 3.5 % NaCl are shown in Figures 5.17 and 5.18. The summary of the Raman spectral shifts of alloy 316 and alloy 444 compared to other observations from other studies prior to this work is shown in Table 5.6. The Raman spectrum of alloy 316 presents bands at 466, 404, 357, and 212 cm^{-1} associated with NiO, γ-Fe_2O_3 and $Mo_7O_{24}^{6-}$ (357 and 212 cm^{-1}) respectively. Raman bands for alloy 444 were observed at 275, 398 and 615 cm^{-1}. These Raman shifts could be attributed to MoO_3, TiO_2 and α-Fe_2O_3 respectively. The Raman spectra of alloy 444 and alloy 316 were observed to be similar in shape. This shape is attributed to the amorphous nature of the corrosion products formed on the alloys. Both alloys exhibited a broad band on their spectra at high intensity. This observation is similar to that obtained for alloy 444 in sulphuric acid and hydrochloric acid which suggested the formation of an amorphous structure and/or fluorescence.

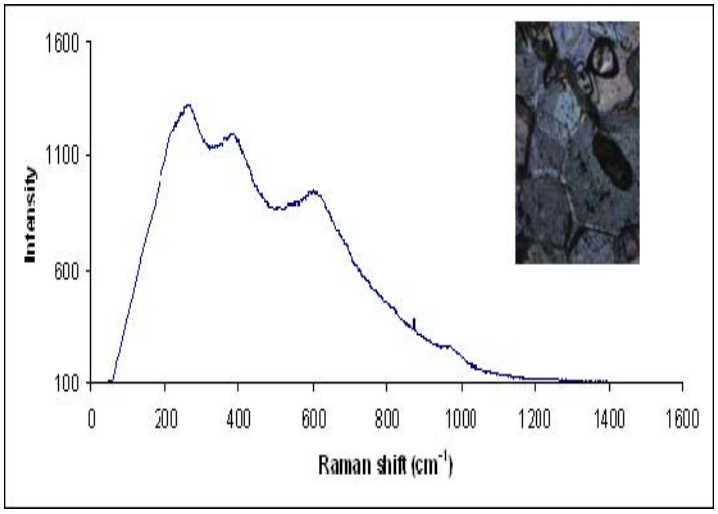

Figure 5.17: Raman spectrum and the image of the overall surface of alloy 444 tested in sulphuric acid containing 3.5 % NaCl.

Table 5.6: Summary of the Raman spectroscopy of the corrosion products formed on alloy 316 and alloy 444 tested in sulphuric acid containing 3.5 % NaCl.

Alloys	**Raman shift (cm^{-1}) from this study**	**Reference (cm^{-1})**	**Probable corrosion product/compound**	**References**
316	466	450	NiO	*Guevara-Lara et al., 2007*
	357	350	$Mo_7O_{24}^{6-}$	*Hart et al. 1976*
	212	210	$Mo_7O_{24}^{6-}$	*Hart et al. 1976*
444	275	282	MoO_3	*Chang et al., 1992*
	398	398	TiO_2	*Guevara-Lara et al., 2007*
	615	613	α-Fe_2O_3	*McCarty and Boehme,1989; Gui and Devine, 1991*

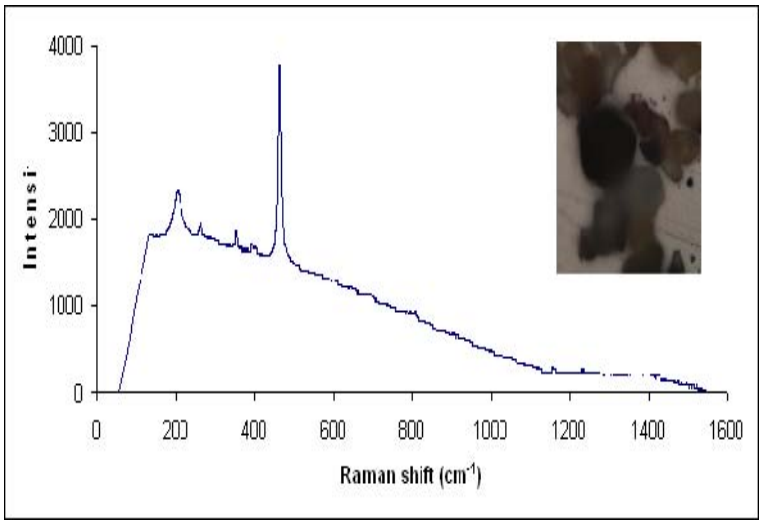

Figure 5.18: Raman spectrum and the image of the overall surface of alloy 316 tested in sulphuric acid containing 3.5 % NaCl.

5.9 THE CORRELATION BETWEEN ALL THE SURFACE ANALYSES TECHNIQUES.

Similar to the observation in sulphuric acid solution, the micrographs obtained from the SEM, Raman spectroscope and optical microscope both of the as-received and after corrosion occurrence were found to be similar. Alloy 444 was observed to be coarser than alloy 316 after the immersion in this solution. The morphology of the as-received samples of alloy 444 and that of alloy 444 after the immersion tests show that there was no difference in the grain sizes. Alloying elements affect the microstructure, which in turn can significantly influence the overall corrosion behavior of the alloy. Chromium, molybdenum and nitrogen are the alloying elements that could increase the resistance of stainless steels to both pitting and crevice corrosion. In a chloride environment, nickel could form a stable passive nickel oxide layer, according to Jiangzhou and Wang (2001); Singh and Singh (2002); Abd El Aal (2003) and Munoz *et al*. (2006. More noticeable pits were observed on the surfaces of the alloys in sulphuric acid solution compared to when chloride ion was added to sulphuric acid, which is contrary to conventional wisdom and expectations. It seems that stable and uniform films were formed on the surface of both alloys on addition of chloride ions to sulphuric acid solution. The reason why there was more corrosion in the sulphate environment compared to one containing both sulphates and chlorides

requires more investigation. However, it was confirmed by similar observations of Ameer *et al.* (2004), who showed that the corrosion rate of the alloys tested was higher in the sulphate medium as compared with the chloride solution at comparable concentration. Betova *et al.* (2002) also reported that the rate of transpassive dissolution of highly alloyed stainless steels is the lowest in chloride solutions and the highest in sulphate containing media. Clayton and Lu (1986) reported that molybdenum additions could aid the development and stability of an amorphous passive film which further provides resistance against $C1^-$ ion attack and subsequent pitting.

CHAPTER SIX

6.0 CORROSION BEHAVIOUR OF ALLOY 316 AND ALLOY 444 IN HYDROCHLORIC ACID

Chapters Four and Five have already dealt with the corrosion behaviour of alloy 444 and alloy 316 in sulphuric acid and sulphuric acid containing 3.5 % NaCl solution. This present chapter deals with the corrosion behaviour of both alloys in hydrochloric acid considering the effect of chloride ion on the alloys in the absence of sulphate ions with detailed discussion.

6.1 WEIGHT LOSS TESTS

The corrosion behaviour of the alloys in 0.1 M hydrochloric acid solutions was studied for 92 days while their behaviour in 1 M solution was evaluated over a period of 12 days.

6.1.1 Corrosion kinetics of both alloys in 1 M hydrochloric acid

The variation of the cumulative weight loss as a function of exposure time for alloy 316 and alloy 444 is shown in Table 6.1 and graphically represented in Figure 6.1. The corrosion rates of alloy 444 and alloy 316 as a function of time is shown in Figure 6.2a and 6.2b and is shown in Table 6.2. Alloy 444 and alloy 316 showed an increase in weight loss with the time of immersion in the 1 M hydrochloric acid solution. This increase in weight loss with time was more significant for alloy 444 than for alloy 316. Typical breakdown of the passive film and repassivation of the alloy behavior was observed in the corrosion rates of both alloys in 1 M hydrochloric acid solution. The corrosion rates of 316 are lower than those of 444, indicating that 316 is the more resistant alloy of the two. Corrosion rates of alloy 444 in 1 M hydrochloric acid solution was observed to increase with time. However, there was instability in the corrosion rates of alloy 316. There was an initial decrease followed by an increase. The corrosion rates of both alloys in 1 M hydrochloric acid were observed to be higher than their corrosion rates in 0.1 M hydrochloric acid solutions.

Table 6.1: Cumulative weight loss of alloy 444 and alloy 316 in 1 M hydrochloric acid.

Time(days)	Cumulative weight loss (g/cm^2)	
	444	316
1	1.39×10^{-2}	2.00×10^{-3}
2	4.80×10^{-2}	5.07×10^{-3}
3	8.80×10^{-2}	6.93×10^{-3}
4	1.28×10^{-1}	8.80×10^{-3}
5	1.87×10^{-1}	1.04×10^{-2}
6	2.67×10^{-1}	1.17×10^{-2}
7	3.10×10^{-1}	1.49×10^{-2}
8	3.80×10^{-1}	1.65×10^{-2}
9	5.17×10^{-1}	1.81×10^{-2}
10	6.11×10^{-1}	2.11×10^{-2}
11	6.75×10^{-1}	2.35×10^{-2}
12	7.71×10^{-1}	2.53×10^{-2}

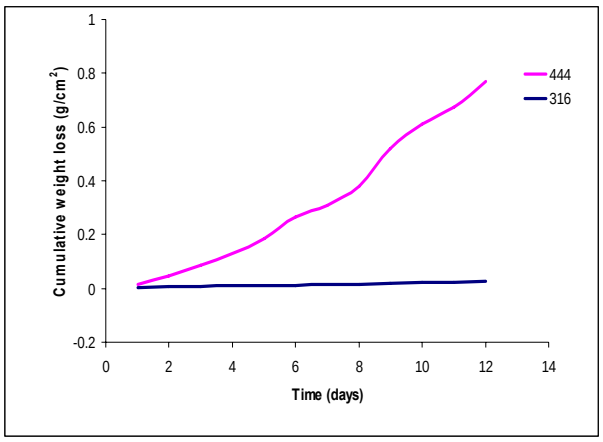

Figure 6.1: Cumulative weight loss of (a) alloy 444 (b) alloy 316 in 1 M hydrochloric acid as a function of immersion time.

Table 6.2: Corrosion rates of alloy 444 and alloy 316 in 1 M hydrochloric acid.

Time(days)	Corrosion rate (μm/yr)	
	444	316
1	6.53×10^{4}	9.13×10^{2}
2	1.13×10^{4}	1.16×10^{3}
3	1.38×10^{4}	1.06×10^{3}
4	1.51×10^{4}	1.01×10^{3}
5	1.76×10^{4}	9.50×10^{2}
6	2.09×10^{4}	8.93×10^{2}
7	2.09×10^{4}	9.75×10^{2}
8	2.24×10^{4}	9.44×10^{2}
9	2.71×10^{4}	9.20×10^{2}
10	2.88×10^{4}	9.62×10^{2}
11	2.89×10^{4}	9.75×10^{2}
12	3.02×10^{4}	9.64×10^{2}

Table 6.3: Summary of the corrosion rates of both alloys in 1 M of all the solutions for 12 days.

Alloy	Corrosion rate (μm/yr)		
	H_2SO_4	HCl	H_2SO_4 + 3.5 % NaCl
316	2.80×10^{1}	9.76×10^{2}	3.25×10^{2}
444	3.26×10^{4}	1.89×10^{4}	4.90×10^{4}

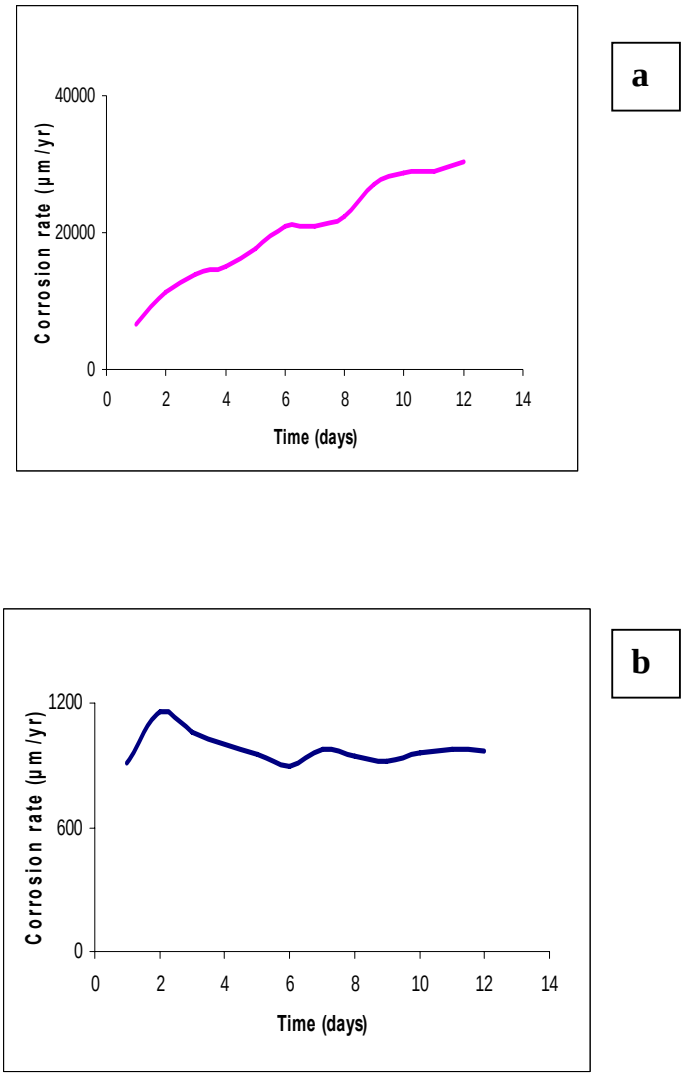

Figure 6.2: Corrosion rates of (a) alloy 444 (b) alloy 316 in 1 M hydrochloric acid as a function of immersion time.

6.1.2 Corrosion behavior of both alloys in 0.1 M hydrochloric acid

The patterns observed for the cumulative weight loss versus the immersion time for both alloys in 0.1 M hydrochloric acid are presented in Figures 6.3 and 6.4. Alloy 316 exhibited lower weight loss in 0.1 M hydrochloric acid compared to alloy 444. The weight losses of alloy 316 in hydrochloric acid were observed to be similar to those obtained in 0.1 M sulphuric acid solution. Alloy 444 exhibited a lower weight loss in 0.1 M hydrochloric acid compared to the other two solutions of study. It was observed that the corrosion rates of both alloys in 0.1 M hydrochloric acid initially increased followed by a steady state decrease with an increase in immersion time. A comparison

of alloy 444 with alloy 316 in all the solutions showed that alloy 316 was more corrosion resistant than alloy 444. This correlates with the higher molybdenum and nickel content of alloy 316.

Table 6.4: Summary of the corrosion rates of both alloys in 0.1 M of all the solutions for 92 days.

Alloy	Corrosion rate (µm/yr)		
	H_2SO_4	HCl	H_2SO_4 + 3.5 % NaCl
316	1.50×10^1	1.60×10^1	1.00×10^1
444	1.65×10^3	6.60×10^2	1.5×10^3

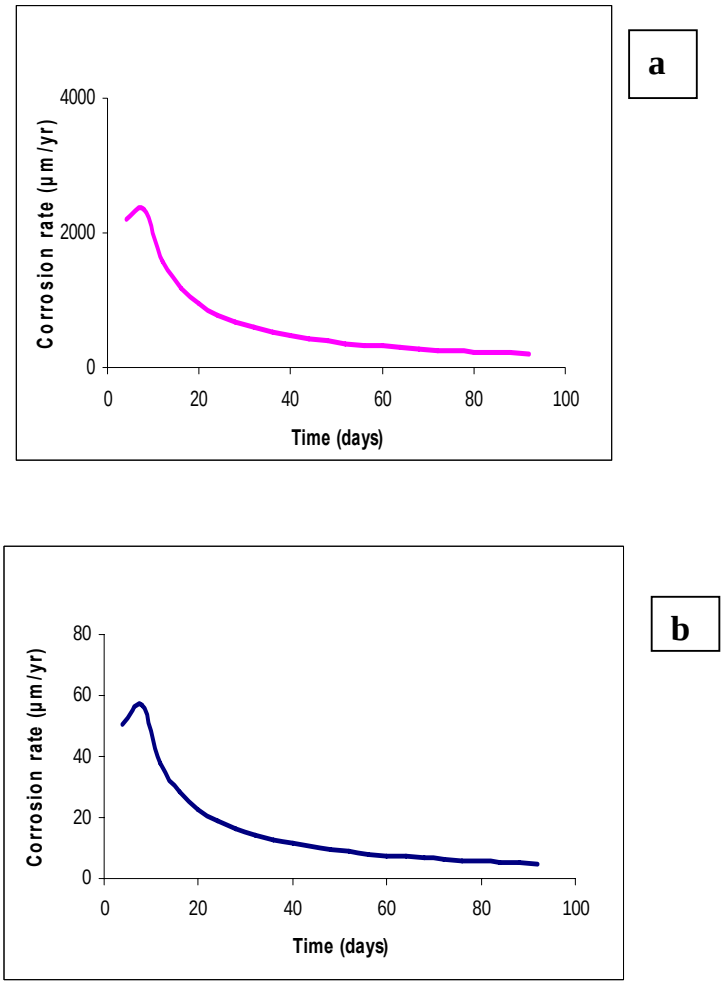

Figure 6.3: Corrosion rates of (a) alloy 444 (b) alloy 316 in 0.1 M hydrochloric acid as a function of immersion time.

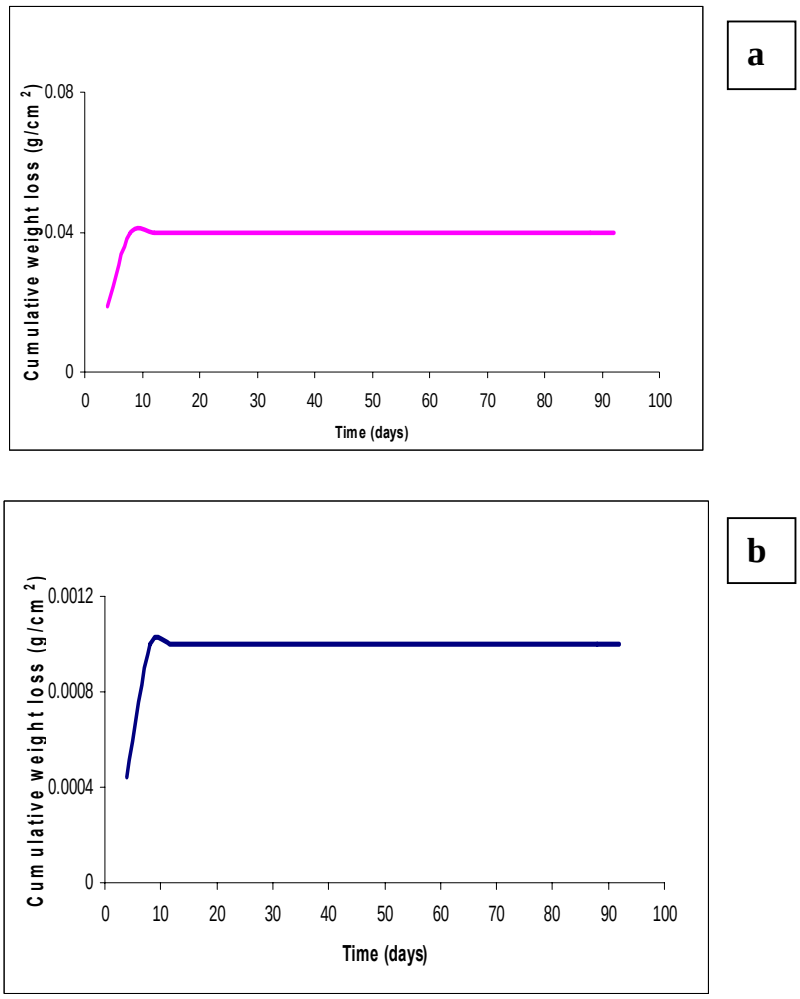

Figure 6.4: Cumulative weight loss of (a) alloy 444 (b) alloy 316 in 0.1 M hydrochloric acid as a function of immersion time.

6.2 OPEN CIRCUIT CORROSION POTENTIAL VARIATIONS WITH TIME OF BOTH ALLOYS IN HYDROCHLORIC ACID

The variation of the OCPs of the alloys in 0.1 M and 1 M hydrochloric acid is shown in Figures 6.5 and 6.6. Alloy 316 exhibited similar behavior as alloy 444 in 0.1 M hydrochloric acid. In 0.1 M hydrochloric acid, the corrosion potential of both alloys was observed to generally shift toward positive values. Similar to the behavior of alloy 444 in 0.1 M hydrochloric acid, there was a small and progressive increase in potential of alloy 444 in 1 M hydrochloric acid from more negative values to positive

values with time. On the other hand, alloy 316 displayed an initial decrease in potential with time before increasing to more positive values. The OCP values for alloy 444 were lower than that of the alloy 316.

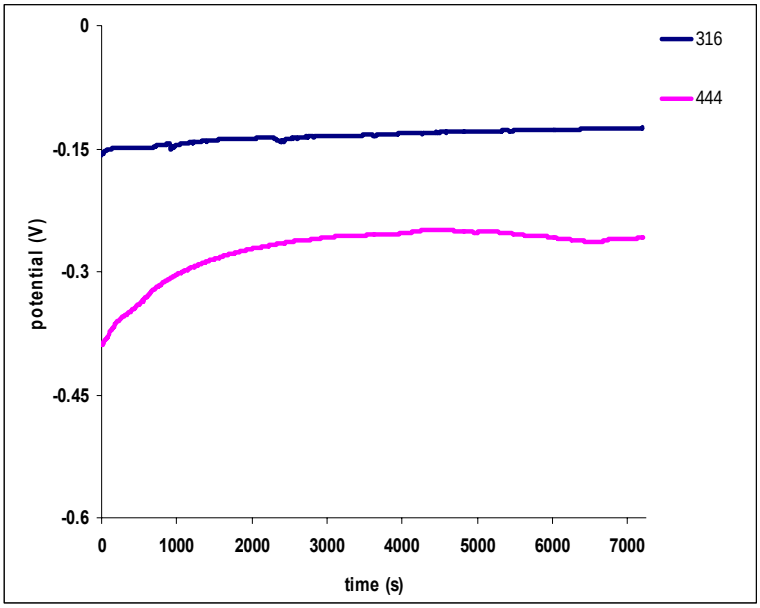

Figure 6.5: Open circuit potential of both alloys in 0.1 M HCl.

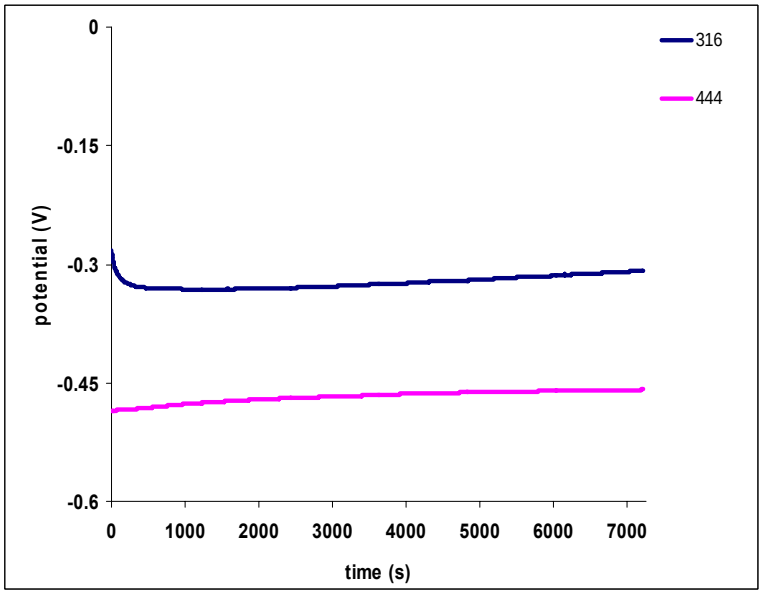

Figure 6.6: Open circuit potential of both alloys in 1 M HCl.

6.3 POTENTIODYNAMIC TESTS

The results for the corrosion potentials, corrosion current, corrosion current densities, and the corrosion rates that were derived from the electrochemical tests for alloys 316 and 444 in 0.1 and 1M hydrochloric acid solutions are summarized in Table 6.5, while Figures 6.7 and 6.8 give a graphical representation of the responses to polarization. It is observed that both alloys display distinct and typical active to passive transition behavior during polarization from active to more noble potentials, with the 444 alloy having more pronounced features in this regard than the curves of the 316 alloy. This behaviour was more distinct in 1 M solution than in 0.1 M solutions. It was observed that in all the solutions investigated, the 316 alloy displayed a more noble corrosion potential than the 444 alloy, thus indicating a lower predisposition to undergo corrosion. The critical current densities are substantially lower for the 316 alloy in comparison to the 444 alloy ones, with a one order of magnitude difference. Alloy 444 displayed a larger passive range than alloy 316 in the 0.1 M solution, but no passive region was observed for both alloys in 1 M of the hydrochloric acid solutions. The passive current densities of alloy 444 were greater than those of alloy 316 in both hydrochloric acid solutions, and the difference between them becomes larger and more noticeable with an increase in the concentration of the hydrochloric acid solution from 0.1 M to 1 M. The same type of phenomenon is seen in the corrosion current densities, where the values from the 444 alloy are always greater than those from the 316 alloys. The type 444 alloy displayed a higher corrosion rate than the type 316 alloy under all experimental conditions investigated. In 0.1 M hydrochloric acid solution, the corrosion rate of the type 444 alloy was two orders of magnitude higher than those of the 316 alloy, but in the 1 M solution the magnitude was one order difference.

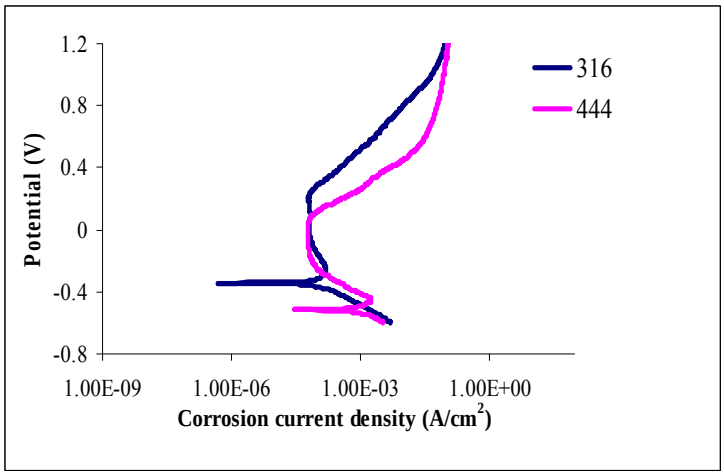

Figure 6.7: Cyclic potentiodynamic polarization curve of both alloys in 0.1 M HCl.

It was observed that when the alloys were immersed in the solution for the electrochemical tests, the solution turned to a dark green colour within the first 10 minutes. The colour change when alloy 316 was immersed was not as intense as it was for alloy 444. Similar observations were made by Pardo *et al.* (2008) when carrying out an investigation on the influence of manganese and molybdenum additions on corrosion resistance of AISI 304 and 316 stainless steels in 30 wt. % H_2SO_4 at 25 and 50 ^{0}C. These authors observed that when the specimen gets in contact with the sulphuric acid medium, the passive layers of the AISI 304 and AISI 316 completely dissolved and the solution turns to dark green colour typical of the Cr (III) species.

Table 6.5: Corrosion data obtained from cyclic potentiodynamic curves of alloy 444 and alloy 316 in 0.1 M and 1 M hydrochloric acid solutions.

Corrosion media	Alloy type	E_{corr} (V)	I_{corr} (A/cm^2)	i_{corr}(A)	i_{crit}(A/cm^2)	$I_{passive}$(A/cm^2)	Corrosion Rate (mm/yr)
0.1M HCl	444	-0.516	1.3E-5	2.9E-5	1.5E-3	1.1E-4	1.4E-1
	316	-0.346	2.2E-7	4.9E-7	1.3E-4	9.6E-5	2.3E-3
1M HCl	444	-0.493	1.8E-5	4.2E-5	3.2E-2	2.1E-3	2.0E-1
	316	-0.356	9.5E-6	2.1E-5	2.0E-3	1.4E-4	9.9E-2

In all the concentrations of sulphuric acid solutions investigated, both alloys displayed a more noble corrosion potential than in the concentrations of hydrochloric acid solution. This indicates a higher tendency of the alloys to undergo corrosion in hydrochloric acid solution. In 0.1 M hydrochloric acid solution, both alloys displayed lower current densities as compared to 0.1 M sulphuric acid. The increase in the concentration increased the current density of alloy 316 in hydrochloric acid. The critical current densities are substantially higher for the 316 alloy in both hydrochloric acid solutions in comparison to sulphuric acid solutions. Alloy 444 shows different trends; the critical current density was lower in 0.1 M hydrochloric acid solution and was higher as the concentration increased to 1 M as compared to the case in the sulphuric acid solutions. The passive current density of alloy 444 was lower in 0.1 M hydrochloric acid solution compared to 0.1 M sulphuric acid and 0.1 M sulphuric acid containing 3.5 % NaCl solution. The passive current density of alloy 316 was lower in 0.1 M hydrochloric acid compared to 0.1 M sulphuric acid containing 3.5 % NaCl solution, but higher compared to 0.1 M sulphuric acid. The addition of nickel had the tendency to reduce corrosion current density of the alloys. These results are in agreement with Potgieter *et al.* (2008) who reported that in the active region of stainless steels, where preferential dissolution of iron and chromium occurred, the formation of the passive oxide film was responsible for a decrease of the current density. Similar results were found by Bojinov *et al*. (2001) in studies of the electrochemical behaviour of anodic films on pure Cr, Fe–Cr alloys and Fe–Cr–Mo alloys in 1 M sulphuric acid solution.

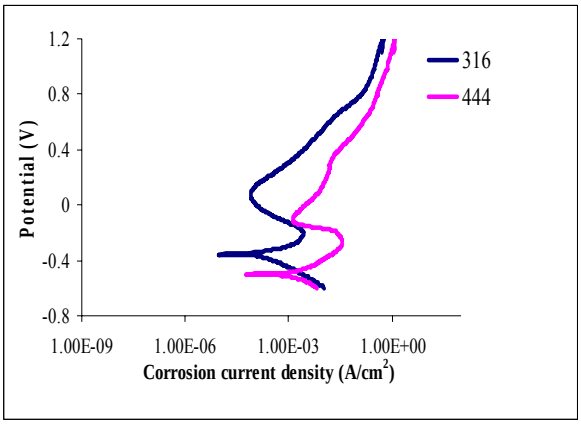

Figure 6.8: Cyclic potentiodynamic polarization curve of both alloys in 1 M HCl.

6.4 THE CORRELATION BETWEEN THE WEIGHT LOSS AND ELECTROCHEMICAL RESULTS

A comparison of the corrosion rates of alloy 444 and 316 determined by mass loss and electrochemical tests both at 0.1 M and 1 M concentrations is shown in Figures 4.9 to 4.12. The value of the electrochemical determination of the corrosion rate, obtained through polarization measurements for both alloys in both concentration of hydrochloric acid were lower than the corrosion rate from the mass loss data. The corrosion rates of alloy 444 in 0.1 M hydrochloric acid of both tests were of the same order of magnitude. However, the corrosion rate of alloy 316 in 0.1 M hydrochloric acid from the mass loss test was two order magnitudes higher than in the electrochemical test. The corrosion rates of alloy 316 in 1 M hydrochloric acid of polarization test were two order magnitudes lower than those obtained from the mass loss tests. The corrosion rate of alloy 444 in 1 M hydrochloric acid for polarization test on the other hand, differed by one order magnitude from the mass loss test value.

Tables 6.3 and 6.4 show the summaries of the corrosion rates obtained from weight loss tests of both alloys in 1 M and 0.1 M concentrations of all the solutions respectively. These summaries give the average obtained by adding the corrosion rates and dividing by the number of days. The corrosion rate of alloy 444 seems to increase in the order hydrochloric acid < sulphuric acid containing 3.5 % NaCl < sulphuric acid although at 1 M concentration, sulphuric acid containing 3.5 % NaCl seems to become the most corrosive medium. The corrosion rate of alloy 316 increased in the order sulphuric acid containing 3.5 % NaCl< sulphuric acid < hydrochloric acid. The order of increase changed to sulphuric acid < sulphuric acid containing 3.5 % NaCl < hydrochloric in 1 M concentration for alloy 316. In 0.1 M concentration, the order of increase in corrosion rates of both alloys in weight loss tests contradicted those obtained from electrochemical test. For alloy 316, the order of increase in electrochemical tests is hydrochloric acid < sulphuric acid < sulphuric acid containing 3.5 % NaCl. The electrochemical test showed that alloy 444 corroded more in sulphuric acid and less in sulphuric acid containing 3.5 % NaCl in 0.1 M solutions. The order of increase in corrosion rate of alloy 316 in 1 M concentration of solution in both test types corresponded with each other, but that of alloy 444 contradicted each other in electrochemical test, where alloy 444 corroded most in sulphuric acid and was more resistant in hydrochloric acid.

6.5 CHRONOAMPEROMETRIC STUDIES

Figure 6.9a and 6.9b show the log corrosion current density versus time curves for the alloy 316 and 444 in hydrochloric acid at 0.2 V and 0.6 V respectively. The curves showed that alloy 316 exhibited an increase of passive current in the middle of the experimental run at 0.6 V. The result from the curve at 0.2 V was similar to the result obtained at 0.6 V, with a difference in the stability time for alloy 316. The behaviour of the two alloys at 0.6 V showed pits and voids opened to the surface, which cause the fluctuations of current density during the potentiostatic tests. The results showed that the alloys in the hydrochloric acid at 0.6 V corroded more than in the sulphuric acid and sulphuric acid containing 3.5 % sodium chloride contained solution. However, at 0.2 V the investigation showed that both alloys formed stable passive films. The result showed more stability for alloy 444 than for alloy 316 at 0.2 V as the current density did not show a distinct increase before achieving film stability. It was observed that the current for alloy 316 decreased from 2.0E-3 A/cm^2 to 2.0E-4 A/cm^2 after about 48 seconds before it gradually increased to reach 3.7E-3 A/cm^2 after 1310 seconds. Current spikes were observed on the alloy 444 curve. However, the curve for the current density remained constant after 2360 seconds at 1.5E-3 A/cm^2.

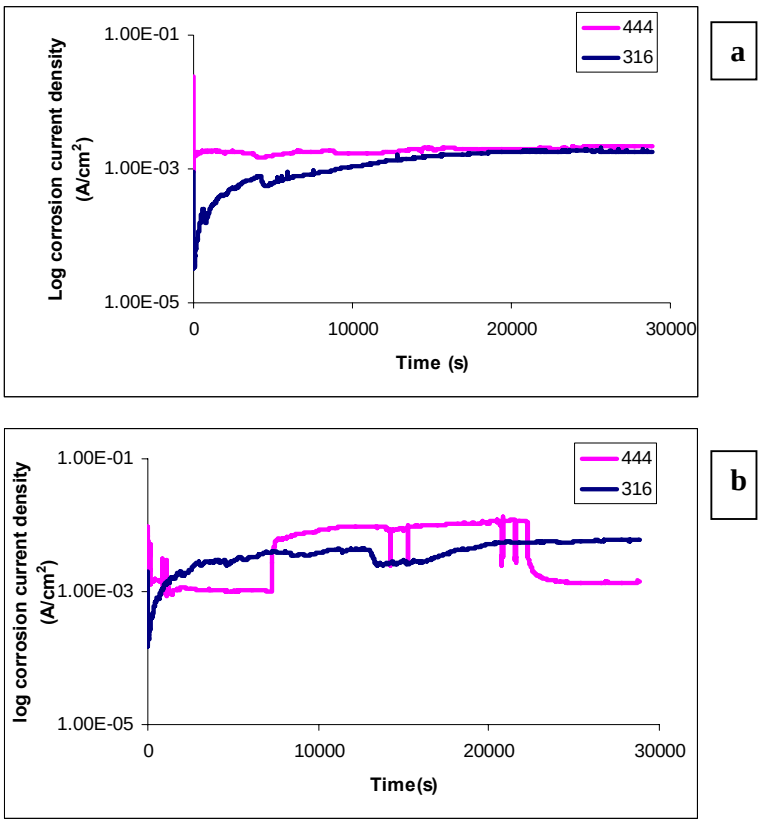

Figure 6.9: Chronoamperometry curves of the alloys 316 and 444 in 0.1 M HCl at (a) 0.2V (b) 0.6 V.

6.6 MATERIAL CHARACTERISATION

6.6.1 Microstructural studies of both alloys in 0.1 M hydrochloric acid

Figure 6.10 shows the optical micrograph of alloy 444 and alloy 316 after their immersion in 0.1 M hydrochloric acid for 92 days. In hydrochloric acid, alloy 316 showed disperse and pits on the grain boundaries while alloy 444 was observed to form deep and large pits. Most of the pits were observed at the grain boundaries for alloy 444. A microstructural transformation was observed for alloy 316, as no grain features were observed on the surface of the alloy. According to Campos *et al.* (2003) a ferrite microstructure is better resistant against chloride attack than the conventional austenitic microstructures, and these results qualitatively confirm it.

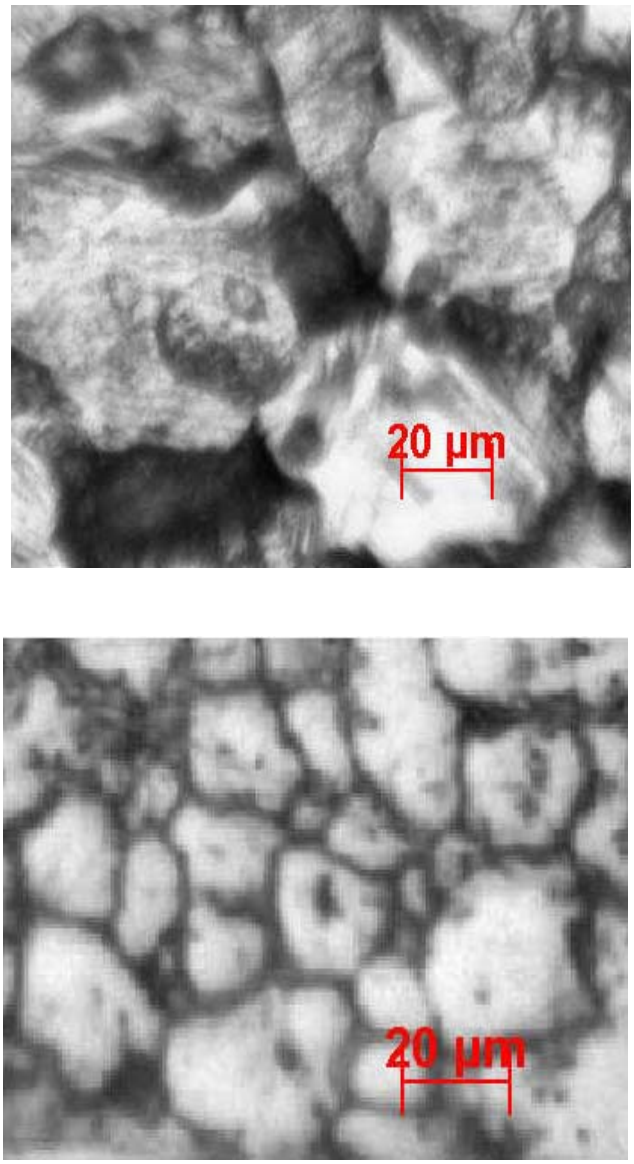

Figure 6.10: Typical optical microstructure of both alloys after immersion in 0.1 M hydrochloric acid for 92 days (a) 444 (b) 316.

6.6.2 Morphological studies of both alloys after immersion tests in hydrochloric acid

The SEM micrographs of the overall surfaces of both alloys in hydrochloric acid solution are shown in Figure 6.11 and 6.12. It can be seen from the SEM micrographs that pits were formed on the surface of both alloys. Some parallel features were observed on alloy 444 which could be due to the corrosion attacks on the surface. The

pits formed on the surface of alloy 316 in hydrochloric acid were more than the pits formed in the sulphuric acid solution. However, the pits formed on the surface of alloy 444 were more in sulphuric acid than in hydrochloric acid. This result confirmed the result from the corrosion rates of both alloys. Similar to the observation in sulphuric acid solution, the grain size of alloy 444 was similar before and after corrosion. The grains of alloy 316 before corrosion appeared finer compared to after the corrosion process. The EDX of the surfaces of both alloys is shown in Figure 6.11 and 6.12 and are summarised in Tables 6.6 and 6.7.

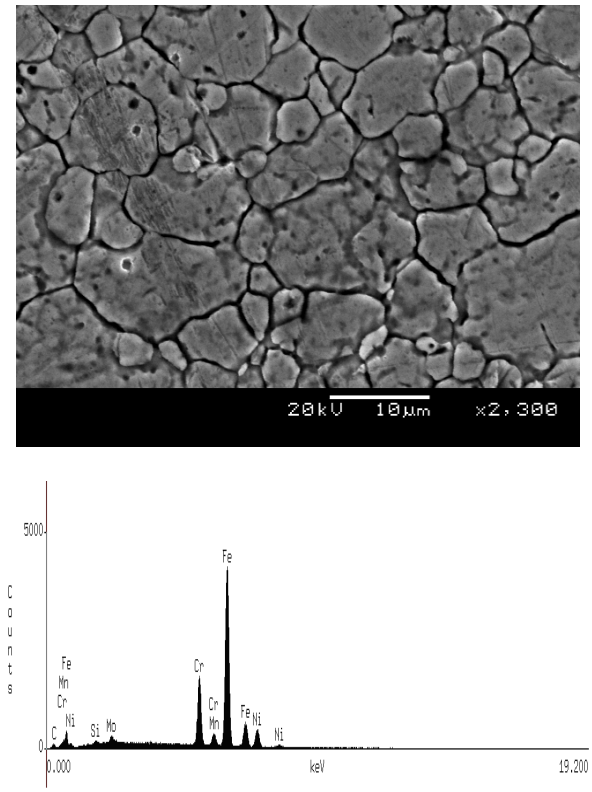

Figure 6.11: SEM/EDX of alloy 316 after immersion in 0.1 M hydrochloric acid for 92 days.

Table 6.6: Summary of EDX obtained for alloy 316 in hydrochloric acid for 92 days.

Element	Si	Cr	Mn	Ni	Mo	C	Fe
Wt %	0.5 ± 0.1	16.4 ± 0.5	1.5 ± 0.1	10.4 ± 0.4	1.3 ± 0.3	0.5 ± 0.1	68.9 ± 0.5

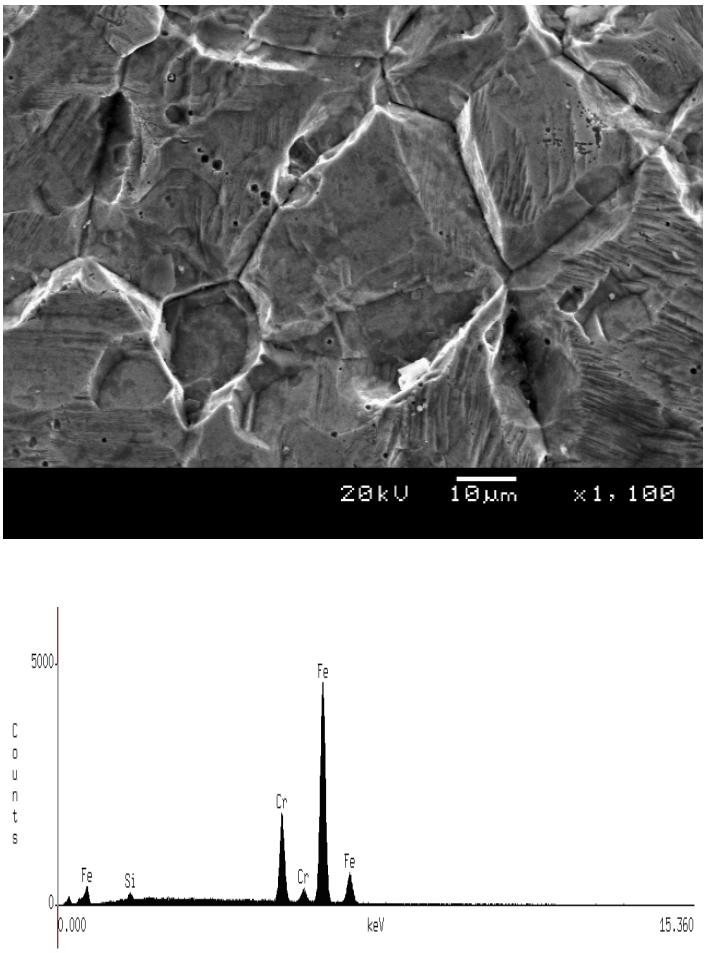

Figure 6.12: SEM/EDX of alloy 444 after immersion in 0.1 M hydrochloric acid for 92 days.

Table 6.7: Summary of EDX obtained for alloy 444 in hydrochloric acid for 92 days.

Element	Si	Cr	Fe	C
Wt %	0.7 ± 0.1	18.5 ± 0.2	78.3 ± 0.5	0.9 ± 0.1

6.6.3 Morphological studies of alloy 316 after corrosion in hydrochloric acid

The SEM micrograph of alloy 316 after exposure to hydrochloric acid solution during polarization tests is shown in Figures 6.13. It can be seen from the micrograph that pits were formed on the surface of the alloy. The pits formed on the alloy in hydrochloric acid were wider than the pits formed in sulphuric acid solution. The

EDX obtained from the investigation revealed three phases. One spectrum showed the corrosion product formed on the surface of the alloy, the second spectrum showed the main surface of the alloy and the third one the pit formed on the surface. The corrosion product(s) contained carbon, chromium, oxygen, iron, silicon and chlorine. This observation shows that the product possibly contained iron chromate, chromium carbide, chromium oxide and iron oxide. On the light phase, carbon, iron, chromium, manganese and nickel were observed. However, in the pit formed on the surface of the alloy oxygen, carbon, aluminium, and manganese were observed. This was an indication that oxides possibly were formed in the pit.

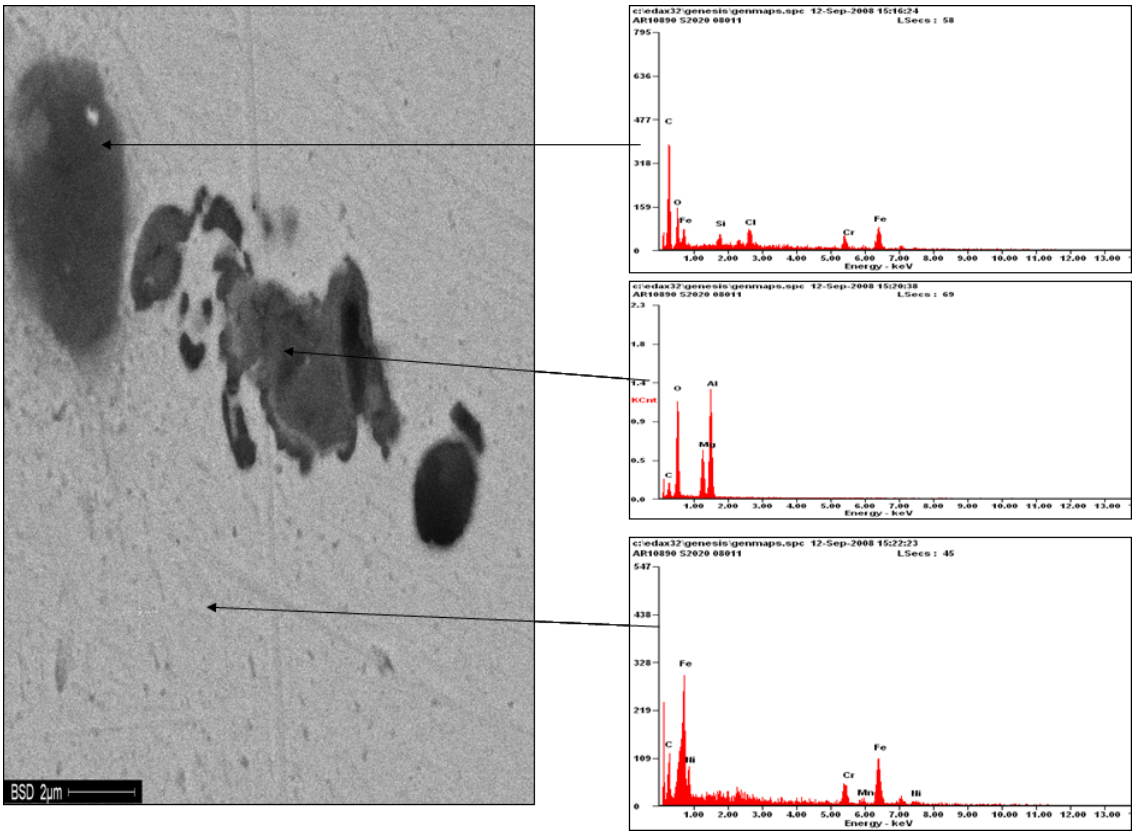

Figure 6.13: SEM scan obtained from the surface of alloy 316 after corrosion in hydrochloric acid.

6.6.4 Morphological studies of alloy 444 after corrosion in hydrochloric acid

The SEM micrograph of alloy 444 after exposure to hydrochloric acid is shown in Figure 6.18. The result revealed that pits were formed on the surface of the alloy. The EDX obtained from the SEM scan are also presented in Figure 6.14. Spectrum 1 showed that iron, chromium, carbon and silicon were the elements present in the

compounds formed on the surface of the alloy tested in hydrochloric acid. This showed that the corrosion products could be of iron-chromate, chromium carbide and probably silicon carbide nature. No oxygen was observed on the surface of the alloy, neither in the pits that formed. The observation showed that the main elements observed in the pit were titanium, iron and carbon, thus indicating that titanium in some form or another could be present in the pit and played a role in the corrosion process.

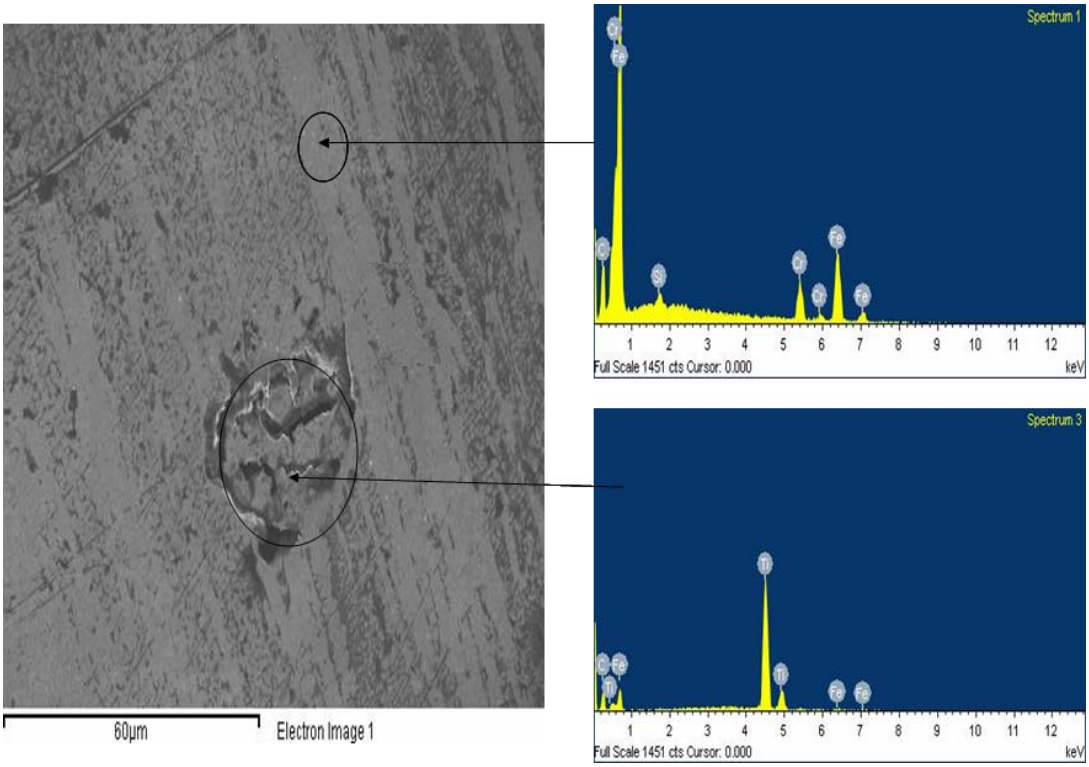

Figure 6.14: SEM scan obtained from the surface of alloy 444 after corrosion in hydrochloric acid.

6.7 PHASE IDENTIFICATION STUDIES

6.7.1 X-ray diffraction of the corrosion products on alloy 316 after polarization

The XRD pattern for alloy 316 studied in hydrochloric acid are shown in Figure 6.15. Four peaks were reflected in the XRD pattern. The XRD patterns from Figure 6.15 indicated that the number of peaks of 316 decreased to four as compared with five that were identified in the as-received sample. The peaks were observed at 2θ positions of 43.6, 44.6, 50.7 and 74.6 ^{0}. Structures of iron, nickel and carbon were

observed. The peak at the 2θ position of 28 ^{0} disappeared and the peak at the 2θ position of 44.6 ^{0} nearly disappeared after the corrosion studies in hydrochloric acid. This could indicate that chromium was dissolved in the solution. This corresponds with the result from the cyclic potentiodynamic polarization studies of the alloy in hydrochloric acid.

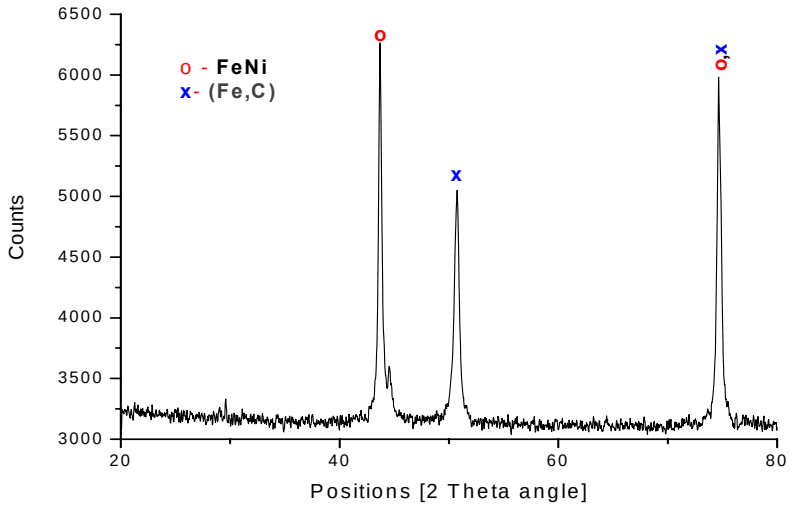

Figure 6.15: X-ray diffraction patterns of alloy 316 after corrosion in hydrochloric acid (00-003-1209, and 00-034-0396).

6.7.2 X-ray diffraction of the corrosion products on alloy 444 after polarization

The XRD spectra obtained from the alloy 444 after the corrosion in hydrochloric acid is shown in Figure 6.16. The result revealed that the main peaks observed in the corrosion products were structures of iron and chromium. No silicon peaks from the substrate were detected in the XRD spectra, as was the case on the as-received sample. In addition, looking at the peaks, they obviously did not show much difference in the XRD spectra between the as-received sample and the alloy after the corrosion in hydrochloric acid. It was observed that the peaks' heights were 2181 and 246 counts at 2θ positions of 44.5 and 64.5 ^{0} respectively.

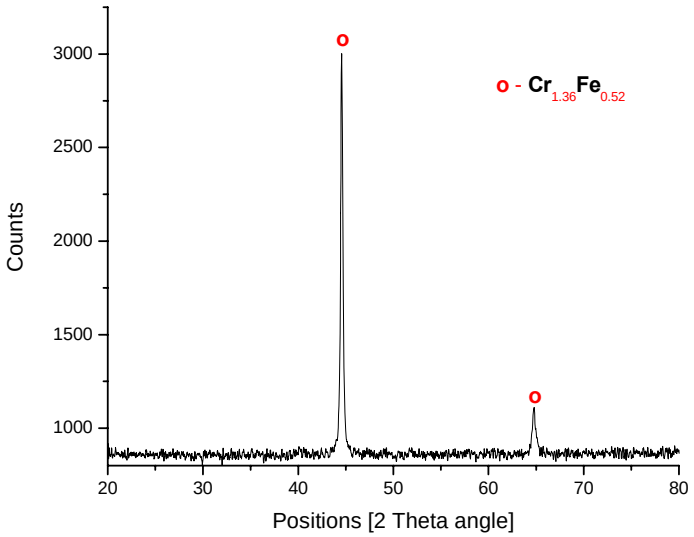

Figure 6.16: X-ray diffraction patterns of alloy 444 after corrosion in hydrochloric acid (00-041-1224).

6.8 RAMAN SPECTRA

6.8.1 Raman spectra of corrosion products formed on alloys in hydrochloric acid

Raman spectra of alloy 444 and alloy 316 after corrosion in hydrochloric acid are shown in Figures 6.17 and 6.18 respectively. The peaks that formed on the alloy 316 spectrum were sharper and had higher intensities compared to the spectrum from the alloy 444. The spectrum for alloy 316 shows Raman shifts at 199, 327, 470, 674 and 1041 cm^{-1} bands. These shifts could correspond to $Mo_8O_{26}^{4-}$, MoO_3, Fe_3O_4, MoO_2 or MoO_3 and Al_2O_3 respectively. On the other hand, the three peaks in Figure 6.16 show Raman shifts for alloy 444 at 217, 299 and 392 cm^{-1} wave numbers. These could correspond to α–Fe_2O_3 (217 and 299 cm $^{-}$1) and TiO_2 (392 cm^{-1}). The summary of the Raman shifts of the corrosion products formed on alloy 316 and alloy 444 in hydrochloric acid compared with the prior findings are presented in Table 6.8.

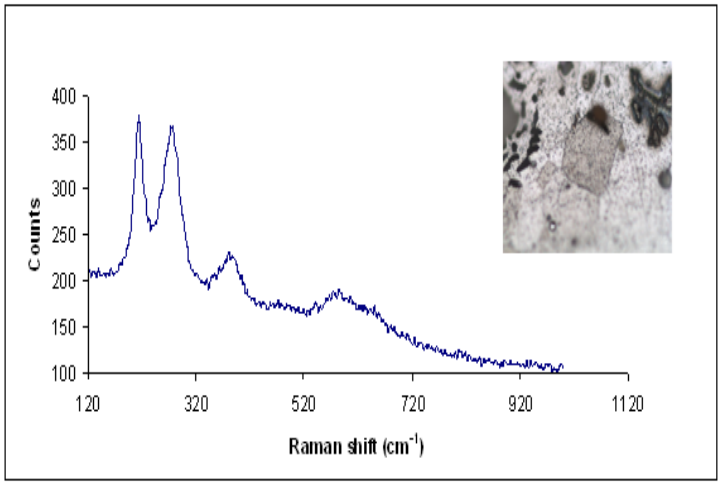

Figure 6.17: Raman spectrum and the image of the overall surface of alloy 444 tested in hydrochloric acid.

Table 6.8: Summary of the Raman spectra of the corrosion products formed on alloy 316 and alloy 444 tested in hydrochloric acid.

Alloys	**Raman shift (cm^{-1}) from this study**	**References (cm^{-1})**	**Probable corrosion product/compound**	**References**
316	199	200	$Mo_8O_{26}^{4-}$	*Hart et al. 1976; Gui and Devine, 1991*
	327	331	MoO_3	*Chang et al., 1992*
	470	472	Fe_3O_4	*McCarty and Boehme,1989; Gui and Devine, 1991*
	674	675	MoO_3 or MoO_2	*Chang et al., 1992*
	1041	1045	Al_2O_3	*Guevara-Lara et al., 2007*
444	217	220	α-Fe_2O_3	*McCarty and Boehme,1989; Gui and Devine, 1991*
	299	299	α-Fe_2O_3	*McCarty and Boehme,1989; Gui and Devine, 1991*
	392	398	TiO_2	*Guevara-Lara et al., 2007*

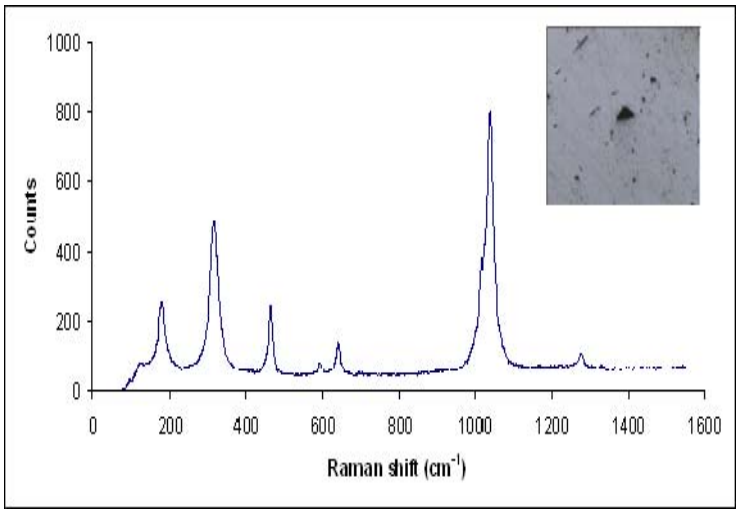

Figure 6.18: Raman spectrum and the image of the overall surface of alloy 316 tested in hydrochloric acid.

6.9 THE CORRELATION BETWEEN ALL THE SURFACE ANALYSES TECHNIQUES.

The microstructure and the morphology of the alloys after the various corrosion tests were observed to be similar. The corrosion products were analyzed by X-ray diffractometer, Raman spectrometer, optical microscope and SEM/EDX. The images obtained using all these techniques were similar. The optical microscope and SEM showed that oxide particles are formed on the surfaces of both alloys during the passivation process. A uniform oxide film developed on the surface of the alloys which confirm the OCP results obtained for both alloys. According to Wegrelius *et al.* (1999), the composition of the film is strongly dependent on the potential. Molybdenum was observed to be a major constituent of the corrosion products formed. Chromium could not be detected by the Raman spectroscope but X-ray diffractometer revealed chromium in the structure of the passive film on both alloys. This could mean that there was chromium dissolution. Chloride was observed to be present on the surface of alloy 316. A similar observation was made by Wegrelius *et al.* (1999). According to these authors, the content of chromium in the hydroxide layer decreases with the potential, and $MoCl_2$ is identified in the film on the molybdenum containing steels. Chloride is present in both the oxide and hydroxide layers. It is suggested that one of the beneficial effects of molybdenum in stainless steels is that it forms soluble oxochloro-complexes, which thereby lower the amount of Cl^- in the

film and makes the steel more resistant to pitting. The XRD and Raman spectroscopes used for this study were not in situ. This could result to some limitations in their uses as many changes could take place on the surface of the studied alloys prior analysis.

CHAPTER SEVEN

7.0 CONCLUSIONS AND RECOMMENDATIONS

7.1 CONCLUSIONS

An electrochemical study and weight loss tests carried out to assess the corrosion behaviour of alloy 316 and alloy 444 in sulphuric acid, hydrochloric acid and sulphuric acid containing 3.5 % NaCl were undertaken. The alloys were analyzed prior to and after corrosion using the SEM/EDX, XRD and Raman spectroscopy. The study thoroughly considered the research questions, problems, hypothesis, and the set aim and objectives. Based on the results obtained from the present study, the following conclusions could be drawn:

The alloys displayed similar corrosion behaviour with considerable difference in their corrosion resistance in all the solutions. This was confirmed by the similar patterns in cumulative weight loss of the alloys, as well as the polarization curves from the electrochemical techniques. Both alloys display similar active to passive transition behavior upon polarization. The passivity of both alloys seems to remain stable with no passivity breakdown and pitting in lower concentrations of all the solutions (0.1M). Little passivation occurred in the 1 M hydrochloric acid solution. E_{corr} of the alloys in all the solutions reached a stable value after a certain period of exposure. This indicates that the corrosion processes of the alloys remain constant with time and they formed relatively stable corrosion products in the media studied.

Although the two alloys exhibited similar corrosion behaviour in all the solutions studied, their corrosion resistances in the different media varied. Alloy 316 was generally more resistant in all the solutions than alloy 444. Alloy 444 was more corrosion resistant in chloride environments (hydrochloric acid and sulphuric acid containing 3.5 % NaCl) than in the sulphuric acid in weight loss tests. Alloy 316 was more resistant in sulphuric acid than in acidic chloride environments. In chloride environments, the corrosion resistance of the two alloys was not significantly different, as evident by their corrosion rates. For instance in 0.1 M sulphuric acid containing 3.5 % NaCl, the corrosion rate of alloy 444 was 0.016 mm/yr while that of alloy 316 was 0.013 mm/yr. In 1 M

hydrochloric acid also, the corrosion rate of alloy 444 was 0.2 mm/yr while that of alloy 316 was 0.1 mm/yr.

The corrosion rates calculated from mass loss tests did not really show good agreement with those calculated from electrochemical measurement results. There was a poor correlation in the corrosion rates obtained from the two techniques for the alloys in all the solutions, and this might be ascribed to the different steady state conditions and thermodynamic stability of the passive oxide layers formed in each case.

XRD and Raman spectroscopy indicated that the corrosion products on alloy 444 in all the solutions were amorphous in nature, while those observed for alloy 316 were more crystalline. SEM analysis showed that alloy 444 formed more and larger corrosion pits in sulphuric acid than alloy 316, while 316 had larger and more pits in chloride environments than alloy 444. This corroborated the different resistances of the two alloys in both sulphate and chloride environments as obtained from the electrochemical investigation. The presence of titanium coupled with molybdenum as observed in the Raman spectra of the corrosion products of alloy 444 in chloride environments, could be responsible for the better corrosion resistance of alloy 444 in chloride environments.

Thus the aims of this investigation which were to study and compare the electrochemical behavior of 444 ferritic and 316 austenitic stainless steels in HCl, H_2SO_4 and $H_2SO_4 + Cl^-$ and to investigate the types and stability of various passive films formed in different media were achieved. Likewise it can be concluded that the hypothesis of the investigation is true, namely that alloy 444 exhibit similar corrosion resistance to alloy 316.

7.2 RECOMMENDATIONS

- It is recommended that alloy 444 can be applied and successfully used to replace alloy 316, especially in chloride environments.
- Since the alloying composition improved the corrosion resistance 444, it is recommended that its molybdenum, niobium and titanium contents be increased, optimised and further compared with alloy 316. An in-depth characterisation of the passive film formed in the acidic chloride media (the chemical composition and the state of the surfaces being formed (films as deposited, heat-treated and/or subjected to anodic polarization) should be carried out using an X-ray photoelectron spectroscopy (XPS) and Auger instrument. Auger is the most commonly used surface technique on metal samples because of the following advantages: High surface sensitivity, acceptable detect-ability for many corrosion problems, simultaneous detection of all elements (except hydrogen and helium), very good small-area analysis (mapping), ability to probe deeper into the surface by sputter profiling, analysis time not excessively long and readily available instrumentation (Hopkins, 1995).
- In-situ spectral and electrochemical investigations should be conducted to shed more light on the mechanism of the corrosion process.

REFERENCES

Aalco (2004). Stainless steel- introduction to grades, properties and applications, Supplier data, UK.

Abd El Aal, E. E. (2003). Breakdown of passive film on nickel in borate solutions containing halide anions. *Corrosion Science, 45,* 759-775.

Abdel, S. H., Eman, E-S. and El-Bitar, T. (2006). The corrosion behavior of niobium bearing cold deformed austenitic stainless steels in 3.5% NaCl. *Materials Letters*, 61, 2827-2832.

Abreu, C.M., Crist´obal, M.J., Losada, R., N´ovoa X.R., Pena, G. and P´erez, M.C. (2004). Comparative study of passive films of different stainless steels developed in alkaline medium. *Electrochimica Acta* ,49, 3049–3056.

Abreu, C.M., Crist´obal, M.J., Losada, R., N´ovoa X.R., Pena, G. and P´erez, M.C. (2006). The effect of Ni in the electrochemical properties of oxide layers grown on stainless steels. *Electrochimica Acta,* 51, 2991–3000.

AK steel (2007a). 444 Stainless steel. www.aksteel.com (Accessed March, 2008).

AK steel (2007b). 316/316L Stainless steel. www.aksteel.com (Accessed March, 2008).

AK steel (2008). AK Steel stainless steels. www.aksteel.com (Accessed April, 2008).

Allegheny Ludlum (1999). Stainless steels chromium-nickel-molybdenum types 316 (S31600), 316L (S31603), 317 (S31700), 317L (S31703). www.alleghenyludlum.com (Accessed April, 2008).

Alonso-Falleiros, N. and Wolynec, S. (1998). Effect of niobium on corrosion resistance to sulfuric acid of 430 ferritic stainless steel. *Materials Research,* 1, 35-39.

Ameer, M.A., Fekry, A.M. and Heakal, F. E-T. (2004). Electrochemical behaviour of passive films on molybdenum-containing austenitic stainless steels in aqueous solutions. *Electrochimica Acta,* 50, 43-49.

Andrews, A. (2005). Electrochemical corrosion measurement of Solid State Sintered Silicon Carbide (SSiC) and Liquid Phase Sintered Silicon Carbide (LPSSiC) ceramic material. MSc. Dissertation, University of the Witwatersrand, Johannesburg. 21-23.

Armitage, W.K. (1985). Chromium aids development of new products. *Metal Bulletin Stainless Survey,* 23-25.

Asami, K., Hashimoto, K., Masumoto, T. and Shimodara, S. (1976). ESCA study of the passive film on an extremely corrosion resistant amorphous iron alloy. *Corrosion Science,* 16, 909-915.

Asami, K. and Hashimoto, K. (1979). X-ray Photo-electron spectroscopic study of surface treatments of stainless steels. *Corrosion Science*, 19, 1007-1017.

Asami, K. and Hashimoto, K. (2003), Importance of initial surface film in the degradation of stainless steels by atmospheric exposure. *Corrosion Science*, 45, 2263–2283.

ASTM G3-89. (2000). Annual books of ASTM standards 2000 convections applicable to electrochemical measurements in corrosion testing, 3, 38-42.

Avesta, S. (1999), Avesta Sheffield Corrosion Handbook for Stainless Steels, 8, SE – 10327.

Beddoes, J. and Parr, J. G. (1999). Introduction to Stainless Steels. ASM International, Materials. Park, OH, 83.

Betova, I., Bojinov, M., Laitinen, T., Makela, K., Pohjanne, P. and Saario, T. (2002). The transpassive dissolution mechanism of highly alloyed stainless steels I. Experimental results and modelling procedure. *Corrosion Science,* 44, 2675-2697.

Berger, H. (1982). Non-destructive evaluation techniques. *Anti-corrosion methods and materials,* 29, 11-13.

Binder, W. O. (1946). Corrosion of metals. American Society for Metals, Cleveland, Ohio, 56.

Bohni, H. (2000). Localized corrosion of passive metals. Uhlig's "Corrosion Handbook", Revie, R.W. (editor), John Wiley and Sons, Inc., Canada, 173-186.

Bojinov, M., Fabricius, G., Laitinen, T., Makela, K., Saario, T. and Sundholm, G. (2001). Influence of molybdenum on the conduction mechanism in passive films on Iron–Chromium alloys in sulphuric acid solution, *Electrochimica Acta,* 46, 1339–1358.

Brooks, A.R., Clayton, C.R., Doss, K. and Lu, Y.C. (1986). On the role of Cr in the passivity of stainless steel. *Journal of the Electrochemical Society,* 133, 2459–2464.

British Stainless Steel Association, (2007). Calculation of pitting resistance equivalent numbers. http://www.bssa.org.uk/topics.php?article=111 (Accessed April, 2008)

Campos, M., Bautista, A., Ca´ ceres, D., Abenojar, J. and Torralba, J. M.(2003). Study of the interfaces between austenite and ferrite grains in P/M duplex stainless steels. *Journal of the European Ceramic Society*, 23, 2813–2819.

Carson, R.O. and Graham, R.G (1977). Effect of molybdenum on the structure and properties of wrought and cast stainless steels. "*Handbook of Stainless Steels"*. Peckner, D.; Bernstein, I.M. (editors) McGraw-Hill, Canada, 13-1.

Chang, S.C., Leugers, M.A. and Bare, S.R. (1992). Surface Chemistry of Magnesium Oxide-Supported Molybdenum Oxide: An In-situ Raman spectroscopic study. *Physical Chemistry,* 96, 10358-10365.

Chernova, G.D. and Tomashov, N. D. (1965). Corrosion of metallurgy alloys. 1. As reported in Snape, E. (1977). Handbook of stainless steels. Peckner, D. and Bernstein I.M. (editors), McGraw-Hill, 12-1 -12-40.

Chiba, A., Sakakura, S., Kobayashi, K. and Kusayanagi, K. (1997). Dissolution amounts of nickel, chromium and iron from SUS 304, 316 and 444 stainless steels in sodium chloride solutions, *Materials Science,* 32, 1995-2000.

Clayton, C.R., and Lu, Y.C. (1986). A bipolar model of the passivity of stainless steel: The role of Mo addition. *Journal of the Electrochemical Society*, 133, 2465–2473.

Cortie, M.B. (1993). History and development of ferritic stainless steels. *Journal of the South African Institute of Mining and Metallurgy,* 93, 165-176.

Cunat, P-J. (2002). The Euro Inox handbook of stainless steels. *Luxembourg Euro Inox Materials And Application Series*, 1.

Cvijovic, Z. and Radenkovic, G. (2006). Microstructure and pitting corrosion resistance of annealed duplex stainless steel. *Corrosion Science*, 48, 3887-3906.

Davies, R.D. (1983). The effect of vanadium and other elements on the mechanical properties and corrosion resistance of ferritic stainless steels. MSc. Dissertation, University of the Witwatersrand, 43-50,114-125.

Davis, J.R. (1994). Atmospheric and aqueous corrosion, in: J.R. Davis (Ed.), ASM Speciality Handbook of Stainless Steel, ASM International, Metals Park, OH, 134–180.

De Abreu, H.F.G., Bruno, A.D.S., Tavares, S.S.M., Santos, R.P. and Carvalho, S.S. (2006). Effect of high temperature annealing on texture and microstructure on an AISI-444 ferritic stainless steel. *Materials Characterization*, 57, 342–347.

Demo, J.J. and Bond, A.P. (1975). Intergranular corrosion and embrittlement of ferritic stainless steels. *Corrosion Science,* 31, 21-22.

Demo, J.J. (1977). Structure and constitution of wrought ferritic stainless steels. In "*Handbook of Stainless Steels"*. Peckner, D.; Bernstein, I.M. (editors) McGraw-Hill, Canada, 5-1.

Doh, S. J., Je J. H., Kim, J. S., Kim, K. Y., Kim, H. S., Lee, Y. D., Lee, J. M. and Hwu, Y. (2003). Influence of Cr and Mo on the passivation of stainless steel 430 (18Cr) and 444 (18Cr–2Mo): In situ XANES study. *Nuclear Instruments and Methods in Physics Research B, 199,* 211–215.

Dowling, N.J.E., Kim, Y.-H., Ahn, S.-K. and Lee, Y.-D. (1999). Effect of alloying elements and residuals on corrosion resistance of type 444 stainless steel. *Corrosion Science*, 55, 187-199.

Dundas, H.J. and Bond, A.P. (1978). Intergranular Corrosion of Stainless Alloys. Steigerwald, R.F. (editor); ASTM, Philadelphia, PA, USA, 154-178.

Enos, D.G. and Scribner, L.L. (1997). The potentiodynamic polarization scan. Technical report, 33, 1-19.

Fielder, J. W. and Johns, D. R. (1989). Pitting corrosion diagrams for stainless steels. UK Corrosion '89 Blackpool.

Fontana, M. G. (1986). Corrosion engineering. McGraw-Hill Series in Materials Science and Engineering. Donnelley R.R and Sons Company, USA. 469.

Gilet, J-Y. (1998). The Ferritic Solution. *International Stainless Steel Forum,* 5.

Grobner, P. J. (1973). The 885 °F (475 °C) embrittlement of ferritic stainless steels. *Metallurgical Transactions,* 4, 251–260.

Gross, C.J. (1980). The effect of manganese on the structure and corrosion properties of 14.5% chromium stainless steels. MSc Dissertation, University of the Witwatersrand, 14, 61-62.

Guevara-Lara, A., Bacaud, R. and Vrinat, M. (2007). Highly active NiMo/TiO_2–Al_2O_3 catalysts: Influence of the preparation and the activation conditions on the catalytic activity. *Applied Catalysis,* 328, 99–108.

Gui, J. and Devine, T. M (1991). In-situ vibrational spectra of the passive film on iron in buffered borate solution. *Corrosion Science,* 32, 1105-1124.

Habazaki, H., Kawashima, A., Asami, K. and Hashimoto, K. (1991). The effect of molybdenum on the corrosion behavior of amorphous Fe-Cr-Mo-P-C alloys in hydrochloric acid. *Materials Science and Engineering,* 13, 1033-1036.

Habazaki, H., Kawashima, A., Asami, K. and Hashimoto, K. (1992). The corrosion behavior of amorphous Fe–Cr–Mo–P–C and Fe–Cr–W– P–C alloys in 6M HCl solution. *Corrosion Science,* 33, 225–236.

Hart, T. R., Adams, S. B and Tempkin, H. (1976). Light scattering in solids (Edited by M. Balkanski, R. L. and S. Porto). Flammarion Sciences, Paris, 254, 259.

Hashimoto, K., Asami, K. and Teramoto, K. (1979a). An X-ray photo-electron spectroscopic study on the role of molybdenum in increasing the corrosion resistance of ferritic stainless steels in HCl. *Corrosion Science,* 19, 3–14.

Hashimoto, K., Asami, K., Naka, M. and Masumoto, T. (1979b). Surface films formed on amorphous Co-Cr alloys in 1N HCl. *Boshoku Gijutsu (Corrosion Engineering),* 28, 271-278.

Hashimoto, K., Asami, K., Kawashima, A., Habazaki, H. and Akiyama, E. (2007). The role of corrosion-resistant alloying elements in passivity. *Corrosion Science,* 49, 42–52.

Haupt, S. and Strehblow, H-H. (1995). A combined surface analytical and electrochemical study of the formation of passive layers on Fe/Cr alloys in 0.5 M H_2S0_4. *Corrosion Science*, 37, 43-54.

He, W. (2002). Atmospheric corrosion and runoff processes on copper and zinc as roofing materials. Doctoral Thesis, Department of Materials Science and Engineering, Division of Corrosion Science, Royal Institute of Technology, SE-10044, Stockholm, Sweden, 12.

Hoar, T. P. and Jacob, W. R (1967). Breakdown of Passivity of Stainless Steel by Halide Ions. *Letters to Nature,* 216, 1299 – 1301.

Holliday, J. E. and Frankenthal, R. P. (1972). Characterization of passivating films on Fe-Cr alloys by Soft X-Ray Spectroscopy. *Journal of the Electrochemical Society,* 119, 1190-1192.

Hopkins, A. G. (1995). Surface Analysis in Baboian. Revised edition, Corrosion Tests and Standards, Philadelphia, American Society for Testing and Materials 55–61.

Horvath, J. and Uhlig, H. (1968). Critical potentials for pitting corrosion of Ni, Cr-Ni, Cr-Fe, and related stainless steels. *Journal of the Electrochemical Society,* 115, 791-795.

Ihrzo, A., Segui, Y., Bui, N. and Dabosi, F. (1986). The conduction mechanisms of passive films on molybdenum-containing stainless steel. *Corrosion Science*, 42, 141–146.

Iorio, L., Cortie, M. and Jones, R. (1994). Technical data: solubility of nitrogen in experimental low nickel austenitic stainless steels. *Journal of the South African Institute of Mining and Metallurgy,* 94, 173-177.

Jargelius-Petterson, R.F.A. (1996). Localized corrosion of stainless steel: ranking, alloying and microstructure effects. *Scandinavian Journal of Metallurgy,* 5,188-193.

Jargelius-Petterson, R.F.A. and Pound, B.G. (1998). Examination of the role of molybdenum in passivation of stainless steels using AC impedance spectroscopy. *Journal of the Electrochemical Society,* 145, 1462–1469.

Jiangzhou, S. and Wang, R. Z. (2001). Experimental research on characteristics of corrosion-resisting nickel alloy tube used in triple-effect $LiBr/H_2O$ absorption chiller. *Applied Thermal Engineering*, 21, 1161–1173.

Jones, D. A. (1996). Principles and prevention of corrosion, Prentice-Hall, Inc., USA, 75-80, 143-153.

Jun'ichi, H., Michio, A., Hiroshige, I. and Osamu, I. (2001). Corrosion resistance of dissimilar welds between Ferritic stainless steel with high corrosion resistance and austenitic stainless steels. *Corrosion Engineering,* 50, 273-278.

Karlsson, L. (2004). Stainless steel past, present and future. *Svetsareno,* 1, 47 – 52.

Kile, D.E. and Eberl, D.D. (2000). Quantitative mineralogy and particle-size distribution of bed sediments in the boulder creek watershed, 173–184.

Kim, J-H., Akiyama, E., Habazaki, H., Kawashima, A., Asami, K. and Hashimoto, K. (1993). Corrosion behavior of sputter-deposited amorphous Cr-Nb and Cr-Ta alloys 12M HCl solution**.** *Corrosion Science,* 34, 1947-1955.

Kish, J. R., Ives, M. B. and Rodda, J. R. (2000). Corrosion mechanism of nickel in hot, concentrated H_2SO_4. *Journal of the Electrochemical Society*, 147, 3637-3646.

Kish, J. R. Ives, M. B. and Rodda, J. R. (2004). Corrosion mechanism of nickel-containing stainless steels in concentrated aqueous solutions of sulfuric acid. *Corrosion*, 60, 523-537.

Kotecki, D. and Armao, F. (2003). Welding of stainless steel. Lincoln Electrical Company, 2-40.

Kozhevnikov, V.B., Tsenta, T.E., Nyazheva, V.M. and Kolotyrkin, Y.M. (1983). X-ray photoelectron investigation of the state of the surface of molybdenum polarized in various ranges of potential. *Protection of Metals (Zashchita Metallov)*, 19, 569-575.

Kruger, J. and Rhyne, K. (1982). Nuclear chemistry. *Waste Management*, 3, 205.

Kruger, J. (2000). Passivity. Uhlig's "Corrosion Handbook", Revie, R.W. (editor), John Wiley and Sons, Inc., Canada, 165-190.

LaQue, F.L. (1969). ASTM special technical publication, 454, 3.

Leffler, B. (2005), Stainless steels and their properties. *Outokumpu Technical article*, 45.
http://www.outokumpu.com/files/Group/HR/Documents/STAINLESS20.pdf. (Accessed April, 2008)

Levey, P.R. (1995). The mechanistic involvement of alloyed nitrogen in the corrosion of stainless steels. MSc Dissertation, University of the Witwatersrand, 3-30.

Leygraf, C., Huktquist, G., Olefjord, I., Elfstrom, B.O., Knyazheva, V.M., Paskeyer, A.V. and Kolotyrkin, Y.M. (1979). Selective dissolution and surface enrichment of alloy components of passivated Fe18Cr and Fe18Cr3Mo single crystals. *Corrosion Science,* 19, 343–357.

Li, X-Y., Akiyama, E., Habazaki, H., Kawashima, A., Asami, K. and Hashimoto, K. (1997). Spontaneously passivated films on sputter-deposited Cr-Ti alloys in 6 M HCl solution. *Corrosion Science,* 39, 935-948.

Li, M.C., Zeng, C.L., Luo, S. Z., Shen, J. N., Lin, H.C. and Cao, C. N. (2003). Electrochemical corrosion characteristics of type 316 stainless steel in

simulated anode environment for PEMFC. *Electrochimica Acta, 48*, 1735-1741.

Lizlovs, E.A. and Bond, P. A. (1969). Anodic polarization of some ferritic stainless steels in chloride media. *Journal of the Electrochemical Society,* 574.

Lorang, G., da Cunha Belo, M., Langeron, J.-P. and Vac, J. (1987). Sputter profiling of passive films in Fe-Cr alloys - a quantitative approach by Auger-electron spectroscopy. *Vacuum Science and Technology (A) -Vacuum Surfaces and Films*, 5, 1213-1219.

Lorang, G., Basile, F., da Cunha Belo, M. and Langeron, J.-P. (1988). Quantitative Auger analysis of passive films formed on stainless steels. *Surface and Interface Analysis*, 12, 424-428.

Lula, R.A. (1986). Manganese stainless steels. The Manganese Centre, France, 22-57.

Lumsden, J.B. and Staehle, R.W. (1972). Application of Auger Electron Spectroscopy to the determination of the composition of passive films in type 316 stainless steel. *Scripta Metallurgica,* 6, 1205-1208.

Lu, Y.C. and Clayton, C.R. (1985).Evidence for a bipolar mechanism of passivity in Mo bearing stainless steels. *Journal of the Electrochemical Society,* 132, 2517–2518.

Maledi, N.B. (2007). Corrosion behaviour of Pt-based superalloys intended for high temperature applications. MSc. Dissertation, University of the Witwatersrand, 76-104.

Malik, A.U., Andijani, I.N. and Ahmed, S. (1994). Corrosion monitoring in SWCC plants Al Khafji plant. Research & Development Center, Al-Jubail and Madeeh Al-Khalidi and Khalid A. Al-Maeeli Al-Khatji Desalination Plant. *Technical Report,* 34, 1040-1056.

Mantel, M. (2000). Effect of double oxide layer on metal–glass sealing. *Journal of Non-Crystalline Solids*, 273, 294-301.

Marcus, P. and Olefjord, I. (1988). A Round robin on combined electrochemical and AES/ESCA characterization of the passive films on Fe–Cr and Fe–Cr–Mo alloys. *Corrosion Science,* 28,589-602.

Maurice, V., Yang, W.P. and Marcus, P. (1996). XPS and STM study of passive films formed on Fe-22Cr-(110) single crystal surfaces. *Journal of the Electrochemical Society,* 143, 1182-1200.

McCarty, K.F. and Boehme, D.R. (1989). A Raman study of the system $Fe_{3-x}Cr_xO_4$ and $Fe_{2-x}Cr_xO_3$. *Solid State Chemistry*, 79, 19-27.

Monypenny, J. H. G. (1951). Stainless iron and steel. Chapman and Hall, London, UK, 288.

Moran, P. (1999). Electrochemical techniques in corrosion science and engineering. Taylor and Francis. 260-290.

Mottu, N., Vayer, M., Dudognon, J. and Erre, R. (2005). Structure and composition effects on pitting corrosion resistance of austenitic stainless steel after molybdenum ion implantation. *Surface and Coatings Technology*, 200, 2131-2136.

Munoz, A. I., Anton, J. G., Guinon, J. L. and Herranz, V. P. (2006). Effects of solution temperature on localized corrosion of high nickel content stainless steels and nickel in chromated LiBr solution. *Corrosion Science*, 48, 3349–3374.

Muwila, A. (2006). The effect of manganese and molybdenum on the corrosion resistance of a low nickel (<2wt %) austenitic stainless steel. MSc Dissertation, University of the Witwatersrand, 7-15.

Naka, M., Hashimoto, K., Asami, K. and Masumoto, T. (1978). Rapidly quenched metals III, Proceedings of 3rd International Conference on Rapidly Quenched Metals, Canter (Ed.) Brighton. *The Metals Society,* 2, 449.

Nakayama, Y., Yamamura, T., Kotoura, Y. and oka, M. (189). In vivo measurement of anodic polarization of orthopaedic implant alloys:comparative study of in vivo and in vitro experiments. *Biomaterials,* 10, 420-424.

Nethercot, D.A. and Gardner, L. (2002). Exploiting the special features of stainless steel in structural design. Proceedings of the Third International Conference on Advances in Steel Structures, Hong Kong, China, 1, 43 – 55.

Newman, R.C. (1985). Dissolution and passivation kinetics of stainless alloys containing molybdenum, II. Dissolution kinetics in artificial pits. *Corrosion Science*, 25, 34l -350.

Nilsson, K. (2006). Corrosion tests of stainless steels in automotive applications. MSc. Dissertation, Lulea University of Technology, 1-70.

Ogawa, H., Omata, H., Itoh, I. and Okada, H. (1978). Auger Electron Spectroscopic and electrochemical analysis of the effect of alloying elements on the passivation behavior of stainless steels. *Corrosion Science,* 34, 52–60.

Okada, H., Ozawa, H., Itoh, I. and Omata, H. (1975). Passivity and its breakdown on iron and iron base alloys. Staehle, R.W. and Okada H. (Editors), Honolulu, NACE, Houston, TX, 82.

Oldham, H.B. and Myland, J.C. (1994). Fundamentals of electrochemical science. Academic Press, Inc., San-Diego, New York, Boston.

Olefjord, I. and Fischmeister, H. (1975). ESCA studies of the composition profile of low temperature oxide formed on chromium steels—II. Corrosion in oxygenated water. *Corrosion Science,* 15, 697-707.

Olsson, C-O. A. (1995). The influence of nitrogen and molybdenum on passive films formed on the austenoferritic stainless steel 2205 studied by AES and XPS. *Corrosion Science*, 37, 467-479.

Olubambi, P.A., Ndlovu, S., Potgieter, J.H. and Borode, J.O. (2008). Mineralogical characterization of Ishiagu (Nigeria) complex sulphide ore. International Journal of Mineral Process, 87 (2008) 83–89.

Osozawa, K. (1980). Atmospheric corrosion resistance of stainless steel. *Boshoku gijutsu* (*Corrosion Engineering*), 29, 403-409.

Pardo, A., Merino, M.C., Coy, A.E., Viejo, F., Arrabal, R. and Matykina, E. (2008). Effect of Mo and Mn additions on the corrosion behavior of AISI 304 and 316 stainless steels in H_2SO_4. *Corrosion Science*, 50, 780-794.

Park, P.-Y., Akiyama, E., Kawashima, A., Asami, K. and Hashimoto, K. (1995). The corrosion behavior of sputter-deposited Cr-Mo alloys in 12 M HCl solution. *Corrosion Science,* 37, 1843-1860.

Peckner, D. and Berstein, I.M. (1977). Handbook of stainless steels. McGraw Hill Company, Canada, 1-2, 4-3, 15-1-15-6.

Pehlke,R.D., and Elllorr, I.F. (1960). Solubility of nitrogen in liquid iron alloys. *Transactions of the American Institute of Mining, Metallurgical and Petroleum Engineers,* 218, 1088-1101.

Pickering, H. W. (1989). The significance of the local electrode potential within pits, crevices and cracks. *Corrosion Science,* 29, 325-341.

Potgieter, J. H., Olubambi, P. A., Cornish, L., Machio, C.N. and Sherif, E-S.M (2008). Influence of nickel additions on the corrosion behaviour of low nitrogen 22%Cr series duplex stainless steels. *Corrosion Science,* 50, 2572-2579.

Pyun, S-I. and Oriani, R. A.(1989). The permeation of hydrogen through the passivating films on iron and nickel. *Corrosion Science,* 29, 485-496.

Qiu, J.H. (1998). Effect of ceramic heat insulating paste on degree of sensitisation of AISI type 304 stainless steel. *British Corrosion Journal,* 33: 318-320**.**

Qiu, J.H. (2002). Passivity and its breakdown on stainless steels and alloys. *Surface and Interface Analysis*, 33, 830-833.

Qvarfort, R. (1998). Some observations regarding the influence of molybdenum on the pitting corrosion resistance of stainless steels. *Corrosion Science*, 40, 215-223.

Redmond, J.D. (1984). Solving brewery stress corrosion cracking problems. *MBAA Technology,* 21, 1-7.

Rigaud, M. (2000). Corrosion testing of refractories and ceramics. Uhlig's "Corrosion Handbook", Revie, R.W. (editor), John Wiley and Sons, Inc., Canada, 1169-1178.

Rocchini G. and Enel S.P.A. (1995). Corrosion rate monitoring with computerized systems. *Werkstoffe und Korrosion*, 46, 582-589.

Rosenfeld, L. and Danilov, I. S. (1967). Electrochemical aspects of pitting corrosion. *Corrosion Science*, 7,129 – 142.

Sakashita, M. and Sato, N. (1977). The effect of molybdate anion on the ion-selectivity of hydrous ferric oxide films in chloride solutions. *Corrosion Science,* 17, 473-486.

Schaeffler A.E. (1949). Metal Progress, 56, 680-680.

Schweitzer, P.A. (2006). Fundamentals of metallic corrosion: Atmospheric and media corrosion of metals. Corrosion Engineering Handbook. CRC Press, New York, 128-132.

Sedriks, A.J. (1986). Role of sulphide inclusions in pitting and crevice corrosion of stainless steels. *International Metals Reviews,* 28, 295-306.

Sekine, I., Hatakeyama, S. and Nakazawa, Y. (1987a). Corrosion behavior of type 430 stainless steel in formic and acetic acids. *Corrosion Science,* 27, 275-288.

Sekine, I., Hatakeyama, S. and Nakazawa, Y. (1987b). Effect of water content on the corrosion behavior of type 430 stainless steel in formic and acetic acids. *Electrochimica Acta,* 32, 915-920.

Sekine, I., and Okano, C. (1989). Corrosion behaviour of mild steels and ferritic Stainless steels in oxalic acid solutions. *Corrosion Science,* 45, 924-932.

Sekine, I., Okano, C. and Yuasa, M. (1990). The corrosion behavior of ferritic Stainless steel in oxalic acid solutions. *Corrosion Science,* 30, 351-366.

Sekine, I., Kawase, T., Kobayashi, M. and Yuasa, M. (1991). The effects of chromium and molybdenum on the corrosion behavior of ferritic stainless steels in boiling acetic acid solutions. *Corrosion Science,* 32, 815-825.

Shahryari, A., Omanovic, S. and Szpunar, J.A. (2008). Electrochemical formation of highly pitting resistant passive films on a biomedical grade 316LVM stainless steel surface. *Materials Science and Engineering,* 28, 94–106.

Sharma, S.C., Somashekar, D.R. and Satish, B.M. (2001). A note on the corrosion characterization of ZA-27/zircon particulate composites in acidic medium. *Material Processing Technology,* 118, 62-64.

Silverman, D. C. (1998). Tutorial on Cyclic Potentiodynamic Polarization Technique. In *Corrosion 98,* Houston, Texas, NACE International, 299.

Silverman, D.C. (2000). Practical corrosion prediction using electrochemical techniques. Uhlig's "Corrosion Handbook", Revie, R.W. (editor), John Wiley and Sons, Inc., Canada, 1179-1225.

Singh, A. K. and Singh, G. (2002). Corrosion of stainless steels in chlorine dioxide solution. *Anti-Corrosion Methods and Materials*, 49, 417–425.

Siow, K.S., Song, T. Y. and Qiu, J. H. (2001). Pitting corrosion of duplex stainless steels. *Anti-Corrosion Methods and Materials*, 48, 31-36.

Snape, E. (1977). Effect of nickel on the structure and properties of wrought and cast stainless steels. Handbook of Stainless Steels. Peckner, D. and Bernstein I.M. (editors), McGraw-Hill, 12-1 -12-40.

Streicher, M.A. (2000). Austenitic and ferritic stainless steels. Uhlig's "Corrosion Handbook", Revie, R.W. (editor), John Wiley and Sons, Inc., Canada, 603.

Sugimoto, K. and Sawada, Y. (1976). Role of alloyed molybdenum in austenitic stainless steels in the inhibition of pitting in neutral halide solutions. *Corrosion Science,* 32, 347–352.

Sugimoto, K., Seto, M., Tanaka, S. and Hara, S. (1993). Corrosion resistance of artificial passivation films of Fe_2O_3-Cr_2O_3-NiO formed by metal organic chemical vapor deposition. *Journal of the Electrochemical Society,* 140, 1586-1592.

Sumita, M., Hanawa, T. and Teoh, S.H. (2004). Development of nitrogen-containing nickel-free austenitic stainless steels for metallic biomaterials—review. *Materials Science and Engineering*, 24, 753-760.

Szklarska-Smialowska, Z. (1986). Pitting corrosion of metals. NACE International, Houston.

Takada, Y., Takahashi, N. and Okuno, O. (2007). Electrochemical behavior and released ions of the stainless steels used for dental magnetic attachments. *The Japanese Society of Magnetic Applications in Dentistry,* 414.

Tanaka, S., Hara, N. and Sugimoto, K. (1995). Corrosion characteristics of Fe_2O_3 and unknown Cr_2O_3 artificial passivation films under potentiostatic control. *Materials Science and Engineering,* 198, 63-69.

Tan, M.W., Akiyama, E., Kawashima, A., Asami, K. and Hashimoto, K. (1995). The effect of air exposure on the corrosion behavior of amorphous Fe–8Cr–Mo–13P–7C alloys in 1M HCl. *Corrosion Science,* 37, 1289–1301.

Teoh, S.H. (2000). Fatigue of biomaterials: a review. *International Journal of Fatigue*, 22, 825–837.

Tochihara, M., Ujiro, T., Yazawa, Y., and Satoh, S. (1986). Atmospheric corrosion of stainless steel used for the eaves of buildings, *Materials Performance,* 58–62.

Truman, J. E. and Crawshaw, B. (1968). Proceedings of conference on stainless steel for the fabricator and user. Birmingham, England, 195-204.

Tsilomelekis, G., Christodoulakis, A. and Boghosian, S. (2007). Support effects on structure and activity of molybdenum oxide catalyst for the oxidative dehydrogenation of ethane. *Catalyst Today,* 127,139-147.

Turan, Y.N. (1991). Effect of nitrogen on the structure and properties of type 310 austenitic stainless steels. MSc. Dissertation, University of the Witwatersrand, 5-16.

Uhlig, H.H. and Revie, R. (1985), Corrosion and Corrosion Control, 3 rd ed., Wiley, New York, 61.

Van Orden, A. C. (1998). Applications and problem solving using the polarization techniques. In *Corrosion 98,* Houston, Tex., NACE International, 301.

Van Warmelo, M., Nolan, D. and Norrish, J. (2007). Mitigation of sensitization effects in unstabilised 12%Cr ferritic stainless steel welds. *Materials Science and Engineering,* 464, 157-169.

Varga, K., Baradlai, P., Barnard, W.O., Myburg, G., Halmosg, P. and Potgieter, J.H. (1997). Comparative study of surface properties of austenitic stainless steels in sulfuric and hydrochloric acid solutions. *Electrochimica Acta,* 42, 25-35.

Viramontes-Gamboa, G., Rivera-Vasquez, B.F. and Dixon, D.G. (2007).The active-passive behavior of chalcopyrite comparative study between electrochemical and leaching responses. *Journal of the Electrochemical Society,* 154, C299–C311.

Vuurman, M.A. and Wachs, I.E. (1992). In-situ Raman spectroscopy of alumina-supported metal oxide catalysts. *Physical Chemistry*, 96, 5008-5016.

Wallen, B. and Olsson, J. (1977). Corrosion resistance in aqueous media. "*Handbook of Stainless Steels"*. Peckner, D. and Bernstein, I. M. (editors) McGraw-Hill, Canada, 16-1 -16-89.

Wallinder, I. O., Bertling, S., Kleja, D. B. and Leygraf, C. (2006), Corrosion-induced release and environmental interaction of chromium, nickel and iron from stainless steel. *Water, Air, and Soil Pollution*, 170, 17–35.

Yang, W., Ni, R.C., Hua, H.Z. and Pourbaix, A. (1984). The behavior of chromium and molybdenum in the propagation process of localized corrosion of steels. *Corrosion Science,* 24, 691–707.

APPENDIX

ACCEPTED FOR PUBLICATION

J.H. Potgieter, V. Adams, N. Maledi, J. Van Der Merwe and P. A. Olubambi, (2009). Corrosion resistance of Type 444 ferritic stainless steel in acidic chloride media. Journal of *Anti-Corrosion Methods and Materials*.